

# Inactivation of waterborne viruses by ozone: Kinetics and mechanisms

**Thèse N° 9370**

Présentée le 9 août 2019

à la Faculté de l'environnement naturel, architectural et construit  
Laboratoire de chimie environnementale  
Programme doctoral en génie civil et environnement

pour l'obtention du grade de Docteur ès Sciences

par

**Camille WOLF**

Acceptée sur proposition du jury

Prof. S. Takahama, président du jury

Prof. T. Kohn, directrice de thèse

Dr M. Templeton, rapporteur

Prof. M. Dodd, rapporteur

Prof. U. von Gunten, rapporteur

2019



---

“ Une personne qui n’a jamais commis d’erreurs n’a jamais tenté d’innover ” *A. Einstein*



# Acknowledgements

To my PhD adviser, Tamar Kohn, thank you for giving me the opportunity to join your laboratory to do my PhD. For the hours you helped me to develop and structure my research during these last 4 years. I really appreciate our meetings; you always had brilliant comments or remarks.

To Urs von Gunten, thank you for the invaluable advice on ozone chemistry in water that you provided me with throughout my PhD. Thanks for welcoming me in your lab to perform ozone experiments and for the opportunity to apply my research in the real world during this exceptional pilot tests.

To Michael Templeton and Michael Dodd, my external experts, for accepting to read and judge my thesis. In addition, thanks to Micheal Dodd for all the nice discussions we had while you were in Switzerland, which helped me to push further my reflections.

To Krista Wigginton for welcoming me in her lab for a month during my second year, that was a great experience.

Thanks to Caroline Gachet, Virginie Bachmann and Elisabeth Salhi for the helping me to perform experiments in the labs.

All LCE members (and LTQE member add-ons) from present and past. I entered this lab as a freshly graduated Master student and I grew up to be proper scientist, thanks to our amazing environment in and outside of the job. To Suzanne and Jason for your help to improve my writing and spelling in English, and also for our passionate debates at Sat. To Qingxia for the 3 years that we spent together at EPFL, for our discussions, activities and your mental support for the end of this project.

To my “twin” in research, Simon Meister, because we survived these 4.5 years with the highs and the lows we had to complete our PhD; we shared more than just work. From late nights in Ann arbour to 14 hours-days in lab, I appreciated all our discussions about science and life.

Thanks to all my team mates for the hours of training and games passed on the ice and for the fourth third, this help me to reach a good work-life balance.

To Adrian and Jess for the several hundred coffees with shared in Sat, and obviously to their advice and help to take a step back and have another persepctive when I encountered difficulties during my PhD. Thanks for your friendship and for all the nice dinners, boardgame afternoons and beer tastings shared together.

To all my friends, for the wine tasting, hiking, dinner or sport, this ensured that I kept one foot in real life and allowed / forced me to relax and enjoy life.

To my family and especially to my parents for their unwavering support all the way through the Bachelor, Master and the PhD. I am thankful that you always let me discover and follow my path. Maman thanks for listenint to me when I tried to explain you my maths or physics, even though you did not understand everything. For all the delicious food you filled in my bag, when I came back to Vallorbe. Sorry for all the stress and the worries you had when I had exams. To Benjamin, my “little” brother for the cooking, brewing, baking together. You will find your path, you are smart and passionate, so I have no doubt. A special thought to two angels who left a bit too early; you always did you best to try answer to my curiosity about the world that surrounded me when I was a kid. You never gave up in front of my numerous questions, even though you did not have all the answers. Your love and attention made me part of the person I am today and no words could say how thankful I am to had the chance to know you.

To Philippine, for sharing my life these last two years of my PhD that were maybe the most challenging and difficult. I know that this was not always easy with the time I spent in the lab or writing, but you kept me on track when I was falling down and always trusted that I was going to achieve it, even though I was not convinced myself. Thanks for your support, your patience and your love.

# Abstract

The growing world population, in conjunction with climate change, cases the global water demand to increase. It is, therefore, crucial to protect existing water resources from chemical pollution and contamination by pathogens. An increasingly popular strategy to meet increased water demand is potable water reuse, which uses wastewater effluent as the water source and treats it to such an extent that it is safe to drink. However, this practise may encompass risks for human health if the treatment train does not ensure a sufficient removal of chemical and microbial contaminants. In the context of both water and wastewater treatment, ozonation has emerged as an efficient treatment method for the control of pathogens, the abatement of organic micropollutants, and the removal of taste and odor compounds. Despite its popularity, information on the inactivation of waterborne viruses by ozone is scarce.

The aim of this thesis was to investigate the kinetics and mechanisms of inactivation of waterborne viruses by ozone. In a first step, the inactivation kinetics of a suite of human viruses and commonly used surrogates (bacteriophages) were determined in well-controlled buffer systems. To this end, we developed a method to control  $O_3$  decay in batch reactors. This allowed us to measure virus inactivation as a function of low ozone exposures. The resulting inactivation rate constant ( $k_{O_3\text{-virus}}$ ) differed between the virus species studied, but all  $k_{O_3\text{-virus}}$  fell within a narrow range of  $10^5\text{-}10^6\text{ M}^{-1}\text{s}^{-1}$ . These high inactivation rate constants indicate that ozone is efficient to inactivate waterborne virus. Increases in temperature and pH resulted in an increased  $k_{O_3\text{-virus}}$ , though the effect was relatively minor.

To determine if more complex, natural water matrices influence virus inactivation by ozone, we investigated the virucidal efficacy of ozone in two surface waters and a secondary wastewater effluent. While inactivation kinetics as a function of ozone exposure initially corresponded well to those observed in buffer solutions, the inactivation curve tailed off at higher ozone exposures. Furthermore, because it is not possible to measure virus inactivation during water treatment in real-time, we tested different if “easy-to-measure” proxies can be used to track virus inactivation. We determined that the applied specific ozone dose, the reduction in  $UV_{254}$ , or the abatement of carbamazepine all correlated to virus inactivation, though some proxy-inactivation relationships were not universal but depended on the water type. The proxies were validated in a pilot-scale ozonation reactor treating Lake Zurich water, and were found to provide good estimates of virus inactivation.

Finally, an immunostaining assay was developed to observe how ozonation affects crucial steps in the life cycle of echovirus 11, a representative of the *Enterovirus* genus. Specifically, we investigated if ozone alters the ability of the virus to enter the host cells, and if it prevents the viral genome from replicating. Preliminary results indicate a loss of internalization after ozone treatment as well as genome replication.

In conclusion, this thesis provides new information on the efficacy and mechanisms of ozone as an inactivating treatment for waterborne viruses, and it delivers tools to monitor virus inactivation during water and wastewater treatment in real-time.

## Keywords

Virus, bacteriophage, ozone, disinfection, kinetics, water treatment, drinking water, wastewater, MS2, Q $\beta$ , T4,  $\Phi$ 174, echovirus 11, human adenovirus, coxsackievirus B5, micropollutant elimination, virus internalization



# Résumé

L'augmentation de la population mondiale, ainsi que le changement climatique, accroît la demande en eau à travers le monde, et avec elle la pression sur les ressources en eau douce. Il est donc crucial de protéger ces ressources de la pollution et des contaminants par des agents pathogènes. Une stratégie qui gagne en popularité pour répondre à cette demande croissante est la réutilisation des eaux usées comme sources d'eau potable. Bien entendu, il existe des risques sanitaires importants liés à une telle pratique si les traitements ne sont pas suffisamment performants. Autant dans le traitement des eaux potables que des eaux usées, l'ozonation a émergé comme une solution efficace d'inactiver les pathogènes, réduire les micropolluants et enlever les odeurs et les goûts désagréables. Malgré sa popularité, les informations sur sa capacité d'inactiver les virus entériques sont rares et insuffisantes.

L'objectif de cette thèse est de comprendre la cinétique et les mécanismes d'inactivation des virus entériques par l'ozone. Dans un premier temps, les cinétiques d'inactivation de plusieurs virus humains et bactériophage (substitut comme modèle) ont été résolues dans une solution tampon bien définie. Pour accomplir ceci, une méthode a été développée pour permettre d'appliquer des expositions d'ozone très faibles, permettant ainsi de mesurer l'inactivation des virus en fonction de l'exposition à l'ozone. Les constantes d'inactivation ( $k_{O_3\text{-virus}}$ ) des virus différaient, mais toutes restaient dans un intervalle étroit de  $10^5\text{-}10^6 \text{ M}^{-1}\text{s}^{-1}$ . Ces constantes élevées prouvent l'efficacité de l'ozone pour inactiver les virus. Une augmentation de la température ou du pH a pour conséquence une augmentation de cette constante, mais cette augmentation reste faible.

Afin de déterminer l'influence des constituants des matrices naturelles sur l'inactivation des virus par l'ozone, nous avons choisi deux eaux de surface et un effluent secondaire d'eaux usées. Alors que la cinétique d'inactivation en fonction de l'exposition à l'ozone correspond initialement bien à celle observée dans les solutions tampons, la courbe d'inactivation présente un plateau avec des expositions à l'ozone plus élevées. De plus, comme il n'est pas possible de mesurer l'inactivation du virus pendant le traitement de l'eau en temps réel, nous avons testé différents types de proxy qui sont des paramètres « faciles à mesurer » pouvant être utilisés pour suivre l'inactivation du virus. Nous avons déterminé que la dose spécifique d'ozone appliquée, la réduction de l'UV<sub>254</sub> ou l'abattement de la carbamazépine étaient tous corrélés à l'inactivation du virus, bien que certaines corrélations dépendent du type d'eau. Ces proxys ont été validés lors d'une expérience d'ozonation dans une pilote traitant l'eau du lac Zurich et se sont révélés être une bonne estimation de l'inactivation du virus.

Enfin, un test d'immunocoloration a été mis au point pour observer comment l'ozone affecte les étapes cruciales du cycle de vie de l'échovirus 11, représentant du genre Enterovirus. Plus précisément, nous avons recherché si l'ozone altère la capacité du virus à pénétrer dans les cellules hôtes et s'il empêche le génome viral de se répliquer. Les résultats préliminaires indiquent une perte d'internalisation après le traitement à l'ozone ainsi que la réplication du génome.

En conclusion, cette thèse fournit de nouvelles informations sur l'efficacité et les mécanismes de l'ozone en tant que traitement inactivant des virus transmis par l'eau, et fournit des outils permettant de surveiller en temps réel l'inactivation des virus lors du traitement de l'eau et des eaux usées.

## Mots-clés

Virus, bactériophage, désinfection, ozone, cinétique, traitement de l'eau, eau potable, eaux usées, adénovirus, caxsackievirus B5, echovirus 11, MS2, Q $\beta$ , T4,  $\Phi$ 174, inactivation entéroviral, internalization de virus, élimination de micropolluant

# Contents

<b>Acknowledgements.....</b>	<b>v</b>
<b>Abstract .....</b>	<b>vii</b>
<b>Keywords .....</b>	<b>viii</b>
<b>Résumé .....</b>	<b>ix</b>
<b>Mots-clés .....</b>	<b>x</b>
<b>Contents.....</b>	<b>xi</b>
<b>List of Figures .....</b>	<b>xv</b>
<b>List of Tables .....</b>	<b>18</b>
<b>List of Equations.....</b>	<b>20</b>
<b>Chapter 1 Introduction .....</b>	<b>21</b>
1.1 Context.....	21
1.2 Water treatment: A multi-barrier approach.....	22
1.2.1 Ozone chemistry and stability in water .....	23
1.2.2 Ozone as a disinfectant.....	25
1.2.3 Disinfection by-products.....	26
1.3 Microbial hazards.....	28
1.3.1 Types of microbes found in wastewater .....	28
1.3.2 Pathogen transmission .....	29
1.3.3 Waterborne viruses as pathogens of concern.....	29
1.4 Research Objectives.....	31
1.4.1 What is the inactivation kinetics of virus by ozone ? .....	31
1.4.2 What is the effect of DOM on inactivation kinetics and which proxy to use for viral inactivation during ozone treatment?.....	32
1.4.3 What are the mechanisms of virus inactivation by ozone?.....	32
<b>Chapter 2 Kinetics of Inactivation of Waterborne Enteric Viruses by Ozone .....</b>	<b>33</b>
2.1 Abstract.....	33
2.2 Introduction .....	33

2.3	Experimental section .....	35
2.3.1	Chemical .....	35
2.3.2	Virus propagation, purification and enumeration.....	35
2.3.3	Ozone Production .....	35
2.3.4	Experimental Procedures .....	35
2.3.5	Simulations and data analysis.....	38
2.4	Results and discussion .....	39
2.4.1	Method validation and temperature-dependence of $k_{O_3-CA}$ .....	39
2.5	MS2 inactivation kinetics by the batch method .....	40
2.5.1	Inactivation of other viruses by ozone .....	41
2.5.2	Estimation of extent of virus inactivation during wastewater ozonation .....	44
2.6	ACKNOWLEDGMENTS.....	46
<b>Chapter 3</b>	<b>Inactivation of Waterborne Viruses by Ozone in Natural Matrices: Proxies for viral inactivation</b>	<b>47</b>
3.1	Introduction .....	47
3.2	Materials and Methods.....	48
3.2.1	Chemicals and solutions .....	48
3.2.2	Phages and bacteria.....	48
3.2.3	Virus propagation, purification and enumeration.....	48
3.2.4	Water matrices .....	49
3.2.5	Ozone production .....	49
3.2.6	O <sub>3</sub> exposure measurements .....	49
3.2.7	Inactivation experiments .....	50
3.2.8	Experiments with proxies .....	50
3.2.9	Pilot experiment .....	51
3.2.10	Data analysis .....	51
3.3	Results and Discussion .....	52
3.3.1	O <sub>3</sub> depletion profiles and exposures .....	52
3.3.2	Virus inactivation as a function of ozone exposure.....	53
3.3.3	Proxies for virus inactivation .....	55
3.4	ACKNOWLEDGMENTS.....	66
<b>Chapter 4</b>	<b>Inactivation mechanisms.....</b>	<b>67</b>
4.1	Introduction .....	67

4.2	Material and Methods .....	69
4.2.1	Virus and cells .....	69
4.2.2	Buffers and media .....	69
4.2.3	Antibodies .....	69
4.2.4	Time lapses and inactivation experiments .....	69
4.2.5	Sample preparation and fixation .....	69
4.2.6	Internalization assay .....	70
4.2.7	Replication assay .....	72
4.3	Confocal microscopy .....	73
4.4	Image analysis .....	73
4.5	Results .....	75
4.5.1	Time laps .....	75
4.5.2	Disinfection .....	79
4.6	ACKNOWLEDGMENTS .....	82
<b>Chapter 5</b>	<b>Conclusion .....</b>	<b>83</b>
5.1	Main conclusion and implications .....	84
5.1.1	Virus inactivation in buffered system .....	84
5.1.2	Virus inactivation in natural matrices .....	84
5.1.3	Virus inactivation mechanism .....	85
5.2	Limitations and further work .....	86
	<b>Supporting information for Chapter 2 .....</b>	<b>87</b>
	Chemicals and solutions .....	87
	Phages and bacteria .....	87
	Viruses and cells .....	87
	Procedure for the purification of MS2 by QA monolith liquid chromatography .....	88
	Activation energy for the reaction of trans-cinnamic acid with ozone .....	89
	HPLC analyses .....	92
	Experimental details for quench-flow experiments to measure the kinetics of MS2 inactivation .....	93
	Experimental details for quench-flow experiments to measure the kinetics of carbamazepine (CBZ) abatement .....	94
	HPLC method to measure benzaldehyde and carbamazepine (CBZ) .....	95
	Comparison of MS2 inactivation measured in batch experiments and by quench-flow .....	96
	Effect of the purification method on $k_{03-MS2}$ .....	97

---

Reproducibility of batch approach and effect of initial virus concentration .....	98
Effect of temperature and pH .....	100
Activation energy of MS2 inactivation by ozone .....	101
<b>Supportive information for Chapter 3 .....</b>	<b>102</b>
S3.1 O <sub>3</sub> depletion profiles in natural matrices .....	102
S3.2 HPLC analyses .....	106
S3.3 Conditions for the SPE online and UPLC MS/MS analysis (adapted from <sup>91</sup> ) .....	107
S3.4 Experimental plan.....	108
S3.5 R Script of the power model.....	109
S3.6 Ozone exposure model : Model parameters and details.....	110
S3.7 Inactivation as a function of the ozone exposure .....	111
S3.8 Proxies as a function of the specific ozone dose: comparison with published data.....	112
S3.9 Bayesian model averaging (BMA).....	114
S3.11 Gerrity et al. extracted data .....	121
S3.12 Pilot experiment .....	123
<b>Supportive information for Chapter 4 .....</b>	<b>125</b>
<b>References .....</b>	<b>127</b>
<b>Curriculum Vitae .....</b>	<b>134</b>

## List of Figures

Figure 1.1 Reaction of ozone with DOM and pathways resulting in hydroxyl radical production. <sup>17</sup> .....	25
Figure 1.2 Scheme of ozone decay (dots) in function of the time to highlight the importance to consider the first phase of decay (black), to correctly calculated the ozone exposure. Dashed area represents the overestimation due to late measurement of ozone (red).....	26
Figure 1.3 Transmission routes of waterborne pathogens, red arrows highlights where water disinfection can be applied.....	29
Figure 1.4 Calculated inactivation rate constant based on reported data highlights inconsistencies through out literature data.....	30
Figure 2.1 Overview over batch approach.....	37
Figure 2.2 Second-order rate constants $k_{O_3-MS2}$ for the inactivation of MS2 with ozone at different temperature (2, 12 and 22°C) and pH (6.5 and 8.5) conditions. ....	41
Figure 2.3. Log inactivation of all selected viruses as a function of the ozone exposure (22°C, pH = 6.5). Each panel contains data from at least two independent experiments.	
Figure 2.4 Second-order rate constants $k_{O_3-MS2}$ for the inactivation of MS2 with ozone at different temperature (2, 12 and 22°C) and pH (6.5 and 8.5) conditions.	41
Figure 2.3. Log inactivation of all selected viruses as a function of the ozone exposure (22°C, pH = 6.5). Each panel contains data from at least two independent experiments. ....	43
Figure 2.4 Calculated inactivation of MS2 and CVF by ozone in wastewater as a function of the specific ozone dose.....	45
Figure 3.1 Natural logarithm of the measured $O_3$ exposure in function of the specific ozone or SWB (red circles) and WW (blue triangles). The inset shows the $O_3$ exposure on a linear scale.....	52
Figure 3.2 Inactivation of MS2 and CVB5 in SWB and WW as function of the ozone exposure computed based on equation 3.2. Solid lines represent the expected inactivation computed based on equation 2.1, using $k_{O_3-virus}$ values of MS2 and CVB5 determined in buffer (Wolf et al., 2018).....	53
Figure 3.3 Inactivation in function of the ozone exposure with power model prediction (black line) and 95% credible interval (dashed line) for SWB (pink) and WW (turquoise) .....	54
Figure 3.4 $\Delta UV_{254}$ (top) and CBZ abatement (bottom) in function of the specific $O_3$ dose applied in the surface water of Lake Geneva and Lake Bret, and secondary effluent wastewater from Dübendorf. ....	55

Figure 3.5 Inactivation of MS2 (black triangles) and CVB5 (red circles) in SWG, SWB and WW in function of the three proxies studied. ....	57
Figure 3.6 Comparison of the inactivation MS2 and CVB5 as function of the $\Delta$ UV254 in WW of this study (black circles) with corresponding data for MS2 by Gerrity et al. (red circles). The data by Gerrity et al. is a compilation of five different wastewaters. 58	
Figure 3.7 Power model (equation 5) with expected mean value (black line) and 95% credible interval (dashed lines) separate by water type (SW: circle and WW: triangle) for the three proxies studied. ....	61
Figure 3.8 (A): Prediction of the mean MS2 inactivation (red line) and 95% CI (black dashed line) in wastewater based on equation 5, superimposed by inactivation data measured by Gerrity et al. (2012). (B): Comparison of the predicted vs measured inactivation for the data generated by Gerrity et al. (2012) <sup>40</sup> The black line indicates a 1:1 relationship. 63	
Figure 3.9 Inactivation measured in the pilot reactor as a function of ozone exposure or proxies. ....	65
Figure 4.1 Schematic overview of the enterovirus life cycle, scheme from Baggen <i>et al</i> (2018) <sup>106</sup> .....	68
Figure 4.2 Immunostaining before permeabilization with Mouse anti-E11 (primary Ab) and Goat anti-Mouse IGG-Alexa 555 (secondary Ab). Only viruses outside of the cell are labelled. ....	71
Figure 4.3 Immunostaining after permeabilization with Mouse anti-E11 (primary Ab) and Goat anti-Mouse IGG-Alexa488 (secondary Ab). Viruses outside are labelled with both Abs (Alexa 555 and Alexa 488). Viruses within the cell are labelled only with Alexa488. 72	
Figure 4.4 Immunostaining after permeabilization with Mouse J2 antibody (primary Ab) and Goat anti-Mouse IGG-Alexa 488 (secondary Ab). Only dsRNA is labelled. ....	73
Figure 4.5 Image analysis pipelines for replication assay A) and internalization assay B). 74	
Figure 4.6 Time laps images of the cells (first column), the virus signal after cell permeabilization (2nd column), the virus signal before cell permeabilization (3rd column) and the replication signal (4th column) from 5 min up to 8h. ....	75
Figure 4.7 A) the area of virus signal inside the cell and B) the mean intensity of replication signal in function of the time post-infection. Each dot represents an individual cell analyzed. The estimated background signals arising from virus-or replication-negative cells are indicated with red lines. ....	77
Figure 4.8 Explanation of Manders coefficients. ....	78
Figure 4.9 Virus-positive cells. ....	79
Figure 4.10 Selection of images analysed to observe loss of internalization or replication with and without ozone treatment. ....	80
Figure 4.11 Comparison of the area of virus signal within the cells and replication signal mean intensity between control and treated sample. ....	81



Figure 4.1 Schematic overview of the enterovirus life cycle .....	85
Figure S4.1 Mander's coefficients. ....	125

## List of Tables

Table 1.1 Validated log reduction values based on challenge testing and operational monitoring sensitivity. (adapted from Potable reuse: GUIDANCE FOR PRODUCING SAFE DRINKING-WATER, WHO 2017) .....	23
Table 1.2 Examples of pathogens and indicators found in wastewater (adapted from WHO, 2017) <sup>8</sup> .....	28
Table 2.1. Summary of measured and reported second-order rate constants for the reaction of CBZ with ozone and corresponding statistics. The error associated with the $k_{O_3-CBZ}$ corresponds to the standard error.....	39
Table 2.2 Second-order rate constants for the inactivation of the selected viruses by ozone ( $k_{O_3-virus}$ ), with corresponding standard errors and adjusted $R^2$ .....	44
Table 2.3 Required oxidant exposures to inactivate, EV, HAdV and CVF by 2 log <sub>10</sub> . Ct values for ozone were determined in this study (Table S10). Ct values for free chlorine and chloramine were determined by Cromeans et al. (2010) in buffer at pH 7 and 5 °C <sup>74</sup> .....	44
Table 3.1 Water quality parameters of real water samples .....	49
Table 3.2 Summary of linear and power model parameters with the mean values, standard deviation and the 95% credible intervals in parentheses.....	62
Table 5.3 Parameters influencing $k_{O_3-virus}$ in buffered water matrix by decreasing importance .....	84
Table 5.4 Parameters influencing $k_{O_3-virus}$ in buffered water matrix by decreasing importance .....	84
Table 5.5 Review of proxies studied, their advantages and limitations .....	85
Figure S2.1 Arrhenius plot of $k_{O_3-CA}$ versus temperature, where the slope corresponds to $E_a/R$ . Two replicate experiments are highlighted in blue and red.	
Table 5.6 Review of proxies studied, their advantages and limitations.....	85
Table S2.1 : Step-gradient sequence applied for MS2 purification by monolith QA.	88
Table S2.2 Reaction rate constants at different temperatures, measured by stopped-flow for the reaction of trans-cinnamic acid and ozone. $k_{obs}$ is the pseudo first-order rate constant of $O_3$ consumption in excess of CA, and $k_{O_3-CA}$ is the second-order rate constant of the reaction of $O_3$ with CA. ....	90
Table S2.3 : Second order rate constants $k_{O_3-CA}$ for the reactions of CA with ozone at 2, 12 and 22°C, calculated using the Arrhenius equation and an activation energy of 21.2 kJ mol <sup>-1</sup> .....	91
Table S2.4 : Ozone concentration [ $O_3$ ], flow rate, aging time, ozone exposure and corresponding MS2 inactivation ( $\ln(N/N_0)$ ) for quench-flow experiments using a 500 $\mu$ L	

loop. Asterisks (*) indicate blank samples used to determine the initial O <sub>3</sub> concentration. In the blank samples, the ozone exposure was not determine (ND).....	93
Table S2.5: Loop volume, ozone concentration [O <sub>3</sub> ], aging time, flow rate, ozone exposures and corresponding CBZ abatement (ln (CBZ/CBZ <sub>0</sub> )) for quench-flow experiments. Asterisks (*) indicate blank sample used to the initial O <sub>3</sub> concentration. In the blank samples, the ozone exposure was not determine (ND).....	94
Table S2.6 : Eluent gradient to analyze benzaldehyde and CBZ by HPLC .....	95
Table S2.7 MS2 inactivation rate constants and effect of purification procedures, and corresponding F-statistics. A p-value > 0.05 indicates that a sample is statistically equivalent to a representative reference experiment (*) obtained under “standard conditions” .....	97
Table S2.8 Second-order MS2 inactivation rate constants for experiments conducted at different MS2 starting concentrations, and corresponding F-statistics. A p-value > 0.05 indicates that a sample is equivalent to a representative reference experiment (*) obtained .....	98
Table S2.9 Contributions of the variables ozone exposure, temperature and pH to inactivation, with corresponding F-test statistics. ....	100
Table S2.10 Data used to estimate activation energy of MS2 inactivation by ozone (T= 2, 12, 22°C) .....	101
Table S3.1 Detailed ions used for CBZ quantification .....	107
Table S3.2 Summary of the experiments that conducted for each water.....	108
Table S3.3 Model parameters and relevant statistics for O <sub>3</sub> exposure model in function of specific O <sub>3</sub> dose [mgO <sub>3</sub> /mgDOC] for the two waters studied. ....	110
Table S3.4 Summary of the O <sub>3</sub> exposure model statistics (estimate, standard deviation, p-value and adjusted R <sup>2</sup> ) .....	111
Table S3.5 Power function and quadratic function parameters (slope, standard deviation, 95% credible intervals) for the three studied waters and comparison with previously published data.....	112
Table S3.6 Summary statistics of Bayesian model averaging for variable selection for the specific O <sub>3</sub> dose as a proxy. Five probable models are presented with their statistics. ....	115
Table S3.7 Summary statistics of Bayesian model averaging for variable selection for ΔUV <sub>254</sub> as a proxy. Five probable models are presented with their statistics. ....	116
Table S3.8 Summary statistics of Bayesian model averaging for variable selection for ΔUV <sub>254</sub> as a proxy. Five probable models are presented with their statistics. ....	117
Table S 3.9 Extracted data from Gerrity et al. (2012) .....	121
Table S3.10 Water parameters of the pilot experiments during the two runs performed .....	123

Table S3.11 Summary of the different sampling points in the pilot reactor together with which proxy measurement locations.....	123
--	-----

## List of Equations

Equation 1.1 Chick-Watson model.....	25
Equation 1.2 Model for inactivation by ozone.....	25
Equation 1.3 $R_{ct}$ concept .....	25
Equation 1.4 Inactivation model including $R_{ct}$ concept .....	26
Equation 1.5 Second order rate constant of ozone reaction with trans-cinnamic acid	31
Equation 2.1 Reaction of trans-cinnamic acid with ozone: stoichiometric production of benzaldehyde.....	36
Equation 2.2 Chick-Watson model for ozone disinfection .....	36
Equation 3.1 Definition of $\Delta UV_{254}$ proxy .....	48
Equation 3.2 Model used to fit the $O_3$ exposure and specific $O_3$ dose .....	52
Equation 3.3 Model for inactivation in function of the $O_3$ exposure in natural matrices	54
Equation 3.4 Model used to fit virus inactivation as function of the different proxies	59
Equation S2.1 Pseudo first-order rate CA reaction with ozone .....	89
Equation S2.2 Arrhenius equation .....	89
Equation S2.3 Statistical model to test for purification effect.....	97
Equation S2.4 Statistical model to test the different replicate.....	98
Equation S2.5 Statistical model to infer pH and Temperature effect on inactivation	100
Equation S3.1 Model for $U_v$ in function of the specific ozone dose.....	112

# Chapter 1 Introduction

## 1.1 Context

An increasing world population and economic growth challenge safe drinking water supplies and ecosystem preservation, as human activities are the main pressure on water systems. Especially in fast developing societies, an increased water demand and high levels of pollution stress freshwater resources.<sup>1</sup> This pollution may stem from either treated or untreated industrial and communal wastewater discharge, and other sources, such as agricultural production, may also contaminate water bodies with fertilizer and pesticides through runoff.<sup>2</sup> Major contaminants include an excess of nutrients (nitrogen, phosphorous) that lead to eutrophication, an excessive increase in plant growth that can deplete oxygen from water sources,<sup>2</sup> or the release of micropollutants<sup>3,4</sup> or pathogens.<sup>5</sup> Minimizing water body contamination is necessary for preserving natural environments and ecosystem biodiversity and for protecting drinking water sourced from lakes, ground water, and rivers.<sup>6</sup> To lower health risks related to drinking water, advanced and efficient treatment technologies to prevent human waste contamination of source water should be a focus of water safety plans. Therefore, technology investments and policy commitments are mandatory to protect public health.<sup>7</sup>

In addition to world population growth, climate change impacts water availability and increases the stress on existing drinking water sources, meaning that areas of water scarcity are increasing. To reduce these effects, more sustainable, climate-independent, resilient, and adaptative drinking water supplies have to be developed and should be located close to high population density centers for maximum impact. Potable water reuse meets these criteria by producing large quantities of drinking water from wastewater through advanced technology in wastewater treatment plants (WWTPs), which can simultaneously reduce the environmental impact of wastewater discharge. However, several challenges have to be overcome for this option to be feasible and highly accessible, one of the biggest being the high concentrations of microbial and chemical contaminants present in wastewater. Complex treatment is required to ensure sufficient levels of safety.<sup>8</sup> These treatments require substantial investment, but this technology is key to ensuring water safety.

Of special concern in water safety, micropollutants are contaminants that can accumulate through a food chain and are highly ecotoxic. Extensive research has been conducted on the detection and removal of micropollutants since the early 1960's when polychlorinated biphenyl compounds (PCB) were detected in wildlife (mussels, fish, and birds).<sup>9</sup> In Switzerland, micropollutant monitoring started in 1975 in Lake Geneva, and in 2006, the first analysis of pharmaceutical contaminants in the lake revealed the presence of several drugs.<sup>10</sup> By 2016, the Swiss government changed the law concerning wastewater discharge, mandating that about 100 WWTPs be upgraded with tertiary treatment steps of either ozonation or activated carbon. The goal is to achieve 80% removal of a dozen indicators of micropollutants.<sup>11</sup>

Ozonation has emerged as promising technology to fulfill these more stringent standards for micropollutant abatement. However, more research is necessary to accurately assess and characterize its efficiency in microbial inactivation, especially for viral pathogens.

## 1.2 Water treatment: A multi-barrier approach

In water treatment, there are multiple levels of barriers protecting public health and water resources from waste and pollutants. The primary treatment of wastewater physically removes suspended solids and reduces heavy metals and organic nitrogen and phosphorus but does not sufficiently remove microbial pathogens or micropollutants. Secondary biological treatments, such as activated sludge or a membrane bioreactor, reduce the biochemical oxygen demand, and suspended solids by 85% or more. Digestion by microorganisms reduce nutrients and organic matter. Virus, bacteria, and protozoa concentrations may also be reduced by 2.5, 3, and  $2\log_{10}$ , respectively.<sup>8</sup> However, most micropollutants and waterborne pathogens can still escape this secondary treatment to be released into the environment.<sup>2-5,7</sup> Therefore, further downstream processes have to be added to conventional wastewater treatment to ensure sufficient removal of health-target compounds or microbes prior to discharge in the environment. These advanced treatments may include a combination of processes such as adsorption, media or membrane filtration, oxidation, and disinfection.

In addition to protecting water sources, multiple treatments are also a required next barrier for ensuring drinking water safety. Drinking water treatment may include pretreatment, flocculation, coagulation, sedimentation, filtration, and disinfection. This combination of processes may reduce by 6  $\log_{10}$  viruses and bacteria, and by 3-4  $\log_{10}$  protozoa. Another important aspect of drinking water production is a good maintenance of drinking water supply system to avoid recontamination post-treatment.

In the case of potable water reuse, where the loop between wastewater release and drinking water production is closed, it is fundamental to ensure sufficient pathogen removal. Therefore, complex treatment trains with multiple barriers between secondary wastewater effluent and drinking water supply are necessary. To ensure health protection, each individual process has to meet performance targets, and the overall treatment must be validated to reliably and consistently produce safe drinking water. Total organic carbon or discrete chemical species are sometimes used as surrogates for the removal of chemical hazards. However, the use of surrogates to monitor microbial disinfection is frequently discussed, and such contradictory results are presented in the literature<sup>12-14</sup> that the World Health Organization (WHO) strongly recommends avoiding microbial surrogates (such as *Escherichia coli*) to estimate microbial pathogen removal, including for human viruses.<sup>15</sup> Because indicator organisms are typically much more susceptible to inactivation than the pathogens they are supposed to indicate, process validation requires evidences of a certain log removal, also called  $\log_{10}$  removal credits (details in Table 1.1), of the microbes of interest. Moreover, an important component of validation is the identification of operational criteria that can assess the online treatment performance.

Table 1.1 Validated log reduction values based on challenge testing and operational monitoring sensitivity. (adapted from Potable reuse: GUIDANCE FOR PRODUCING SAFE DRINKING-WATER, WHO 2017)

Treatment process	LRV <sub>OMS</sub>		
	Bacteria	Viruses	Protozoa
Secondary wastewater treatment (without disinfection)	1	0.5	0.5
Soil-aquifer treatment	system specific		
Membrane bioreactor	4	1.5	2
Microfiltration	4	0	4
Ozone-biological activated carbon	4	4	0
Reverse osmosis	1.5-2	1.5-2	1.5-2
Ultraviolet light disinfection	6	6	6
Ultraviolet light/advanced oxidation process disinfection	6	6	6
Chlorination	6	6	0
Drinking water treatment plant (coagulation, flocculation, filtration, chlorination)	6	6	3-4

Advanced oxidation processes (AOPs) are some of the most important components to micropollutant or microbial risk removal, several of which have been implemented in existing water reuse treatment trains.<sup>16</sup> In parallel to AOPs, standard ozonation is of interest due to its high potential for micropollutant abatement and microbial inactivation, and it has been used for more than 100 years in drinking water production.<sup>17</sup> However, its application to wastewater treatment is more recent, where its main goals is micropollutant abatement.

### 1.2.1 Ozone chemistry and stability in water

Ozone is a strong oxidant that is unstable in aqueous solutions due to various different effects, not all of which are fully understood. Essentially, ozone instability increases in basic solutions due to a higher OH<sup>-</sup> concentration and increased formation of hydroxyl radicals (<sup>•</sup>OH), which are also strong oxidants. A lower pH and temperature increase ozone stability and solubility in water.

In drinking or wastewater, the presence of natural dissolved organic matter (DOM) significantly contributes to ozone decay, potentially due to its preferential reaction with the electron rich moieties of the DOM. Ozone has a high reactivity towards olefins and aromatics that is dependent on the accessibility of these functional

groups and their surrounding substituents. For example, its reactivity towards nitrogen-containing compounds varies significantly with the type of functional groups involved. Its reactivity towards aliphatic amines depends on the lone pair accessibility such that this reactivity is knocked down by complexation or protonation of the amine. In aromatic amines, a high electron density in the aromatic cycle may compete for ozone reactivity, though when the nitrogen is in an aromatic heterocycle, it has a low reactivity towards ozone.<sup>18,19</sup> Amides exhibit extremely low reactivity due to the presence of a carboxyl group that draws a lone pair of electrons. A similar effect is observed for sulfonamide compounds.<sup>17</sup>

Other organic and inorganic are affected by ozone to various degrees. Disulfide bonds are typically involved in bridges in secondary protein folding, so they are present in protein of microbes found in wastewater. Sulfur-containing compounds react with ozone in their low oxidation states as thiols (RSH) or disulfides (RSSR), though cysteine and methionine amino acids have high reaction rate constants for the reaction ozone at  $1 \times 10^9$  and  $6 \times 10^6 \text{ M}^{-1}\text{s}^{-1}$  at pH 7, respectively.<sup>20</sup> Considering the very slow reactivity of ozone with C-H bonds, saturated compounds lacking heteroatom reactive sites are “ozone refractory”, meaning they are typically not directly abated by ozone. Nevertheless, due to  $\cdot\text{OH}$  production during the ozonation of drinking or wastewater, they can be eliminated by alternative pathways with hydroxyl radicals.<sup>17</sup> Inorganic constituents of the water matrix, such as low oxidation state metal ions or inorganic anions, may also contribute to ozone decay. One particularly concerning one is bromide ( $\text{Br}^-$ ), whose reaction with ozone leads to the formation of bromate ( $\text{BrO}_3^-$ ), which has been identified as potential human carcinogenic compound.<sup>7,17</sup>

The quantity of conducted research into ozone for abating micropollutants highlights its potential, and, in fact, ozone has been used as a disinfectant for more than a century, including as a primary disinfectant for drinking water and wastewater. However, the complexity of ozone decay kinetics in water challenge the precise quantification of ozone exposure during laboratory experiments and water treatment. This decay kinetics are also largely dictated by the multitude of possible reactions with the DOM present in water matrices and can vary greatly depending on the concentration and specific DOM composing the water sample. Figure 1 shows how ozone can react with DOM moieties to form various radicals, and due to these reactions, ozone decay kinetics are often multiphasic.<sup>17,19</sup> The formation of  $\cdot\text{OH}$  radicals are of special interest as an intermediate in ozone decomposition because higher  $\cdot\text{OH}$  formation actually increases ozone consumption, and  $\cdot\text{OH}$  is itself also likely to react with micropollutants or pathogens present in water. Alkalinity is also an important parameter of the water matrix, because  $\text{CO}_3^{2-}$  ions act as  $\cdot\text{OH}$  scavengers, and therefore it increased ozone stability.



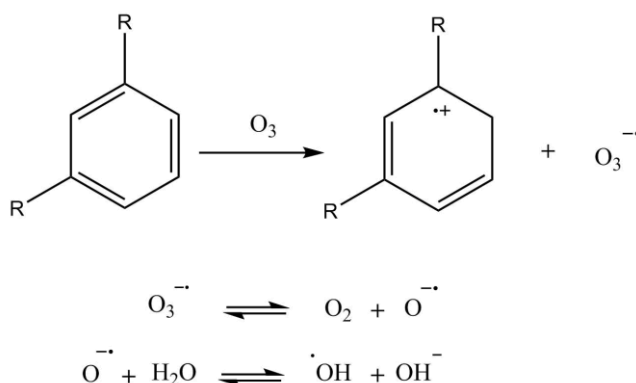
**DOM model**

Figure 1.1 Reaction of ozone with DOM and pathways resulting in hydroxyl radical production. <sup>17</sup>

### 1.2.2 Ozone as a disinfectant

To evaluate the efficiency of a given disinfectant, its kinetics have to be characterized. At the beginning of the last century, the Chick-Watson model (Equation 1.1) was proposed to describe disinfection kinetics,<sup>21</sup> and is represented as

Equation 1.1 Chick-Watson model

$$\ln\left(\frac{N}{N_0}\right) = -k \int [Disinfectant]^n dt$$

With this equation, inactivation can be described by the product of the inactivation rate constant ( $k$ ) and the exposure to the disinfectant. As seen previously, ozone reacting with DOMs also generates  $\cdot OH$  radicals that are also able to inactivate pathogens. Therefore, both processes may be considered to determine overall pathogen inactivation, which can be represented as

Equation 1.2 Model for inactivation by ozone

$$\ln\frac{[N]}{[N_0]} = -\left(k_{O_3} \int [O_3] dt + k_{\cdot OH} \int [\cdot OH] dt\right)$$

The  $R_{ct}$  concept was introduced by Elovitz and von Gunten, where<sup>22</sup>

Equation 1.3  $R_{ct}$  concept

$$R_{ct} = \frac{\int [\cdot OH] dt}{\int [O_3] dt}$$

which represents the ratio of  $\cdot OH$  exposure over ozone exposure in a given water sample. Generally, the  $R_{ct}$  is equal to  $10^{-8}$ – $10^{-9}$ (M/M) in surface water. This concept is useful for determining microbial inactivation based on the inactivation rate constants, the  $R_{ct}$ , and the ozone exposure.

The total inactivation is expressed in the transformed formula below as a function of their rate constant, the  $R_{ct}$  and the ozone exposure. Moreover, the importance of each disinfection process can be directly compared.

Equation 1.4 Inactivation model including  $R_{ct}$  concept

$$\ln \frac{[N]}{[N_0]} = -(k_{O_3} + k_{\cdot OH} R_{ct}) \int [O_3] dt$$

As one can see here,  $k_{\cdot OH}$  has to be much higher than  $k_{O_3}$  to be important in the disinfection process because of the low  $R_{ct}$  value of the  $\cdot OH$  radical, so its contribution to disinfection is generally neglectable in drinking water disinfection.<sup>23</sup> Here, the important variable to determine is the ozone exposure which is represented by the area under the ozone decay curve. As highlighted by Buffle *et al.*,<sup>18</sup> the initial phase of ozone decay (0 to 5s) is crucial for precisely determining ozone exposure in natural matrices. As highlighted by Figure 1.2, if this first phase is not measured (black dots), the real exposure can be overestimated (dashed area), resulting in an underestimation of the inactivation rate constant.

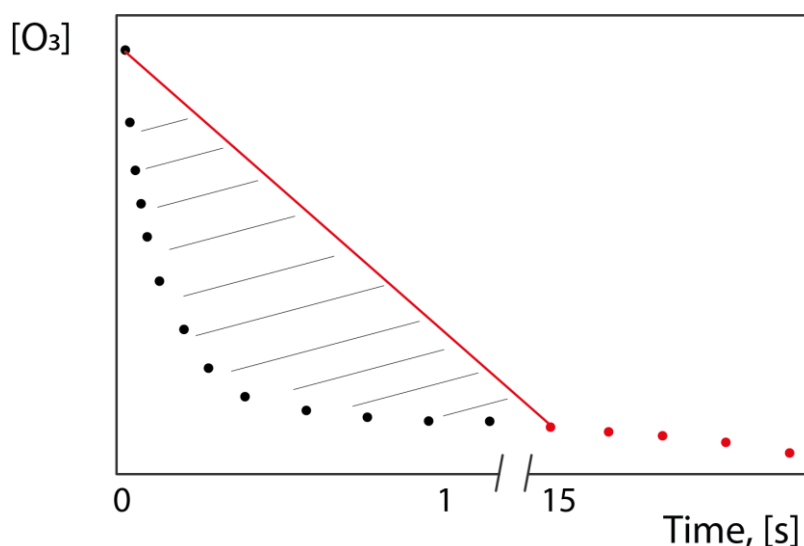


Figure 1.2 Scheme of ozone decay (dots) in function of the time to highlight the importance to consider the first phase of decay (black), to correctly calculate the ozone exposure. Dashed area represents the overestimation due to late measurement of ozone (red).

By comparing the required exposure for 2 log<sub>10</sub> inactivation (also called CT<sub>99</sub>), ozone has been recognized more efficient than chlorine. Especially against several pathogens of concern that are known to be chlorine resistant.<sup>24–29</sup> For 99% inactivation, the required CT (in mg\*min/l) were lower for O<sub>3</sub> by factor 10 for *Legionella pneumophila* and *Giardia lamblia*, and even 100 for *Cryptosporidium parvum*.<sup>30</sup>

### 1.2.3 Disinfection by-products

During disinfection, disinfection by-products (DBPs) are formed due to the reaction of ozone with natural organic matter (NOM), and it is necessary to consider these by-products due to their potential chronic exposure. A major reason for concern in by-product formation is the presence of bromide (Br<sup>-</sup>) in natural water, which can be found in the broad range from 10–1000 µg/l.<sup>17</sup> In low levels or the absence of Br<sup>-</sup>, a variety of organic DBPs are formed, most of which are biodegradable and will be eliminated by a biological filtration

step after ozonation. In the presence of bromide, bromoorganic compounds can be formed, though generally in concentrations below the threshold for drinking water. Therefore, the main by-product concern is bromate ( $\text{BrO}_3^-$ ) because of its carcinogenic effects. The maximum contaminant level has been established to  $10 \mu\text{g l}^{-1}$  by EU and USEPA. For  $\text{Br}^-$  levels above  $50\text{--}100 \mu\text{g/l}$ , bromate formation become already a problem. To mitigate bromate formation, ammonia can be added to scavenge hypobromous acid ( $\text{HOBr}$ ), a precursor of bromate. In addition, lowering the pH can shift bromate precursor equilibrium and reduce its formation. Combining these two measures can decrease bromate formation by up to 50%.

This illustrates the fine balance that must occur between the reduced microbial content and formation of toxic and possible cancerogenic DBPs in terms of health risks. The health benefits and the losses of different strategies of treatment can be compared using the disability adjusted life year (DALY) metric. This DALY may represent the lost years of “healthy” life.<sup>31</sup> Havelaar *et al.* estimate risks of *C. parvum* as  $10^{-3}$ /person-years. Applying ozone may reduce this risk by  $\sim 7$ -fold, but bromate level may rise higher than drinking water standards. However, the authors estimated the net benefit of preventing gastroenteritis in general and premature death with acquired immunodeficiency syndrome to be approximately 1 DALY/million person-year. According to the authors, health benefits by reducing *C. parvum* outcompete the losses due to renal cell cancer by a factor of  $>10$ .<sup>32</sup> To establish overall treatment goals, though, accurate inactivation kinetics are key because an underestimation of the required exposure may lead to insufficient inactivation, but an overestimation may uselessly increase the risk of DPB formation. In addition, an increased understanding of inactivation kinetics will allow a better evaluation of health benefits and losses during risks assessment analysis.

## 1.3 Microbial hazards

### 1.3.1 Types of microbes found in wastewater

Table 1 shows several examples of relevant enteric pathogens and their related indicators linked to water-borne disease, and includes data for bacteria, viruses, parasites, and helminths, as well as their general concentration range in typical untreated wastewater.

Table 1.2 Examples of pathogens and indicators found in wastewater (adapted from WHO, 2017)<sup>8</sup>

Pathogen	Illness	Number in untreated wastewater (per liter)
<b>Bacteria</b>		
<i>Escherichia coli</i>	Gastroenteritis /Microbial indicator	$10^5$ – $10^{10}$
Enterococci	/Microbial indicator	$10^6$ – $10^7$
Campylobacter	Gastroenteritis, Guillain-Barré syndrome	$<1$ – $10^5$
Mycobacteria (non-tuberculous)	Respiratory illness (hypersensitivity pneumonitis), skin infections	$<1$ – $10^6$
<i>Salmonella Typhi</i>	Typhoid	$<1$ – $10^5$
Other Salmonella	Gastroenteritis, reactive arthritis	$<1$ – $10^5$
Shigella	Dysentery	$<1$ – $10^4$
<i>Vibrio cholerae</i>	Cholera	$<1$ – $10^6$
<b>Viruses</b>		
Somatic coliphage	Microbial indicator	$<1$ – $10^9$
F-RNA phage	Microbial indicator	$<1$ – $10^7$
Adenoviruses	Gastroenteritis, respiratory illness, eye infections	$<1$ – $10^4$
Noroviruses	Gastroenteritis	$<1$ – $10^6$
Enteroviruses	Gastroenteritis, respiratory illness, nervous disorders, myocarditis	$<1$ – $10^6$
Rotavirus	Gastroenteritis	$<1$ – $10^6$
<b>Protozoa</b>		
Cryptosporidium	Gastroenteritis	$<1$ – $10^5$
<i>Entamoeba histolytica</i>	Amoebic dysentery	$<1$ – $10^2$
Giardia	Gastroenteritis	$<1$ – $10^5$
<b>Helminths</b>		
Ascaris	Abdominal pain, intestinal blockage	$<1$ – $10^3$
Trichuris	Abdominal pain, diarrhea	$<1$ – $10^2$

### 1.3.2 Pathogen transmission

Waterborne pathogens generally follow the fecal-oral transmission route, but several other routes may also lead to infection, as highlighted by Figure 1.3. First, transmission can occur via direct infection through the consumption of contaminated water or during recreational activities. Secondly, contaminated water may be used for irrigation or wash water, resulting in the contamination of food. For example, the raw consumption of contaminated lettuce has been known to lead to infections.<sup>33</sup> Contamination from hand-to-hand, hand-to-food, or flies-to-food are also important routes of transmission.<sup>34</sup> If wastewater is sufficiently treated before release or not released at all in a reuse scenario, the global risk of infection can be reduced by minimizing the exposure that occurs through any of the transmission routes.

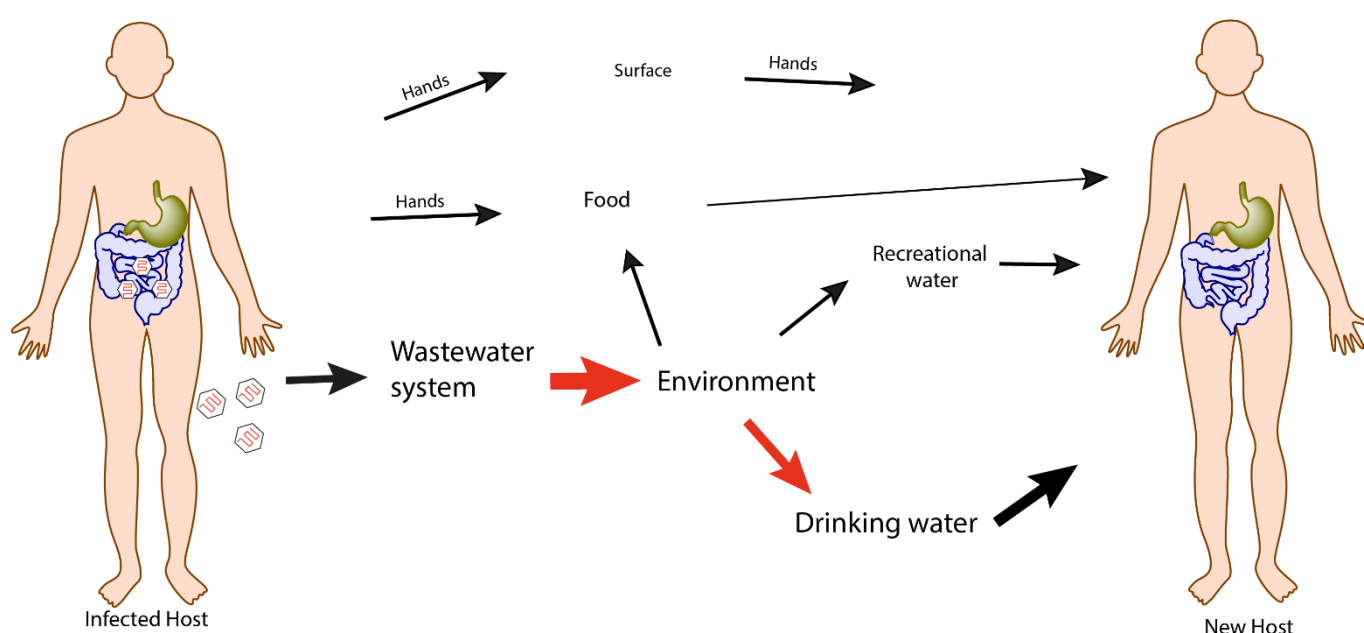


Figure 1.3 Transmission routes of waterborne pathogens, red arrows highlights where water disinfection can be applied.

### 1.3.3 Waterborne viruses as pathogens of concern

#### **Inactivation kinetics**

Among all waterborne pathogens, the WHO considers waterborne viruses to be of moderate to high health concern. Despite several differences in physical structure and genome morphology, these non-enveloped viruses, have several common features of concern. They persist for long periods in the environment, have an extremely low infectious dose ( $<100$ )<sup>35</sup>, and are shed in high numbers in feces—up to  $10^{11}$  per gram of stool for rotavirus, even when the infection is asymptomatic. Hence, fecally contaminated drinking water, if not adequately disinfected, may cause large outbreaks of viral gastroenteritis. In addition, exposure through swimming or showering may also lead to ocular or respiratory infections.<sup>36</sup>

As highlighted in the previous section, ozone has a high potential as a disinfectant. However, despite its historical use in water disinfection, only few studies have attempted to characterize its kinetics in relation to

viral inactivation. Precise ozone exposure values are challenging to obtain due to the variety and complexity of ozone decay profiles encountered in natural matrices. A recent study by Sigmon *et al.*<sup>14</sup> compiled data on viral inactivation by ozone to measure the similarities and differences between indicators and actual pathogenic viruses. Specifically, they measured the overall effect of ozonation on pathogen reduction by comparing the reduction of several pathogenic viruses and bacteria in buffer and wastewater. However, they did not derive inactivation rate constants and did not consider the initial rapid ozone decay phase. Vaughn *et al.* estimated an inactivation rate constant for rotavirus to be around  $\sim 10^4 \text{ M}^{-1}\text{s}^{-1}$  in buffer, but they also did not measure ozone exposure in the initial rapid decay phase between 0 and 10 s.<sup>37</sup>

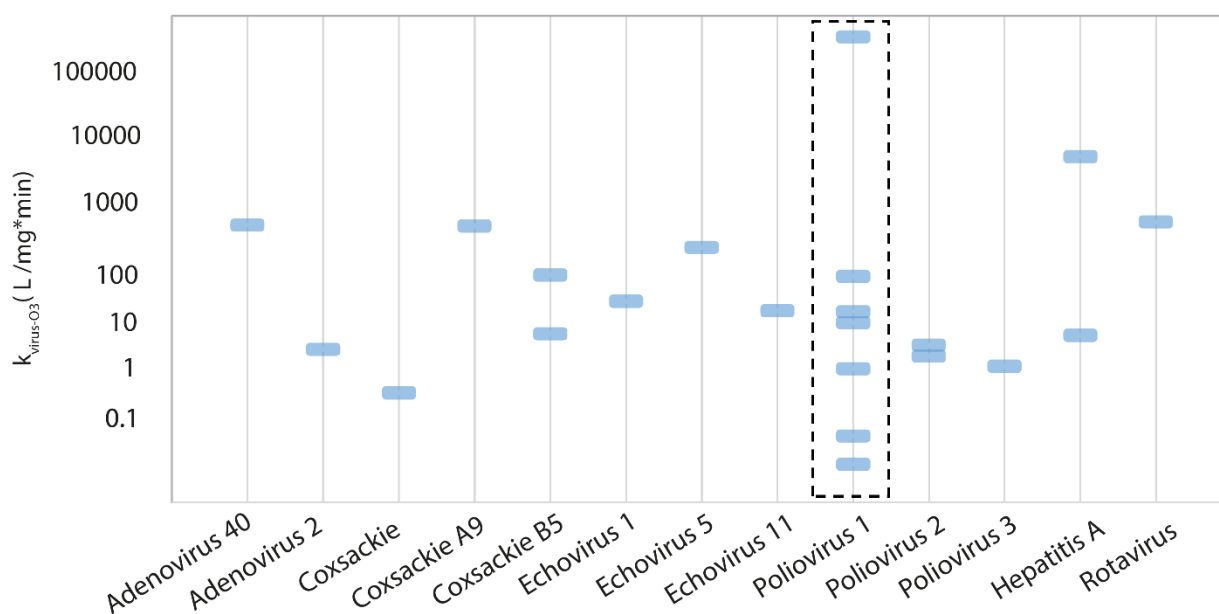


Figure 1.4 Calculated inactivation rate constant based on reported data highlights inconsistencies through out literature data.

Understanding the kinetics of ozone decay and disinfection is essential to its application in water treatment. Additionally, the monitoring of treatment performance is necessary to meet the validation criteria for water reuse. Therefore, to measure the efficiency of the disinfection processes, robust tools must be developed to monitor viral inactivation through water treatment.

### Molecular mechanism

As very few studies exist that address viral inactivation by ozone at all, even fewer address the mechanisms by which ozone can inactivate viruses. Roy *et al.*<sup>38</sup> published a study on inactivation of Poliovirus 1 by ozone, demonstrating a reduction of viral infectivity after treatment with various concentrations of ozone. They showed that ozone damages VP1 and VP2 polypeptide chains, two of the three proteins forming viral capsid subunits. These damages did not lead to breaking the viral capsid. However, the associated changes in protein conformation did not seem sufficient to reduce the host cell attachment capacity of the virus; thus, this impairment of the viral coat is not the predominant cause of inactivation. They also observed that the viral RNA was damaged during ozonation, which was therefore interpreted as the major cause of viral inactivation.

In contrast, Kim *et al.*<sup>39</sup> worked with bacteriophage f2 and demonstrated that ozone inactivation coincided with a loss in host attachment due to a breakup of the capsid protein. Additionally, they found that naked

RNA was inactivated by ozonation to a lesser extent than RNA inside the phage particle. The authors attributed this to a secondary reaction of RNA with radicals formed by reaction of coat protein subunits with ozone. Overall, these authors established that the main bacteriophage targets of ozone were the viral proteins, whereas the degradation of the genome was secondary.

Finally, Shinriki *et al.*<sup>40</sup> determined that in addition to degradation of the genome, the main mode of action of ozone on tobacco mosaic virus was crosslinking of the coat proteins that prevented the virus from uncoating inside of the host, and hence releasing its genome. With all of these studies taken together, it can thus be concluded that both protein and genome damage by ozone play an important role in inactivation and that their interplay is complex and poorly understood.

A mechanistic understanding of the molecular targets of ozonation is important for anticipating the disinfection of viruses that cannot be assessed experimentally. Virus species lacking a convenient cell culture system to measure their infectivity, such as norovirus. Furthermore, ozone target sites have to be determined to better understand the variability in viral disinfection kinetics, i.e., why some viruses are more ozone-resistant than others. Finally, a combination of disinfectants with different modes of action may be needed to eliminate a maximum number of viral species, which can only be understood through a detailed investigation of the mechanisms. A robust understanding of the modes of action of ozone is therefore necessary to design such a combined system.

## 1.4 Research Objectives

### 1.4.1 What is the inactivation kinetics of virus by ozone ?

To precisely resolve viral inactivation, the kinetics were first studied in a buffered system. These systems have the advantage of being a simplified water matrix with a well-controlled composition. As highlighted previously, the most challenging part in ozone inactivation is quantifying the precise exposure. In this study, an experimental method was developed to measure viral inactivation by controlling ozone decay kinetics through the addition of excess trans cinnamic acid (CA) to the buffer system containing t-BuOH to exclude  $\cdot\text{OH}$  radicals. This procedure allowed to study ozone inactivation kinetics in a simplified and reproducible system. The reaction rate constant ( $k_{\text{O}_3\text{-CA}}$ ) have been established at different temperatures and the Arrhenius activation energy was measured. Knowing the  $k_{\text{O}_3\text{-CA}}$  and the initial concentration of the reactants, the ozone exposure can be computed by resolving the second order decay equation below.

Equation 1.5 Second order rate constant of ozone reaction with trans-cinnamic acid

$$\frac{\partial[\text{O}_3]}{\partial t} = k_{\text{O}_3\text{-CA}} \times [\text{CA}]_t \times [\text{O}_3]_t$$

This would be impossible in natural matrices, because the kinetics of ozone are not controlled. Using this method, the influence of pH and temperature on the inactivation rate constant ( $k_{\text{O}_3\text{-virus}}$ ) were established for MS2. Then, the inactivation kinetics of nine different viruses were determined at room temperature and pH 7 for four bacteriophages and five human viruses, including two environmental isolates. The goals were, first, to measure the precise  $k_{\text{O}_3\text{-virus}}$ , and second, to observe if different viral species had significant differences in inactivation efficiency with  $\text{O}_3$ . Additionally, we verified whether bacteriophages would be good surrogates

for human viruses in ozone disinfection studies and if significant differences were measured between laboratory and environmental virus strains.

#### 1.4.2 What is the effect of DOM on inactivation kinetics and which proxy to use for viral inactivation during ozone treatment?

Once the kinetics were established, one bacteriophage (MS2) and one enteric virus (CVB5 Env1) were selected to establish the inactivation kinetics in natural matrices for several reasons. First, MS2 is easy to work with and can be propagated with a high titer, and experiments outside of a BSL2 environment are possible. CVB5 was one of the most “resistant” viruses observed in the buffer system, and it is an environmental strain that may better represent circulating viral species. To cover the different types of natural water matrices, three were selected, two raw surface waters (SW) and one secondary wastewater effluent (WW) samples. These matrices may represent the different types of water in which ozonation may be applied as treatment. They include different types and concentrations of dissolved organic matter (DOM). In this chapter, we investigated whether the natural matrix constituents significantly change  $k_{O_3\text{-virus}}$ . As a second goal, proxies for viral inactivation during ozonation were tested.

More specifically, the ozone exposure was calculated for the different samples. The specific ozone dose ( $\text{mgO}_3/\text{mgDOC}$ ) correlated to ozone exposure in wastewater,<sup>41,42</sup> we measured precisely ozone exposure for a range of specific ozone doses in one SW sample and the WW sample. A model was developed to predict ozone exposure based on the specific ozone dose applied, and batch experiments were performed with the MS2 and CVB5 viruses to compare the inactivation with the previously measured  $k_{O_3\text{-virus}}$ .

We also chose to investigate and validate previously mentioned proxies for surface water and wastewater application in this study. For example, Gerrity *et al.* and Gamage *et al.* showed the potential of UV absorbance reduction at 254 nm ( $\Delta\text{UV}_{254}$ ) and the specific ozone dose as proxies for MS2 inactivation in wastewater.<sup>43,44</sup> Additionally, carbamazepine abatement has also been considered as a proxy for virus inactivation by ozone. This micropollutant has similar reaction kinetics as the viruses with ozone. In addition, carbamazepine will be monitored punctually during wastewater treatment in Switzerland as part of a new regulation.<sup>11</sup>

#### 1.4.3 What are the mechanisms of virus inactivation by ozone?

For a multi-barrier approach to water treatment, understanding the ability of a disinfectant to damage either the genome or capsid proteins is important. Successive disinfection steps have to be complementary to avoid resistant pathogens passing through the treatment train, wherefore, synergistic processes are preferred.

In this chapter, the effect of ozone damage on viral life cycle functions (internalization, or replication) are investigated. An immunocytochemistry assay was developed to measure internalization of the virus and its ability to replicate.



## Chapter 2 Kinetics of Inactivation of Waterborne Enteric Viruses by Ozone

Reproduced with permission from : C. Wolf, Urs von Gunten; Tamar Kohn. 2018. "Kinetics of Inactivation of Waterborne Enteric Viruses by Ozone." *Environ. Sci. Technol.* 2018, 52 (4), 2170–2177. DOI: 10.1021/acs.est.7b05111 > Copyright [2018] American Chemical Society.

The author of this thesis, Camille Wolf, developed the experimental methods, performed the experiments, analyzed the data and wrote the paper.

### 2.1 Abstract

Ozone is an effective disinfectant against all types of waterborne pathogens. However, accurate and quantitative kinetic data regarding virus inactivation by ozone is scarce, due to the experimental challenges associated with the high reactivity of ozone towards viruses. Here, we established an experimental batch system that allows tailoring and quantifying very low ozone exposures and simultaneously measuring virus inactivation. Second-order ozone inactivation rate constants ( $k_{O_3\text{-virus}}$ ) of five enteric viruses (laboratory and two environmental strains of coxsackievirus B5: CVF, CVEnv1 and CVEnv2, human adenovirus: HAdV, and echovirus 11: EV) and four bacteriophages (MS2, Q $\beta$ , T4 and  $\Phi$ 174) were measured in buffered solutions. The  $k_{O_3\text{-virus}}$  of all tested viruses ranged from  $4.5 \times 10^5$  to  $3.3 \times 10^6 \text{ M}^{-1}\text{s}^{-1}$ . For MS2,  $k_{O_3\text{-MS2}}$  only depended weakly on temperature ( $2 - 22^\circ\text{C}$ ,  $E_a = 22.2 \text{ kJmol}^{-1}$ ) and pH (6.5 – 8.5), with an increase of  $k_{O_3\text{-MS2}}$  with increasing pH. The susceptibility of the selected viruses towards ozone decreases in the order  $Q\beta > CVEnv2 > EV \approx MS2 > \Phi174 \approx T4 > HAdV > CVF \approx CVEnv1$ . Based on the measured  $k_{O_3\text{-virus}}$  and typical ozone exposures applied in water and wastewater treatment, we conclude that ozone is a highly effective disinfectant for virus control.

### 2.2 Introduction

Ozone ( $O_3$ ) has been applied to drinking water disinfection and chemical oxidation for over a century.<sup>17</sup> Ozone is known to efficiently inactivate bacteria, and protozoans, including chlorine resistant pathogens such as *Cryptosporidium parvum* oocysts, *Giardia* cysts and *Legionella*.<sup>23,26–28</sup> In addition, ozone can be applied for taste and odor control, as well as for the oxidation of inorganic contaminants.<sup>45</sup> More recently, the application of ozone has been extended to wastewater treatment,<sup>46–49</sup> where its main purpose is to contribute to the abatement of micropollutants in secondary wastewater effluent and the reduction of their load to the aquatic environment. Finally, ozone is becoming an integral part of many potable reuse trains, where it can be applied for pre-oxidation of effluent organic matter, micropollutant abatement and disinfection.<sup>16</sup>

Ozone has also been recognized as an effective treatment against waterborne viruses. This property is particularly desirable in the context of potable reuse, where guidelines require a stringent treatment goal of up to 12 log<sub>10</sub> virus removal from raw wastewater to tap water.<sup>50</sup> Previous studies have reported inactivation data for different enteroviruses, adenoviruses and several bacteriophages.<sup>14,38,51,52</sup> However, reproducible measurements of kinetic parameters for viral inactivation remain sparse, and the reported efficacy of ozone toward a given virus varies dramatically. For example, as reviewed by Finch and Fairbairn (1991), the reported inactivation of poliovirus type 1 ranges from 0.5 log<sub>10</sub> at an estimated ozone exposure (ozone concentration integrated over exposure time<sup>49</sup>) of 3.9 mg\*min/L (15 min at 0.26 mg/L ozone) to 4 log<sub>10</sub> at an estimated exposure of only 1.7\*10<sup>-4</sup> mg\*min/L (0.1 s at 0.1 mg/L ozone).<sup>51</sup> In a less extreme example, Roy *et al.* (1981) reported a 2 log<sub>10</sub> inactivation of coxsackievirus B5 at an ozone exposure of 0.072 mg\*min/L (0.48 min at 0.15 mg/L ozone),<sup>53</sup> whereas Sigmon *et al.* (2015) determined an ozone exposure of 0.51 mg\*min/L to achieve the same extent of inactivation.<sup>54</sup>

These differences in reported kinetic data are in part associated with different experimental setups to measure virus inactivation by ozone. For example, in experiments using bubble contactors inactivation may be limited by ozone transfer from the gas phase to the bulk solution.<sup>54</sup> Compared to experiments using dosing of stock solutions of dissolved ozone, bubble contactors are thus likely to report slower inactivation kinetics. The biggest experimental challenge, however, is the quantification of the very low ozone exposures associated with virus inactivation. Although some studies report inactivation as a function of ozone residual or ozone concentration applied and time of exposure<sup>38,51</sup> permitting rough estimates of exposure values - the majority of prior studies did not provide sufficient data to evaluate virus inactivation in terms of ozone exposure. Furthermore, due to the extremely rapid kinetics of viral inactivation, substantial measurement uncertainties remain even when exposures were reported. For example, while both Sigmon *et al.* (2015)<sup>14</sup> and Thurston *et al.* (2005)<sup>52</sup> reported inactivation as a function of the ozone exposure, their first measured ozone concentration was only obtained after 10 to 15s. However, the initial phase ( $\leq 10$ s) of the ozone decay has been identified as crucial to determine ozone exposures for fast reactions.<sup>18</sup> Experimental approaches that do not capture this initial phase will result in an overestimation of ozone exposure, and by consequence to an overestimation of the exposure required to achieve a given virus inactivation.

The experimental challenges discussed above highlight the need for a reliable experimental approach to measure virus inactivation kinetics at low ozone exposures. The resulting kinetic information is of particular importance with respect to the use of ozone in wastewater, where competing reactions of ozone with matrix constituents (e.g., dissolved organic matter) lead to rapid ozone consumption, and hence low ozone exposures. For example, a typical specific ozone dose of 0.5 mg O<sub>3</sub>/ mg dissolved organic carbon (DOC) applied to nine different secondary wastewater effluents yielded ozone exposures of 0.16 – 2.2 mg\*min /L (0.2-2.8\*10<sup>-3</sup> Ms).<sup>41</sup> To estimate the extent of virus inactivation by ozonation of wastewater, virus susceptibilities to low ozone exposures must thus be known.

An existing experimental approach is the use of quench-flow systems.<sup>18</sup> However, such experiments require specialized equipment, which is not practical for use with biosafety level II material. In this context, the first aim of this study was to develop and validate a simple batch method to measure second order virus inactivation rate constants at low ozone exposures. This method was then used to explore the range of susceptibilities of different viruses toward ozone, which in turn allowed an estimation of virus inactivation during wastewater ozonation.

## 2.3 Experimental section

### 2.3.1 Chemical

The quality and sources of all chemicals are listed in the Supporting Information (SI).

### 2.3.2 Virus propagation, purification and enumeration

Five human enteric viruses (Faulkner strain and two environmental strains of coxsackievirus B5: CVF, CVEnv1 and CVEnv2; human adenovirus type 2: HAdV; and echovirus 11 Gregory strain: EV) and four bacteriophages (MS2, Q $\beta$ , T4 and  $\Phi$ 174) were included in this study. The information on sources of all viruses, their host cells and their propagation procedures is provided in the SI.

All viruses were purified using a polyethylene glycol (PEG)-chloroform method, as described previously.<sup>55</sup> For MS2, a second purification method adapted from Oksanen *et al.* (2012)<sup>56</sup> using a CIM monolithic column (QA 1 ml, BIA Separation) was performed to study the effect of purification on inactivation. Details of the procedure are given in Table S1, SI. Virus stock solutions were kept in phosphate buffered saline (PBS; 5 mM NaH<sub>2</sub>PO<sub>4</sub>, 10 mM NaCl, pH=7.5) and stored at 4°C. Phages were enumerated by the double-agar-layer method as described previously<sup>55</sup> and infective phage concentrations are expressed in plaque forming units (PFU)/mL. Enteric viruses were enumerated by the most probable number (MPN) assay as detailed elsewhere,<sup>57</sup> and concentrations are expressed as most probable number of cytopathic units (MPNCU)/mL.

### 2.3.3 Ozone Production

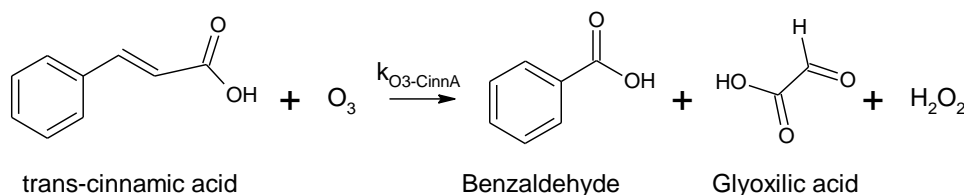
Ozone gas was produced by an ozone generator (Innovatec; model CMG 3-3 or CMG 3-5, Rheinbach, Germany) from pure oxygen (Carbagaz) and the resulting ozone/oxygen mixture was bubbled through Barnstead Nanopure (ThermoFisher) /MilliQ (Millipore) water cooled in an ice bath.<sup>58</sup> Ozone stock solutions reached concentrations ranging from 0.8 to 1.25 mM. For each stock solution produced, the ozone concentration was measured by direct spectrophotometry using an absorption coefficient  $\epsilon_{260} = 3200 \text{ M}^{-1} \text{ cm}^{-1}$ .<sup>17</sup>

### 2.3.4 Experimental Procedures

#### **Approach to produce and quantify low ozone exposures**

To measure viral inactivation at low ozone exposures, we used an experimental setup in which the ozone stability was controlled by a compound with known ozone reactivity added in excess of the ozone dose. Specifically, we performed inactivation experiments in solutions containing excess concentrations of trans-cinnamic acid (CA) in presence of tert-butanol (t-BuOH) to avoid any interferences with hydroxyl radicals ( $\cdot\text{OH}$ ). CA was chosen because it is highly reactive towards ozone ( $k_{\text{O}_3\text{-CA}} = 3.8 \times 10^5 - 1.2 \times 10^6 \text{ M}^{-1} \text{ s}^{-1}$ ),<sup>59,60</sup> it does not affect viral infectivity at concentrations used for the experiments, and its reaction with O<sub>3</sub> produces benzaldehyde with a 1:1 stoichiometry (Equation 2.1).<sup>60</sup>

Equation 2.1 Reaction of trans-cinnamic acid with ozone: stoichiometric production of benzaldehyde.



Once the reaction between  $O_3$  and CA is completed, the concentration of benzaldehyde can be used to precisely determine the initial ozone concentration. The theoretical ozone decay resulting from the reaction of ozone with CA can be modelled using three parameters: the second-order rate constant for the reaction of ozone with CA ( $k_{O3-CA}$ ), the initial  $O_3$  concentration (determined from final benzaldehyde concentration) and the initial CA concentration. The ozone decay curve is then integrated over time to determine ozone exposure.<sup>61</sup>

In this experimental approach,  $k_{O3-CA}$  is a key parameter to estimate the ozone exposure. Therefore, it is crucial to adapt  $k_{O3-CA}$  in the ozone decay model to the applied experimental conditions (pH and temperature). To obtain  $k_{O3-CA}$ , the kinetics of ozone decay in the presence of excess CA were determined under pseudo-first order conditions at different temperatures, using a Hi-Tech Scientific SF-61DX2 stopped-flow spectrometer (TGC Scientific). The experimental procedure was modified from Heeb *et al* (2017)<sup>62</sup> and details are given in the SI. Based on the resulting rate constants (Table S2, SI) the activation energy ( $E_a$ ) was determined via the Arrhenius equation (Figure S1, SI). This, in turn, allowed us to calculate  $k_{O3-CA}$  at any selected temperature (Table S3, SI).

### Batch ozonation experiments

The steps involved in obtaining a virus inactivation curve are summarized in Figure 2.1. Specifically, a series of batch reactions was run with different initial  $O_3$ :CA ratios (A), to establish different ozone exposures. After complete depletion of  $O_3$ , samples were withdrawn for benzaldehyde quantification by HPLC (see SI) to determine the ozone concentration in each reactor. Additionally, residual infective viruses were enumerated. Subsequently, the determined ozone concentration and the initial CA concentration were used to model the ozone exposure in each reactor (B). Finally, the inactivation in each reactor was evaluated as a function of the corresponding ozone exposure (C), and the inactivation rate constant ( $k_{O3-Virus}$ ) was determined from a least-squares fit to the linear portion of the following model:

Equation 2.2 Chick-Watson model for ozone disinfection

$$\ln\left(\frac{N}{N_0}\right) = -k_{O3-Virus} * \int_0^t [O_3](t) dt$$

where  $N$  and  $N_0$  are the infective virus concentrations at times  $t$  and  $0$ , respectively,  $[O_3](t)$  is the time-dependent ozone concentration, and  $\int_0^t [O_3](t) dt$  is the ozone exposure at exposure time  $t$ .

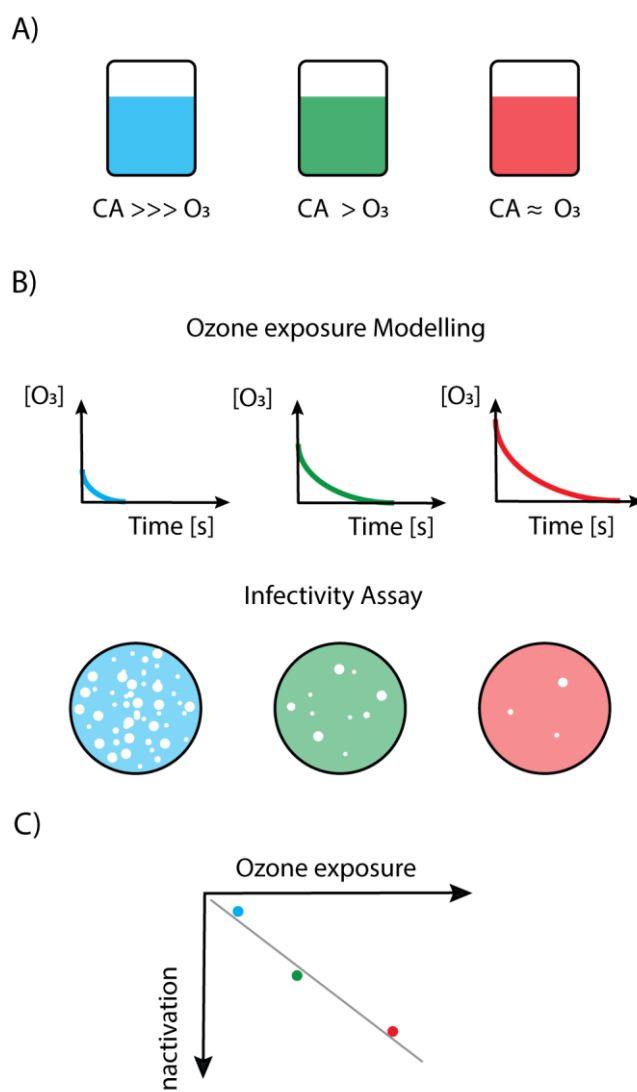


Figure 2.1 Overview over batch approach. (A) Viruses are inactivated in batch reactors with different O<sub>3</sub>: CA ratios, whereby CA is in excess. The closer the O<sub>3</sub>:CA ratio is to unity, the higher is the resulting ozone exposure. (B) Ozone decay is simulated based on the ozone concentration (determined by quantification of benzaldehyde) and initial CA concentration, and the ozone exposure in each reactor is calculated. The residual infective virus concentration in each reactor is quantified by an infectivity assay. (C) Inactivation is plotted versus the ozone exposure to obtain the inactivation rate constant, according to Equation 2.2

Experimental solutions were freshly prepared the day of the experiment with a range of CA (90-180  $\mu\text{M}$ ) in PBS. 20 mM t-BuOH was added to scavenge  $\cdot\text{OH}$  produced during ozonation, to ensure that kinetic parameters pertained to the inactivation by ozone only. Inactivation curves for all viruses were obtained at pH 6.5 and a temperature of 22°C. For MS2, additional experiments were conducted over a range of pH values (6.5-8.5) and temperatures (2-22°C) to assess the influence of these parameters on the second order ozone inactivation rate constants. Virus ozonation was performed in 50 mL glass reactors filled with the experimental solution, capped and sealed to limit ozone outgassing. Viruses were added to the reactors at concentrations of  $10^7$  - $10^9$  PFU/mL (coliphages) or  $10^5$  MPNCU/mL (human enteric viruses). An ozone stock solution was injected into the reactors to reach a concentration of 20 to 175  $\mu\text{M}$ , and the reactors were mixed (650 rpm)

for 30 s. A syringe connected to a 0.22  $\mu\text{m}$  filter (Infochroma) was simultaneously inserted to avoid overpressure during  $\text{O}_3$  injection and was removed after the injection. After 2.5 to 3 min, when  $\text{O}_3$  was completely depleted, 100  $\mu\text{L}$  aliquots were withdrawn, were diluted 10x into PBS containing 0.1  $\mu\text{M}$  EDTA (coliphages) or in culture media (human viruses), and viruses were enumerated as described above. The role of EDTA was to prevent virus inactivation by a Fenton-type reaction of  $\text{H}_2\text{O}_2$  (produced during the reaction of  $\text{O}_3$  with CA; Scheme 1) with trace metals present in PBS.<sup>63</sup> No inactivation of viruses by  $\text{H}_2\text{O}_2$  was observed if the samples were diluted in culture media.  $\text{O}_3$  decay was then modelled and integrated to determine the ozone exposure in each reactor. All experiments were conducted at least in duplicate.

In addition to viruses, the kinetics of carbamazepine (CBZ) abatement by ozone was also measured to validate the experimental system.<sup>17</sup> For these experiments, CBZ (5  $\mu\text{M}$ ) was mixed with CA (150- 170 $\mu\text{M}$ ) in PBS adjusted to pH 3, and containing 20 mM t-BuOH. The lower pH was used to increase  $\text{O}_3$  stability. CBZ concentrations were quantified by HPLC as described in the SI.

### **Quench-flow ozonation experiments**

**MS2 inactivation.** To confirm the inactivation rate constants obtained in the batch system, the inactivation of MS2 was additionally measured by quench-flow, using a procedure adapted from Czekalski *et al.* (2016). Specifically, a MS2 suspension ( $\sim 10^9$  PFU/mL) in PBS at pH 6.5 and 5 mM t-BuOH, was mixed at a 10:1 ratio with an ozone solution (500  $\mu\text{M}$ , prepared in 1mM HCl solution, kept at 4°C) in reaction loops (40  $\mu\text{L}$  and 500  $\mu\text{L}$ ) with different flow rates, to yield a range of ozone exposures (Table S2.4 SI). Ozone was quenched after defined contact times by mixing the sample at a 11:1 ratio with 100 mM CA in Nanopure water at pH  $\sim 7$ . Quenched samples were collected in a sterile syringe, and were used to quantify MS2 infectivity by plaque assay and benzaldehyde concentrations by HPLC. The residual ozone concentration and ozone exposure was determined as described previously<sup>64</sup>, and the inactivation rate constant was determined using Equation 1.

The initial MS2 concentration was measured in the same experimental setup in ozone-free samples consisting of the MS2 solution and milliQ water at a 10:1 ratio. Similarly, the experimental ozone concentration was measured at the start and end of each experiment at the shortest contact time in virus-free solutions consisting of milliQ water and an  $\text{O}_3$  solution at a 10:1 volumetric ratio. The decay of the ozone feed solution in the quench-flow system during the experiments (15-25 min) was less than 2 %.

**Second order rate constant for the reaction of CBZ with ozone.** The second order rate constant for the reaction of CBZ with ozone was also quantified by the quench-flow setup. For these measurements, the experimental solution consisted of 5  $\mu\text{M}$  CBZ and 5 mM t-BuOH in milliQ water at pH 3. The experiments were conducted as described above, except that ozone was quenched by 100 mM CA solution at a 11:2 volumetric ratio. Prior to the experiment, the starting concentration of CBZ was measured in the same experimental setup in ozone-free solutions (CBZ solution and milliQ water at a volumetric ratio of 10:1). The  $\text{O}_3$  concentrations were measured at the shortest contact time in CBZ-free experiments (milliQ water and  $\text{O}_3$  solution at a 10:1 volumetric ratio). The decay in the ozone feed solution (pH $\sim 3$ ) throughout the experiment (40-60 min) was less than 2 %. Quenched reaction mixtures were withdrawn for CBZ and benzaldehyde quantification. Details on contact times, flow rates, residual ozone concentrations and the derived ozone exposures are listed in Table S2.5.

### **2.3.5 Simulations and data analysis**

Simulations of ozone depletion were performed in R<sup>65</sup> using the packages “caTools”<sup>66</sup>, “flux”<sup>67</sup> and “desolve”<sup>68</sup>. Statistical analyses were performed in R<sup>65</sup> using the “ggplot2”<sup>69</sup> and “multcomp”<sup>70</sup> packages.

Rate constants of the different viruses were compared by ANCOVA with Tukey's post hoc test, allowing for an  $\alpha$ -type error of 5%.

## 2.4 Results and discussion

### 2.4.1 Method validation and temperature-dependence of $k_{O_3-CA}$

To validate the batch ozonation approach developed herein, it was applied to measure the kinetics of the abatement of CBZ. The obtained second order rate constant  $k_{O_3-CBZ}$  was then compared to a previous value from literature,<sup>71</sup> as well as to the value measured by the quench-flow system in this study. As summarized in Table 2.1, the  $k_{O_3-CBZ}$  values obtained in the batch and the quench-flow system were within the error statistically equivalent ( $p$ -value = 0.057). The larger error in the batch system may be explained by the fact that the ozone exposure is simulated, whereas in the quench-flow approach it is directly measured. Furthermore, the measured  $k_{O_3-CBZ}$  values were within a factor of two of the previously reported values, which is typical for such kinetic measurements. This suggests that the batch ozonation approach can accurately determine reaction kinetics with ozone.

Table 2.1. Summary of measured and reported second-order rate constants for the reaction of CBZ with ozone and corresponding statistics. The error associated with the  $k_{O_3-CBZ}$  corresponds to the standard error.

Method	$k_{O_3-CBZ}$ , [ $M^{-1}s^{-1}$ ]	Adjusted $R^2$	Condition	Reference
Batch	$(5.5 \pm 0.8) \times 10^5$	0.90	$22 \pm 2^\circ C$ $pH = 3.00 \pm 0.03$	This study
Quench-flow	$(6.1 \pm 0.1) \times 10^5$	0.99	$22 \pm 2^\circ C$ $pH = 3.00 \pm 0.03$	This study
Competition kinetics	$\sim 3 \times 10^5$	-	$20^\circ C$ $pH = 7$	Ref. 22

The batch approach generated ozone exposures ranging from approximately  $10^{-7}$  Ms ( $8 \times 10^{-5}$  mg x min  $L^{-1}$ ) to approximately  $10^{-5}$  Ms ( $8 \times 10^{-3}$  mg x min  $L^{-1}$ ). The upper end of this range is determined by the requirement that the  $O_3:CA$  ratio has to be below unity.

This batch method can be applied over a range of temperatures, as long as the ozone depletion is modelled using  $k_{O_3-CA}$  for the corresponding temperature. To this end,  $k_{O_3-CA}$  was measured at different temperatures, and an activation energy  $E_a$  of 21.2 kJ/mol was determined (see Figure 2.1 and Table S2.3, SI for details). The  $k_{O_3-CA}$  measured at  $22^\circ C$  ( $7.6 \times 10^5 M^{-1} s^{-1}$ ) corresponds well to previously reported values ( $3.8 \times 10^5$  and  $1.2 \times 10^6 M^{-1} s^{-1}$ ).<sup>59,60</sup>

In summary, the batch ozonation approach developed herein can be applied to determine kinetic parameters for ozone-sensitive substances/organisms at different temperatures. Furthermore, as the method does not require any specialized equipment, it is well suited for applications in any laboratory, including laboratories handling biohazardous materials.

## 2.5 MS2 inactivation kinetics by the batch method

### *Influence of virus solution conditions on inactivation*

An important prerequisite of the batch approach used herein is that CA be the main sink for ozone. This condition can be readily met for ozonation of chemical substances such as CBZ, which are typically available at high purity. The purity of stock solutions of viruses, in contrast, is compromised by residues from the culture media and host cells used during virus propagation. To ensure that impurities in the virus solutions do not influence ozone inactivation kinetics, three purification approaches were compared. For MS2 coliphage as the benchmark virus, we tested purification by PEG-chloroform, purification by ion exchange chromatography on a monolithic column, and absence of purification (simple filtration using a 0.45  $\mu\text{m}$  Durapore filter, Millipore). In addition, the inactivation kinetics were measured for different starting concentrations of MS2 ( $10^6$ - $10^9$  PFU/mL), as dilution can be used as a method to reduce impurities from the stock solution.

Second-order inactivation rate constant for MS2 ( $k_{\text{O}_3\text{-MS}_2}$ ) were statistically equivalent for all procedures as long as purification was applied (p-value = 0.14, Table S2.8). In contrast,  $k_{\text{O}_3\text{-MS}_2}$  decreased significantly if no purification was used (p-value =  $5.3 \times 10^{-4}$ ). In the absence of purification, the culture media constituents thus likely protected the viruses from inactivation. Furthermore, the initial MS2 concentration did not affect  $k_{\text{O}_3\text{-MS}_2}$  to a significant extent (p-value >0.05; Table S2.8).

Replicate experiments using different MS2 stock solutions purified by the PEG-chloroform method indicated that this purification procedure yielded consistent kinetic data across different viral batches (Table S2.8 and Figure S2.2, SI). Therefore, the PEG-chloroform method was used for all further virus inactivation experiments.

### *Rate constant for the inactivation of MS2 by ozone*

Based on multiple replicate batch experiments, a  $k_{\text{O}_3\text{-MS}_2}$  of  $(1.9 \pm 0.1) \times 10^6 \text{ M}^{-1} \text{ s}^{-1}$  was determined at pH 6.5 and 22 °C. Under the same experimental conditions, quench-flow determination of  $k_{\text{O}_3\text{-MS}_2}$  yielded a value of  $(1.0 \pm 0.1) \times 10^7 \text{ M}^{-1} \text{ s}^{-1}$  (Figure S2.2). This difference of about a factor of 5 in measured  $k_{\text{O}_3\text{-MS}_2}$  values approximately corresponds to that of reported second-order rate constants for the abatement of organic substances by ozone in different studies (e.g., reported values of  $k_{\text{O}_3\text{-CA}}$  vary by a factor of 3 between measurements by quench-flow<sup>59</sup> and by competition kinetics<sup>60</sup>). The greater  $k_{\text{O}_3\text{-MS}_2}$  obtained in the quench-flow system may be explained by the differences in the experimental procedures. First, mixing may be less efficient in the batch experiments, which are conducted in greater volumes. Second, the ozone exposures in batch experiments are simulated not measured, which may introduce an error in the resulting  $k_{\text{O}_3\text{-MS}_2}$ . However, despite the difference in the absolute values, both methods confirm the very high susceptibility of MS2 to ozone. Furthermore, the discrepancies in  $k_{\text{O}_3\text{-MS}_2}$  values observed herein are minor compared to the vast differences in ozone susceptibilities for the same virus in different studies (see introduction).

### *Effects of temperature and pH*

To investigate temperature- and pH-dependence of virus inactivation by ozone, MS2 inactivation was investigated over a pH range of 6.5-8.5 and temperature range of 2 – 22°C, roughly characteristic of water and wastewater treatment (Figure 2.2).



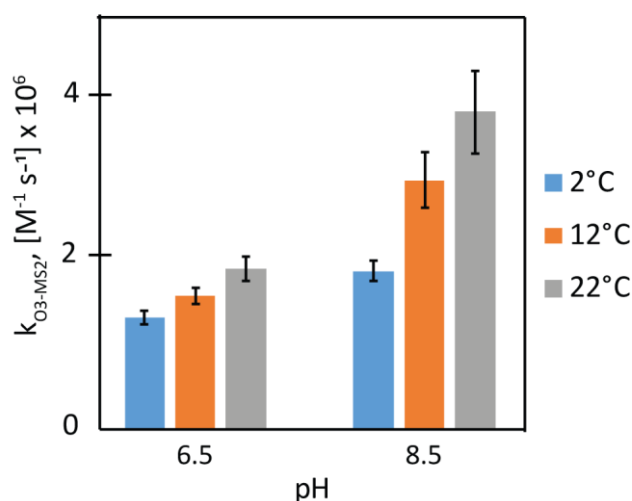


Figure 2.2 Second-order rate constants  $k_{O_3-MS2}$  for the inactivation of MS2 with ozone at different temperature (2, 12 and 22°C) and pH (6.5 and 8.5) conditions.

Increases in temperature and pH both accelerated inactivation, though the effects were minor (see Table S2.9). Specifically, an increase in pH from 6.5 to 8.5 enhanced  $k_{O_3-MS2}$  by a factor 1.4 (2°C) to 2 (22°C), whereas a temperature shift by 10°C resulted in a 1.2 (pH 6.5) to 1.4 (pH 8.5)-fold increase in  $k_{O_3-MS2}$ . This temperature dependence of  $k_{O_3-MS2}$  indicated an activation energy of MS2 inactivation by ozone of 12.2 to 23.4 kJ/mol at pH 6.5 and pH 8.5, respectively (see Table S2.10 and Figure S2.4, SI). These values correspond well to that previously reported by Roy *et al.* (1981) of 15 kJ/mol.<sup>72</sup> Similarly low activation energies for the reaction with ozone are also encountered for highly reactive organic compounds (e.g., the  $E_a$  for the reaction of CA with ozone determined herein corresponds to 21.2 kJ/mol). Such low temperature dependence of the reaction indicates that reaction rate constants are close to the upper end of ozone reactions. In contrast, the  $E_a$  for the reaction of ozone with *C. parvum*, a more ozone-resistant pathogen, is significantly higher (51.7 kJ/mol).<sup>73</sup> Due to the rather modest effect of temperature and pH, additional viruses were only tested at a single temperature and pH condition (pH 6.5 and 22°C). The somewhat lower pH compared to that encountered in wastewater was chosen to increase ozone stability throughout the experiment, and thus reduce a source of variability. Given its low pH dependence, however,  $k_{O_3-virus}$  measured at pH 6.5 is still representative of water and wastewater treatment conditions.

### 2.5.1 Inactivation of other viruses by ozone

After validation of the batch method and optimization of the experimental parameters using MS2, the batch method was applied to eight additional bacteriophages and enteric viruses. Representative inactivation curves are shown in Figure 2.3, and the resulting second order inactivation rate constants ( $k_{O_3-virus}$ ) are summarized in Table 2.2.

The investigated viruses spanned a range of genome types (CV, EV, MS2 and Q $\beta$ : single-stranded RNA;  $\phi$ X174: single-stranded DNA; HAdV and T4: double-stranded DNA) and lengths, as well as different protein contents and capsid configurations. Despite this diversity, all second-order inactivation rate constants were of similar magnitude, spanning a range from  $4.5 \times 10^5$  to  $3.3 \times 10^6 \text{ M}^{-1}\text{s}^{-1}$  (Table 2.2). These high rate constants confirm the high ozone efficiency for virus inactivation. Nevertheless, minor yet statistically significant differences were observed among the ozone reactivities of the different viruses. Interestingly, the biggest differences

were found among closely related viruses. For example, one of the most susceptible (CEnv2) and the most resistant viruses (CEnv1 and CVF) are representatives of the same virus strain (coxsackievirus B5). Similarly, MS2 was more resistant than its closely related counterpart Q $\beta$ . The causes underlying these differences are currently not understood and are the subject of ongoing investigations.

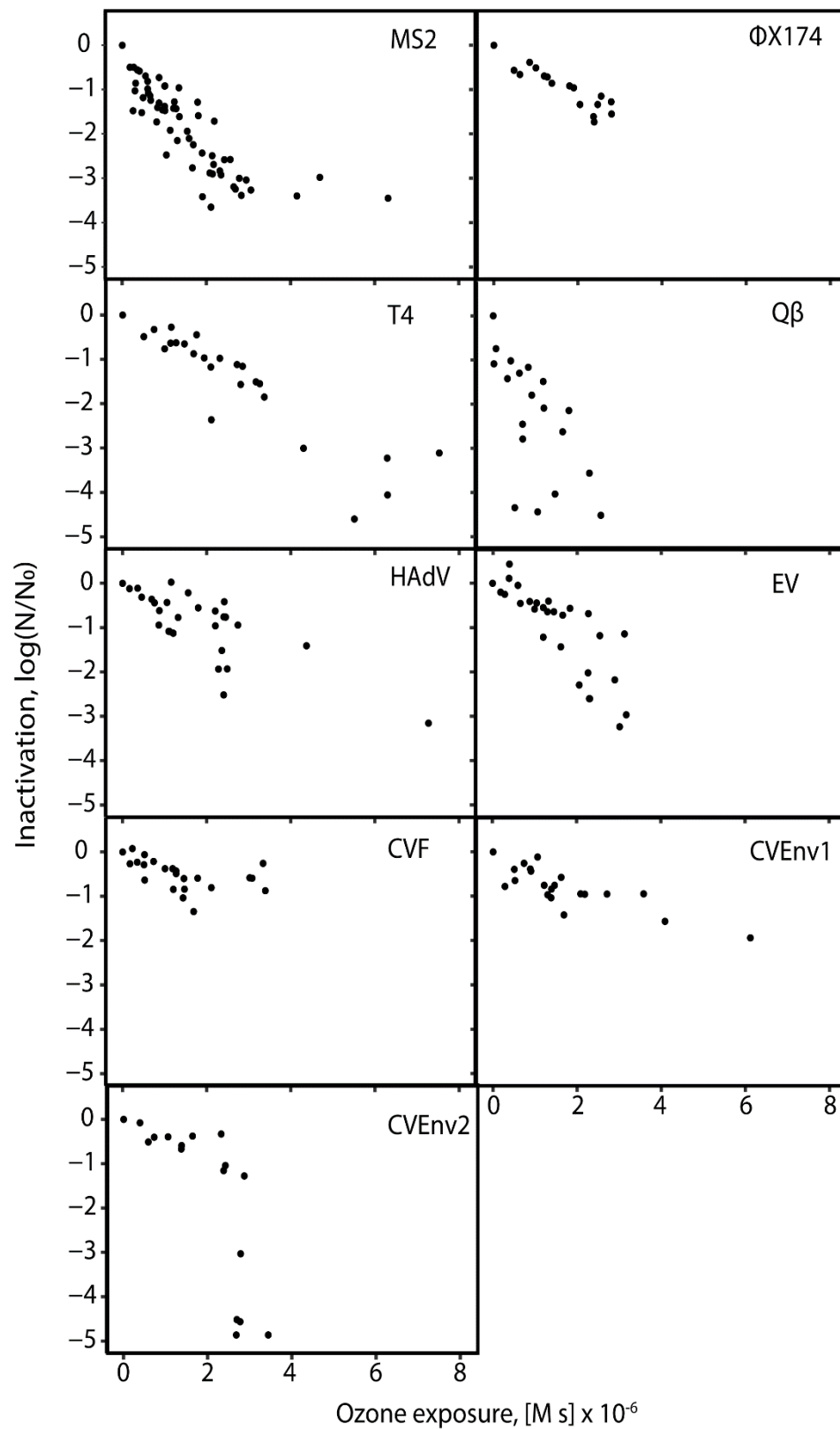


Figure 2.3. Log inactivation of all selected viruses as a function of the ozone exposure (22°C, pH = 6.5). Each panel contains data from at least two independent experiments.

Table 2.2 Second-order rate constants for the inactivation of the selected viruses by ozone ( $k_{O_3\text{-virus}}$ ), with corresponding standard errors and adjusted  $R^2$ .

Viruses	$k_{O_3\text{-virus}}, [M^{-1} s^{-1}]$	$R^2$
MS2	$(1.9 \pm 0.2) \times 10^6$	0.73
Q $\beta$	$(3.3 \pm 0.7) \times 10^6$	0.50
$\Phi$ X174	$(1.2 \pm 0.1) \times 10^6$	0.86
T4	$(1.3 \pm 0.1) \times 10^6$	0.83
HAdV	$(9.0 \pm 1.2) \times 10^5$	0.63
EV	$(1.9 \pm 0.2) \times 10^6$	0.69
CVF	$(4.4 \pm 1.4) \times 10^5$	0.27
CVE <sub>env</sub> 1	$(4.9 \pm 0.7) \times 10^5$	0.66
CVE <sub>env</sub> 2	$(2.5 \pm 0.6) \times 10^6$	0.56

Interestingly, the ozone reactivities of the viruses tested herein exhibited a similar trend as observed by Sigmon *et al.* (2015), namely MS2>EV>T4>HAdV  $\approx$   $\phi$ X174>CVF. Higher stability of CVF compared to other enteric viruses tested was also observed for disinfection by free chlorine, whereas this trend did not apply to disinfection by chloramine (Table 2.3).

Table 2.3 Required oxidant exposures to inactivate, EV, HAdV and CVF by 2 log<sub>10</sub>. Ct values for ozone were determined in this study (Table S10). Ct values for free chlorine and chloramine were determined by Cromeans *et al.* (2010) in buffer at pH 7 and 5 °C<sup>74</sup>

Virus	Ozone, [Ms] / [mg min L <sup>-1</sup> ]	Free chlorine [Ms] / [mg min L <sup>-1</sup> ]	Chloramine [Ms] / [mg min L <sup>-1</sup> ]
EV	$\sim 2.4 \times 10^{-6} / 1.9 \times 10^{-3}$	$\sim 7.8 \times 10^{-4} / 0.7$	$\sim 1.1 / 940$
HAdV	$\sim 5.1 \times 10^{-6} / 4.1 \times 10^{-3}$	$\sim 3.4 \times 10^{-5} / 0.3$	$\sim 0.9 / 795$
CVF	$\sim 1.0 \times 10^{-5} / 8.0 \times 10^{-3}$	$\sim 4.75 \times 10^{-3} / 4.2$	$\sim 0.7 / 590$

Finally, the high  $k_{O_3\text{-virus}}$  determined in this study imply that hydroxyl radicals ( $\bullet$ OH), which are typically produced during ozonation, do not significantly contribute to the inactivation of viruses of water and wastewater. The ratio of the  $\bullet$ OH to the O<sub>3</sub> exposures ( $R_{ct}$ )<sup>22</sup> typically corresponds to  $\sim 10^{-6}$  to  $10^{-8}$  during lake water and wastewater ozonation, respectively.<sup>18</sup> This implies that in order for  $\bullet$ OH to play a significant role in inactivation, its reactivity toward viruses would have to exceed that toward ozone by a factor of  $10^6$  to  $10^8$ . However, rate constants for  $\bullet$ OH previously measured in our laboratory correspond to  $7.0 \times 10^9 \text{ M}^{-1} \text{ s}^{-1}$  for MS2,  $4.0 \times 10^9 \text{ M}^{-1} \text{ s}^{-1}$  for HAdV and  $1.7 \times 10^9 \text{ M}^{-1} \text{ s}^{-1}$  for  $\phi$ X174,<sup>75</sup> whereas those for inactivation by ozone were only 3-4 orders of magnitude lower (Table 2.2). The contribution of hydroxyl radicals to inactivation during ozonation can thus be considered negligible.

## 2.5.2 Estimation of extent of virus inactivation during wastewater ozonation

As highlighted above, inactivation of viruses by ozone differ both between and within different virus serotypes and families. However, these differences may not be relevant in the context of water and wastewater

treatment, as the applied ozone exposures are generally large and the inactivation of viruses by ozone is efficient. Based on the  $k_{O_3\text{-virus}}$  determined herein, we estimated inactivation for specific ozone doses from 0.25-1 mg  $O_3$ /mg dissolved DOC. Based on previously determined relationships between specific ozone doses and ozone exposures in secondary wastewater effluent, the corresponding ozone exposure during wastewater treatment can be estimated as  $6 \times 10^{-6}$  to  $8 \times 10^{-3}$  Ms,<sup>42</sup> which is in the upper range or above the ozone exposures applied in this study ( $10^{-7}$  –  $10^{-5}$  Ms). Figure 2.4 shows the calculated extent inactivation of CVF (most resistant human virus studied; Table 2.2) and MS2 in a wastewater as a function of the specific ozone dose. At the lowest specific ozone dose of 0.25 mg  $O_3$ /mg DOC, the inactivation of CVF is minor, whereas MS2 exceeds 4 log<sub>10</sub> inactivation. This example illustrates that viruses may escape inactivation if low specific ozone doses are applied to wastewater. Furthermore, it indicates that at low specific ozone doses, MS2 may not be a good surrogate for enteric viruses. At specific ozone doses  $\geq 0.3$  mg  $O_3$ /mg DOC, both viruses are estimated to be inactivated by  $\geq 9$  log<sub>10</sub> (Figure 2.4). Typical specific ozone doses for enhanced wastewater treatment for micropollutant abatement with ozone are in the order of 0.5-0.6 mg  $O_3$ /mg DOC.<sup>41,76,77</sup> Under such conditions, an efficient inactivation of viruses can be expected. We caution, however, that these estimates are based on inactivation rate constants derived from the linear regression of the inactivation curves shown in Figure 2.3. The linear relationship between ozone exposure and inactivation may break down at higher exposures, as some studies have reported tailing inactivation curves.<sup>78</sup> Furthermore, a recent study has shown that flocs present in wastewater effluent can protect microorganisms from inactivation by ozone,<sup>64</sup> and this factor remains to be tested for viruses. Overall, ozone thus has a high potential as a wastewater disinfectant for viruses, but this potential should be confirmed during ozonation in real wastewater systems. This is done in Chapter 3.

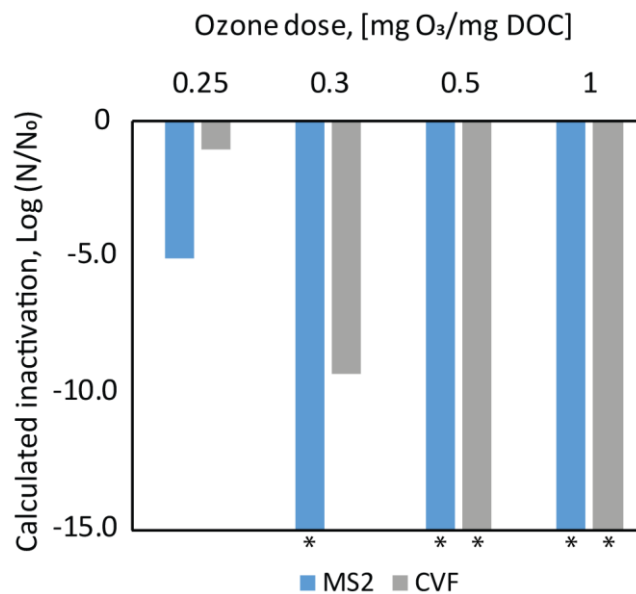


Figure 2.4 Calculated inactivation of MS2 and CVF by ozone in wastewater as a function of the specific ozone dose

## 2.6 ACKNOWLEDGMENTS

This study was funded by the Swiss National Science Foundation (Grant 205321\_169615). Elisabeth Salhi, Virginie Bachmann, Ursula Schönenberger, and Caroline Gachet Aquillon are acknowledged for help in the laboratory, and Michèle Heeb is acknowledged for assistance with the stopped-flow experiments.

# Chapter 3 Inactivation of Waterborne Viruses by Ozone in Natural Matrices: Proxies for viral inactivation

The author of this thesis, Camille Wolf, developed the experimental methods, performed the majority of experiments, analyzed the data and wrote the paper (to be submitted). Most ozone decay batch experiments and ~80% of the experiment measuring and  $\Delta UV_{254}$  were conducted by Annalisa Pavese.

## 3.1 Introduction

Human viruses are present in raw sewage at concentrations of  $10^6$  to  $10^7$  virus particles/L.<sup>79</sup> If discharged into the environment in an infective state, they can cause health risks to recreational water users, or consumers of drinking water, if these waters are used as water resources. The removal and/or inactivation of viruses during water and wastewater treatment is thus an important measure to prevent waterborne diseases. A particularly critical case is potable water reuse, where guidelines aim for 9.5 (Australia) to 12 log<sub>10</sub> (California, USA) enteric virus removal as performance target for a complete treatment train.<sup>80</sup>

A promising approach to strongly reduce infective virus concentrations is ozonation. Ozone is a powerful oxidant that has a long tradition in treatment trains for drinking water<sup>81</sup>, and is increasingly implemented for wastewater<sup>82</sup> and potable water reuse throughout the world.<sup>16</sup> In Chapter 2, we determined the inactivation kinetics of a suite of human enteric viruses and bacteriophages by ozone in well-controlled buffered solutions, and inactivation rate constants ( $k_{O_3-Virus}$ ) on the order of  $10^6 \text{ M}^{-1}\text{s}^{-1}$  were determined as a function of the ozone exposure<sup>83</sup>, according to Equation 2.2. However, in natural water or wastewater, virus inactivation remains difficult to predict. First, inactivation kinetics may be mitigated by different matrix constituents,<sup>14</sup> resulting in lower values of  $k_{O_3-Virus}$ . Second, the extent of virus inactivation is a function of ozone exposure, and this parameter is difficult to measure or estimate in real-time during treatment, due to the high ozone demand of many wastewater or raw drinking water matrices.<sup>18</sup> To overcome this problem, relationships between the ozone exposure and the specific ozone dose (mgO<sub>3</sub>/mgDOC) have been established<sup>42</sup>, and can be invoked to estimate the ozone exposure in a given water matrix. However, these relationships differ between different water matrices, and are time-consuming and experimentally challenging to establish. Overall, knowledge of the specific ozone dose is not a sufficient parameter to estimate virus inactivation in water or wastewater treatment.

Alternatively, inactivation may be monitored based on an “easy-to-measure” proxy. Proxies are an indirect measure of the ozone exposure, and can be used as surrogate parameters to predict virus inactivation. Buffle *et al.* (2006) demonstrated that during ozonation of wastewater, the UV absorbance at 254 nm of the matrix decreases ( $\Delta UV_{254}$ , details in Equation 3.1) as a function of the specific ozone dose, which in turn determines the ozone exposure.<sup>19</sup> Gerrity *et al.* (2012) and Carvajal *et al.* (2017) measured the abatement of micropollutants and/or the inactivation of fecal indicator organisms, which also depend on the ozone exposure, in function of  $\Delta UV_{254}$ . They then established correlations between  $\Delta UV_{254}$  and micropollutant abatement as well as

the inactivation of the indicator organisms.<sup>43,84</sup> This allowed them to estimate the abatement of these chemical and biological pollutants based solely on the measurement of  $\Delta UV_{254}$ , without the need to determine the ozone exposure.

Equation 3.1 Definition of  $\Delta UV_{254}$  proxy

$$\Delta UV_{254} = 1 - \left( \frac{[UV_{254}]}{[UV_{254}]_0} \right)$$

In this study, we explore if  $\Delta UV_{254}$  can be used as a proxy for virus inactivation. Additionally, we investigate if micropollutants with similar ozone reactivity as viruses may serve as alternative proxies. We investigate micropollutants as an additional proxy, because in Switzerland their abatement in wastewater is regularly monitored in the framework of the Swiss water protection act, a new regulation aiming to reduce discharge of micropollutant in the environment.<sup>11</sup> This is achieved by monitoring a suite of indicator compounds, among them carbamazepine (CBZ), which has a similar ozone reactivity as viruses ( $5.5 \times 10^5 \text{ M}^{-1} \text{ s}^{-1}$ ).<sup>83</sup> Therefore, CBZ was chosen as second proxy for virus inactivation in this study.

The objectives of this study were (1) to investigate the influence of natural matrices on  $k_{O3-Virus}$ , (2) to evaluate potential proxies ( $\Delta UV_{254}$  or CBZ abatement) for virus inactivation during ozonation of environmental matrices, and (3) to validate these proxies for virus inactivation in a pilot scale ozonation reactor. As model organisms we used MS2 coliphage and an environmental strain of coxsackievirus B5 (CVB5). These viruses were selected because they exhibited significant differences in  $k_{O3-Virus}$  in buffered solutions, and thus spanned a range of possible inactivation kinetics.<sup>83</sup> Furthermore, MS2 inactivation has previously been correlated to  $\Delta UV_{254}$  by *Gerrity et al.*, which will enabled a comparison with results of this study.

## 3.2 Materials and Methods

### 3.2.1 Chemicals and solutions

Sodium chloride (NaCl), sodium monophosphate ( $\text{NaH}_2\text{PO}_4$ ) and sodium di-phosphate ( $\text{Na}_2\text{HPO}_4$ ) were purchased from Acros. Ortho-phosphoric acid ( $\text{H}_3\text{PO}_4$ ) was purchased from Fluka. Carbamazepine ( $\text{C}_{15}\text{H}_{12}\text{N}_2\text{O}$ ), benzaldehyde ( $\text{C}_7\text{H}_6\text{O}$ ) and 1 M HCl were purchased from Sigma-Aldrich. HPLC grade solvents were purchased from Biosolve chimie SARL. Indigo trisulfonate was purchased from (Sigma).

### 3.2.2 Phages and bacteria

Coliphages MS2 (DSMZ 13767) and its host *Escherichia coli* (DSMZ 5695) were purchased from the German Collection of Microorganisms and Cell Cultures (DSMZ, Braunschweig, Germany). MS2 phages were propagated and purified by PEG purification, except for Pilot experiment where MS2 stocks was directly diluted. The phages were enumerated using double agar layer plaque assay, as described previously.<sup>55</sup>

### 3.2.3 Virus propagation, purification and enumeration

An environmental strain of the human enteric coxsackievirus B5 (CVB5) was isolated from the Vidy wastewater treatment plant (Lausanne, Switzerland), as described elsewhere.<sup>85</sup> CVB5 was propagated on buffalo green monkey kidney (BGMK) cells. BGMK cells were cultivated in minimum essential medium (MEM; Invitrogen), was supplemented with penicillin ( $20 \text{ U mL}^{-1}$ ; Invitrogen), streptomycin ( $20 \mu\text{g mL}^{-1}$ ; Invitrogen), and 2 or 10% fetal bovine serum (FBS; Invitrogen), and cells were incubated at  $37^\circ\text{C}$  in 5%  $\text{CO}_2$  and 95%



humidity. Viruses were purified using a polyethylene glycol (PEG)-chloroform method, as described previously.<sup>55</sup> Virus stock solutions were stored in phosphate buffered saline (PBS; 5 mM NaH<sub>2</sub>PO<sub>4</sub>, 10 mM NaCl, pH=7.5) at 4°C. Phages were enumerated by the double-agar-layer method as described previously<sup>55</sup> and infective phage concentrations are expressed in plaque forming units (PFU)/mL. Enteric viruses were enumerated by the most probable number (MPN) assay as detailed elsewhere,<sup>86</sup> and concentrations are expressed as most probable number of cytopathic units (MPNCU)/mL.

### 3.2.4 Water matrices

Virus ozonation was studied in two surface waters (SW) that serve as drinking water sources, and in a secondary wastewater (WW) effluent. Surface waters were obtained from Lake Geneva (SWG; St-Sulpice) and Lac de Bret (SWB; Puidoux, Switzerland) and were collected at the intake of the drinking water treatment plants. Secondary wastewater effluent (WW) was obtained from the wastewater treatment plant in Dübendorf, Switzerland. The dissolved organic carbon (DOC) concentrations of SWG, SWB and WW were 1.2, 5.2 and 6.2 mg/L, respectively. The water samples (~30 L) were filtered through a 0.45µm filter (PES, Merck Millipore Ltd.) and stored at 4°C in dark until used. Further details pertaining to the composition of the three water matrices are provided in the Table 3.1. DOC was measured by catalytic combustion at 720 °C, followed by IR detection of CO<sub>2</sub> (Shimadzu TOC-L CSH), alkalinity by titration with HCl (0.1 mol/L) (Metrohm 809 Titrando), respectively. For NO<sub>2</sub><sup>-</sup>, a spectrophotometric determination of nitrite-nitrogen after the reaction to a reddish azo-dye (Griess-reaction) was used.

Table 3.1 Water quality parameters of real water samples

Water	DOC, [mgC/L]	NO <sub>2</sub> <sup>-</sup> , [µgN/L]	Alkalinity, [mmol/L]	pH
<b>SWG</b>	1.2	< 1.0	1.77	8.2
<b>SWB</b>	5.2	10.8	3.6	8.2
<b>WW</b>	6.2	172.7	6.3	8.2

### 3.2.5 Ozone production

An ozone generator (Innovatec; model CMG 3-3/CMG 3-5, Rheinbach, Germany) was used to generate ozone gas from pure oxygen (99.999%, Carbagaz). The resulting ozone/oxygen mixture was bubbled through Nanopure (Barnstead Nanopure, Thermofisher) or MilliQ (Millipore) ice cooled water.<sup>61</sup> Concentration of ozone stock solutions ranged from 0.8 to 1.25 mM as determined by direct spectrophotometry with a molar absorption coefficient for ozone of  $\epsilon_{260} = 3200 \text{ M}^{-1} \text{ cm}^{-1}$ .<sup>87</sup>

### 3.2.6 O<sub>3</sub> exposure measurements

Ozone exposures in SWB and WW were determined as a function of the specific ozone dose. Specifically, ozone depletion profiles were measured in SWB and WW for a range of specific ozone doses (0.01-0.9 and 0.04-1.5 mgO<sub>3</sub>/mgDOC, respectively). The integration of the ozone depletion profile over time yielded the ozone exposure.<sup>61</sup> Depletion profiles for low specific ozone doses were measured by quench-flow as described below. For higher specific ozone doses, the initial part of the depletion profile (up to 0.5 mgO<sub>3</sub>/mgDOC) were measured by quench-flow and the later parts by the indigo blue method described below. The measured O<sub>3</sub> depletion profiles are shown in the SI. Because of the low DOC content of SWG, the applied ozone doses to achieve the desired range of specific O<sub>3</sub> doses were very low, and O<sub>3</sub> depletion profiles

were difficult to measure accurately. Therefore, the dependence of the ozone exposure on the specific ozone dose was not assessed for SWG.

*Measurement of ozone depletion profiles by quench-flow.*  $O_3$  was spiked into water matrices at different specific ozone doses ranging from 0.01 to 0.6 and from 0.04 to 0.6  $mgO_3/mgDOC$  for SWB and WW, respectively. Ozone was quenched after defined contact times by mixing the sample at a 10:1 ratio with 100 mM cinnamic acid (CA) in Nanopure water at pH  $\sim 7$ . Quenched samples were collected in a sterile syringe, and were used to determine benzaldehyde concentrations by HPLC (details in SI), as described previously.<sup>83</sup> Benzaldehyde is produced from the reaction of CA with ozone in a 1:1 stoichiometry, and its concentration in the quenched sample therefore corresponds to the residual ozone concentration. For each specific ozone dose, the residual ozone concentration was measured at different time points to establish an ozone depletion curve versus time. Ozone exposures were calculated using the *auc()* function (“catTools”)<sup>66</sup> in R<sup>65</sup>. Decay in the ozone feed solution over the course of the experiment was in the range of 1-5 %.

*Measurement of ozone depletion profiles in a batch system.*  $O_3$  was spiked into 500 ml Schott bottles with a dispenser to achieve specific ozone doses from 0.25 to 0.86 for SWB and 0.75 to 1.5  $mgO_3/mgDOC$  for WW. Samples were withdrawn periodically from 30 s to 60 min and were added to an indigo quenching solution (0.1-1 mM).<sup>88</sup> For shorter time ranges (5 to 15 s), smaller reactors (10 mL) were used and the Indigo solution was added directly and under constant mixing (650rpm) into the vials to quench the residual ozone. The difference in absorbance at 600 nm ( $\Delta UV_{600}$ ) was used to determine the residual  $O_3$  concentration as described previously.<sup>58</sup>

### 3.2.7 Inactivation experiments

*Batch experiments.* The inactivations of MS2 and CVB5 in the three matrices tested were measured in 50 mL or 100 mL glass batch reactors. MS2 or CVB5 were spiked to 400-500 mL of the water matrix under consideration at room temperature ( $22 \pm 2^\circ C$ ) to yield initial concentrations of  $\sim 10^{8-9}$  PFU/mL for MS2 and  $\sim 10^{4-6}$  MPNCU/mL for CVB5, respectively. Ozone was then added to reach specific ozone doses ranging from 0.01-0.25  $mgO_3/mgDOC$  for SWG, 0.01 to 0.58  $mgO_3/mgDOC$  for SWB and 0.04 to 1  $mgO_3/mgDOC$  for WW. Upon addition of ozone, the reactors were mixed for 30 s, and were then kept at room temperature without further stirring until complete depletion of  $O_3$  (1 h). After one hour, aliquots were withdrawn and the concentrations of residual infective viruses were determined.

### 3.2.8 Experiments with proxies

To test their potential as a proxies, the abatement of carbamazepine (CBZ) and the change in  $UV_{254}$  absorbance in the high DOC matrices (SWB and WW) were measured in the same experimental reactors as the inactivation of viruses. CBZ was spiked into a subset of batch reactors at concentration between 0.67-0.9 and 0.88-1.02  $\mu M$  in SWB and WW, respectively. These CBZ concentrations did not affect the  $UV_{254}$  absorbance of the matrix and did not alter the ozone exposure for the applied specific ozone doses. The CBZ concentration and  $UV_{254}$  in each reactor before the addition of  $O_3$  and after complete  $O_3$  consumption were measured by HPLC-UV and spectrophotometry, respectively, as detailed in the Supporting Information, S3.2-3.3.

To investigate the use of CBZ as proxy for virus inactivation in SWG, a lower concentration of CBZ (0.04  $\mu M$ ) was used to prevent an increase in the ozone demand of the water. After the experiment, the remaining CBZ was quantified by online solid phase extraction followed by ultra-performance liquid chromatography and tandem mass spectrometry (UPLC-MS/MS; Xevo TQ MS, Waters). Samples were diluted 1:1 with acidified

Evian water (pH ~2.5) and deuterated CBZ compounds were spiked in every sample as internal standards. The analytical method was adapted from previous work,<sup>89–91</sup> and details are found in Supportive information S3.2. CBZ concentrations were calculated based on calibration curves using all 8 calibration points for high concentration and only the 5 lowest standard for low concentration. Correlation coefficients for the calibration curves were typically >0.990. The analytical limit of quantification (LOQ) was defined as the concentration of the lowest standard with a signal-to-noise ratio > 10 and equal to 1.2 ng/l. The result of the blank, containing only internal standard in Evian water, was subtracted from every standards and samples if its signal-to-noise ratio was higher than 10, prior to standard curves and samples concentration determination. The uncertainty associated with the sample concentrations, calculated as the relative standard deviation, was <30% for the large majority of the compounds<sup>90</sup>.  $\Delta UV_{254}$  was measured using a 10 cm quartz cuvette. A summary of the type of experiment realized and virus specie used for each water matrix is presented in Table S3.2, SI.

### 3.2.9 Pilot experiment

The potential of the CBZ abatement  $\Delta UV_{254}$  as proxies was validated in a pilot-scale ozonation reactor operated at the Lengg water treatment plant (Zürich, Switzerland). The detailed setup of the pilot plant is described elsewhere.<sup>92</sup> Briefly, Lake Zürich water (DOC=1.4 and 1.6 mg/L) was treated in an ozone reactor with a 2 m<sup>3</sup> volume on two consecutive days. The reactor was operated at a flow rate of 10 m<sup>3</sup>/h, and two ozone concentrations (0.3 mgO<sub>3</sub>/L or 0.8 mgO<sub>3</sub>/L), resulting in specific ozone doses of 0.2 or 0.5 mgO<sub>3</sub>/mgDOC (Table S3.10). Water samples (100 mL) were taken prior to ozone addition, immediately after ozone addition, at four points along the ozone reactor, as well as at the reactor effluent. Residual ozone was quenched using 1 mL of 1.5 M sodium thiosulfate (Sigma) (for proxy and MS2 analysis) or by an indigo solution (to quantify ozone).<sup>58</sup> An unquenched effluent sample was used to measure  $UV_{254}$  absorbance after complete ozone depletion.

The O<sub>3</sub> exposure in the plug-flow system (previously characterized)<sup>93</sup> was determined based on the retention time<sup>92</sup> and the measured O<sub>3</sub> concentration at each sampling point. CBZ abatement was quantified using solid phase extraction, followed by UPLC-MS as described elsewhere.<sup>94</sup>  $\Delta UV_{254}$  was measure as previously described. Prior to MS2 enumeration, the samples were preconcentrated 50-fold using a 100 kD Amicon filter (Millipore).

### 3.2.10 Data analysis

Data analysis was performed in R<sup>65</sup>. A R function was construct to compute automatically the ozone exposure from ozone concentration measured in function of the time for each specific ozone dose, this function requires the packages “caTools”<sup>66</sup>, “flux”<sup>67</sup>. The “ggplot2”<sup>69</sup> and “ggmcmc”<sup>95</sup> packages were used to construct graphics. A frequentist linear regression in R was used to fit ozone exposure-specific ozone dose relationship (Equation 3.2). Bayesian model selection (BMA)<sup>96</sup> was performed using the BAS package.<sup>97</sup>

Bayesian analysis were performed using the “runjags”<sup>98</sup> package which interfaces with the Jags<sup>99</sup> software, using Markov chain Monte Carlo (MCMC) sampling. Censored inactivation data and detection limits were incorporated in the analysis formulated with Jags as described elsewhere.<sup>100</sup> Detection limits were set according to the maximum log<sub>10</sub> inactivation measurable for each experiment independently. Parameter estimates were assumed to be normally distributed, and prior knowledge of the mean value and standard deviation of these distributions were included. These priors originate from previously published literature.<sup>44,84</sup>

When no prior knowledge was available, a non-informative normal prior or flat prior were used for the mean, and a uniform flat prior for the standard deviation. The model structure is presented in a detailed script in Text S3.5, SI. The number of simulations was set to  $10^5$ , of which the first  $10^4$  were considered as the burn-in. Visual inspection of traceplots, plots and Geweke's diagnostics confirmed convergence of chains. Diagnostics plots were constructed using the “*ggmcmc*”<sup>95</sup> and “*coda*”<sup>101</sup> packages (data not shown).

### 3.3 Results and Discussion

#### 3.3.1 O<sub>3</sub> depletion profiles and exposures

The ozone exposure as a function of the specific ozone dose is shown in Figure 3.1 for SWB and WW. The ozone depletion curves for the different specific ozone doses are shown in the SI (Figure S3.1 and Figure S3.2). The resulting ozone exposure ranged from  $10^{-7}$  to  $10^{-2}$  Ms. The ozone demand in WW was higher than in SWB water for same ozone dose. Consequently, the ozone exposure was higher in SWB than in WW for similar specific ozone doses in the range tested.

The relationship between specific ozone dose and resulting ozone exposure, has been log-linearised and was fitted using the following function:

Equation 3.2 Model used to fit the O<sub>3</sub> exposure and specific O<sub>3</sub> dose

$$\ln(O_3 \text{ exposure}) = a * \ln(\text{specific } O_3 \text{ dose}) + b$$

The modeled parameters a and b (Equation 3.2) are  $-3.4 \pm 0.4$  and  $2.9 \pm 0.2$  in SWB and  $-4.7 \pm 0.4$  and  $3.7 \pm 0.2$  in WW, respectively (for model fits, see SI, Figure S3.4 and Table S3.3). Using these models, the ozone

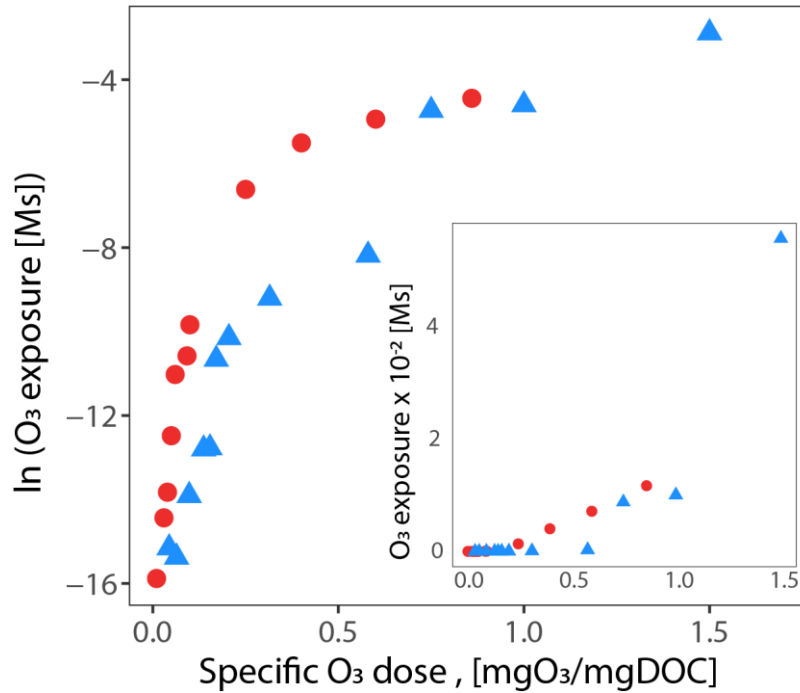


Figure 3.1 Natural logarithm of the measured O<sub>3</sub> exposure in function of the specific ozone or SWB (red circles) and WW (blue triangles). The inset shows the O<sub>3</sub> exposure on a linear scale.

exposure could be estimated for any specific ozone dose applied in subsequent inactivation experiments in SWB or WW.

### 3.3.2 Virus inactivation as a function of ozone exposure

In Figure 3.2, the inactivation of MS2 and CVB5 in SWB and WW is shown as a function of the ozone exposure, estimated based on Equation 3.2. The inactivation curve exhibited a rapid initial decrease in infective virus concentrations at low exposures, followed by a pronounced tail. Viruses (MS2 and CVB5) were detectable up to an exposure of  $1.15 \times 10^{-5}$  and  $1.14 \times 10^{-3}$  Ms in SWB, respectively, compared to  $2.3 \times 10^{-3}$  to  $8.75 \times 10^{-3}$  Ms in WW. Beyond these exposures, the inactivation exceeded the measurable inactivation range of  $9 \log_{10}$  for MS2 and  $5 \log_{10}$  for CVB5. Inactivation was generally lower in WW than in SWB for similar exposures, indicating that matrix constituents in wastewater have a protective effect on the virus.

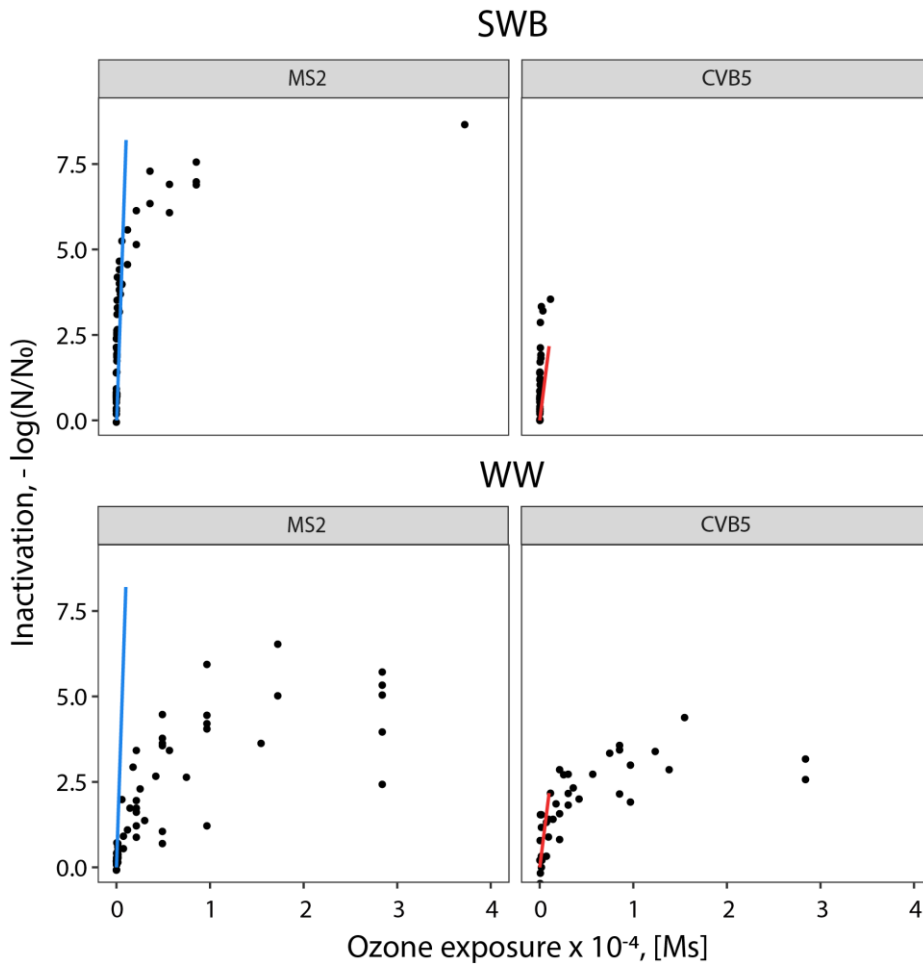


Figure 3.2 Inactivation of MS2 and CVB5 in SWB and WW as function of the ozone exposure computed based on equation 3.2. Solid lines represent the expected inactivation computed based on equation 2.1, using  $k_{O_3\text{-virus}}$  values of MS2 and CVB5 determined in buffer (Wolf et al., 2018).

The blue and red lines in Figure 3.2 show the extent of inactivation predicted according to Equation 2.2, using

inactivation rate constants ( $k_{O3-MS2} = 8.2 \times 10^5 \text{ M}^{-1}\text{s}^{-1}$ ;  $k_{O3-CVB5} = 2.2 \times 10^5 \text{ M}^{-1}\text{s}^{-1}$ ) measured in homogeneous buffer solutions.<sup>83</sup> In these buffer solutions, the observed exposures ranged up to  $1 \times 10^{-5} \text{ Ms}$ , which corresponds to an inactivation up to 8.2 or 2.2  $\log_{10}$  for MS2 and CVB5, respectively. For CVB5, this prediction corresponds reasonably well to the observed inactivation in SWB and WW. In contrast, MS2 inactivation is well estimated in fast initial phase in SWB, but rapidly overestimates the inactivation in WW. This highlights that inactivation rate constants determined in model systems have limited value for estimating virus inactivation during treatment of real matrices. They can predict the log-linear portion of the inactivation in real water matrices, but fail to consider the strong tail observed at higher ozone exposures, in particular in DOC-rich matrices (WW). The increased complexity of the matrices thus results in a curved inactivation profile.

Instead of the log-linear model as described by Equation 2.2, virus inactivation in natural matrices could be fitted using a power model (such as equation 3.3), as proposed by Peleg and Cole (1998).<sup>102</sup>

Equation 3.3 Model for inactivation in function of the  $O_3$  exposure in natural matrices

$$\text{Log} \left( \frac{N}{N_0} \right) = \alpha_0 * O_3 \text{ exposure}^{\alpha_1}$$

The model fits are presented in Figure 3.3 below, and incorporate uncertainties associated with ozone exposure calculations. This results in a high uncertainty on the predicted inactivation, especially for SWB. Model coefficient are shown in Table S3.4.

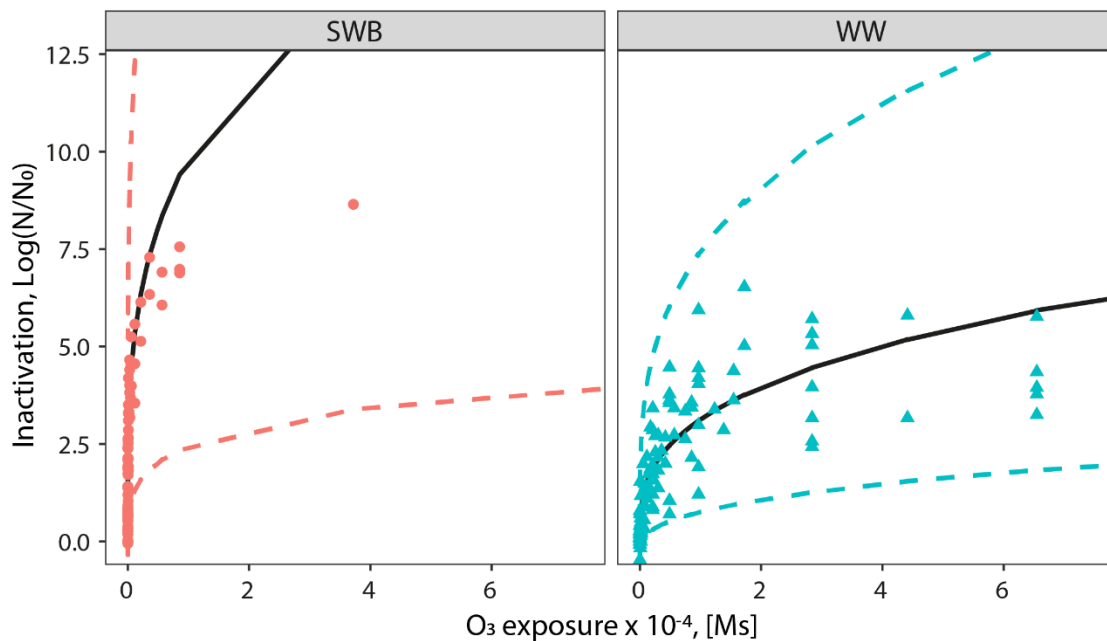


Figure 3.3 Inactivation in function of the ozone exposure with power model prediction (black line) and 95% credible interval (dashed line) for SWB (pink) and WW (turquoise)

### 3.3.3 Proxies for virus inactivation

Above, we established a relationship between inactivation and  $O_3$  exposure that predicts virus inactivation in natural matrices reasonably well (Equation 3.3). Nevertheless, estimating virus inactivation based on  $O_3$  exposure is impractical, because ozone exposure during wastewater treatment is typically not known. In addition, the uncertainties in the model presented above are not suitable for accurate predictions. Alternatively, virus inactivation could be monitored using proxies that vary with the specific  $O_3$  dose in a similar way as the  $O_3$  exposure.

#### **$\Delta UV_{254}$ and CBZ abatement as a function of the specific ozone dose**

To evaluate the utility of  $\Delta UV_{254}$  or CBZ abatement as proxies for virus inactivation, we first tested their response to different specific ozone doses. This step served to validate that these two proxies vary with the specific ozone dose over a similar range as the ozone exposure. The relationship between  $\Delta UV_{254}$  or CBZ abatement and the specific ozone dose is presented in Figure 3.4.

As shown in previous studies,<sup>43,44,84</sup> the  $\Delta UV_{254}$  dependence on the specific ozone dose can be described by a power function.<sup>43,44,84</sup> Here, we therefore also used a power function to fit the data (Equation S3.1), and model coefficients corresponded well to those previously published (Table S3.5)

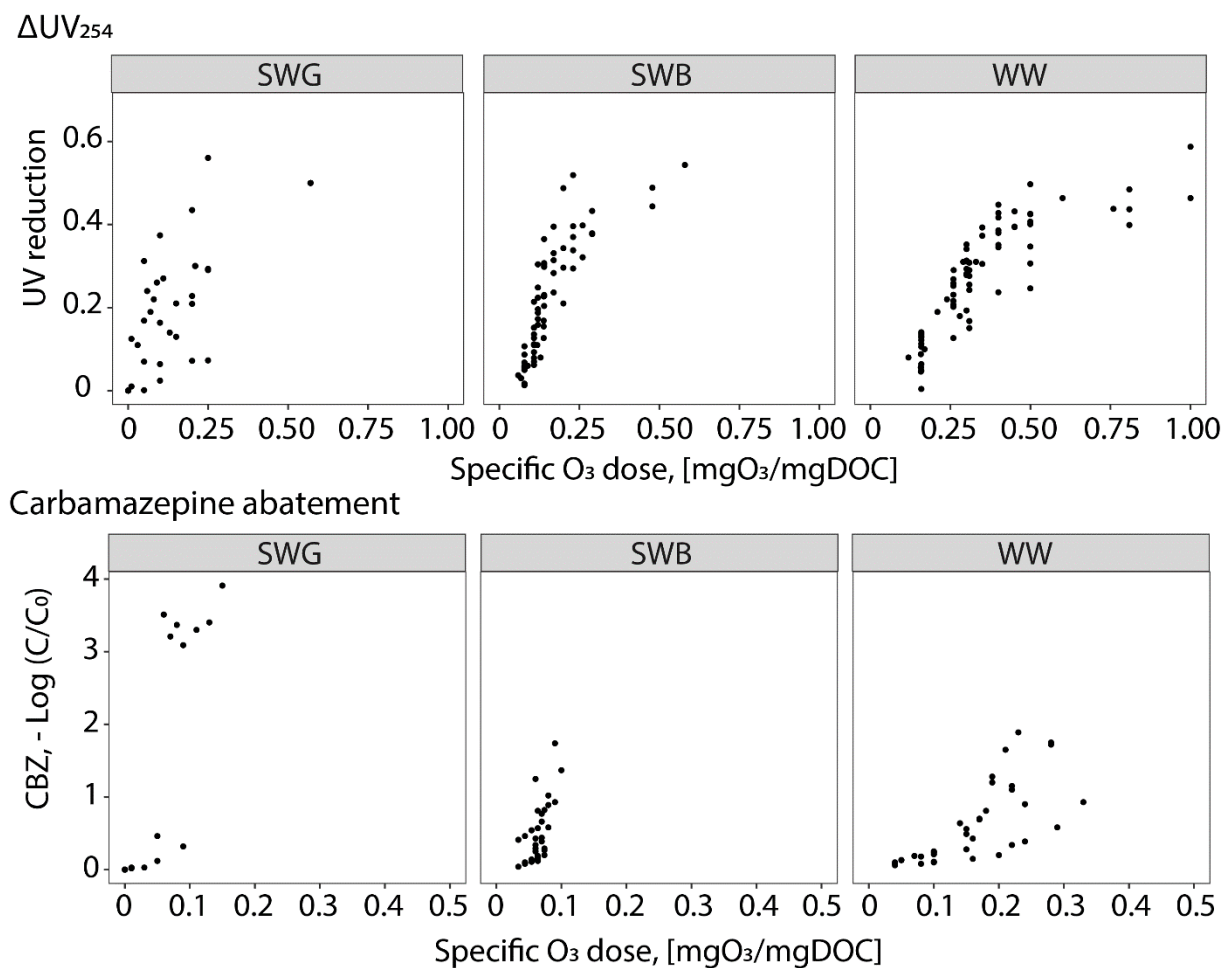


Figure 3.4  $\Delta UV_{254}$  (top) and CBZ abatement (bottom) in function of the specific  $O_3$  dose applied in the surface water of Lake Geneva and Lake Bret, and secondary effluent wastewater from Dübendorf.

In contrast to  $\Delta UV_{254}$ , CBZ abatement exhibited a lag-phase at low specific ozone doses. This lag-phase may be explained by competition with reactive moieties of the dissolved organic matter (DOM) with a higher reactivity towards ozone than CBZ. Hence, at low specific doses, ozone is preferentially consumed by DOM, resulting in a reduced CBZ abatement. Once the reactive moieties are oxidized (for  $\sim 0.07$  and  $0.15$   $\text{mgO}_3/\text{mgDOC}$  for SWs or WW, respectively), residual ozone is available for the abatement of CBZ. The abatement of CBZ in WW as a function of specific  $\text{O}_3$  dose corresponded well to that observed by Lester *et al*<sup>103</sup> (Figure S3.5). The two surface waters used in this study exhibited similar trends, even though their [DOC] differed and they are really different than the WW. Hence, the relationship between CBZ abatement and specific  $\text{O}_3$  dose depends more on the type of water than on the DOC concentration.

#### ***Correlation between virus inactivation and specific ozone dose, $\Delta UV_{254}$ or CBZ***

In a next step, virus inactivation was measured for a range of the specific  $\text{O}_3$  doses, and was evaluated as a function of  $\Delta UV_{254}$  or CBZ abatement measured in the same sample. Furthermore, because the ozone exposure is driven by the specific ozone dose, the specific ozone dose itself was also assessed as a predictor for virus inactivation. The inactivation of MS2 and CVB5 as a function of A) the specific ozone dose, B)  $\Delta UV_{254}$  and C) CBZ abatement are shown in Figure 3.5.

For the specific  $\text{O}_3$  dose the relationship is approximately log-linear for all waters tested, though the data is more scattered in wastewater. Higher inactivation was observed in the two SWs compared to WW for similar specific  $\text{O}_3$  doses.



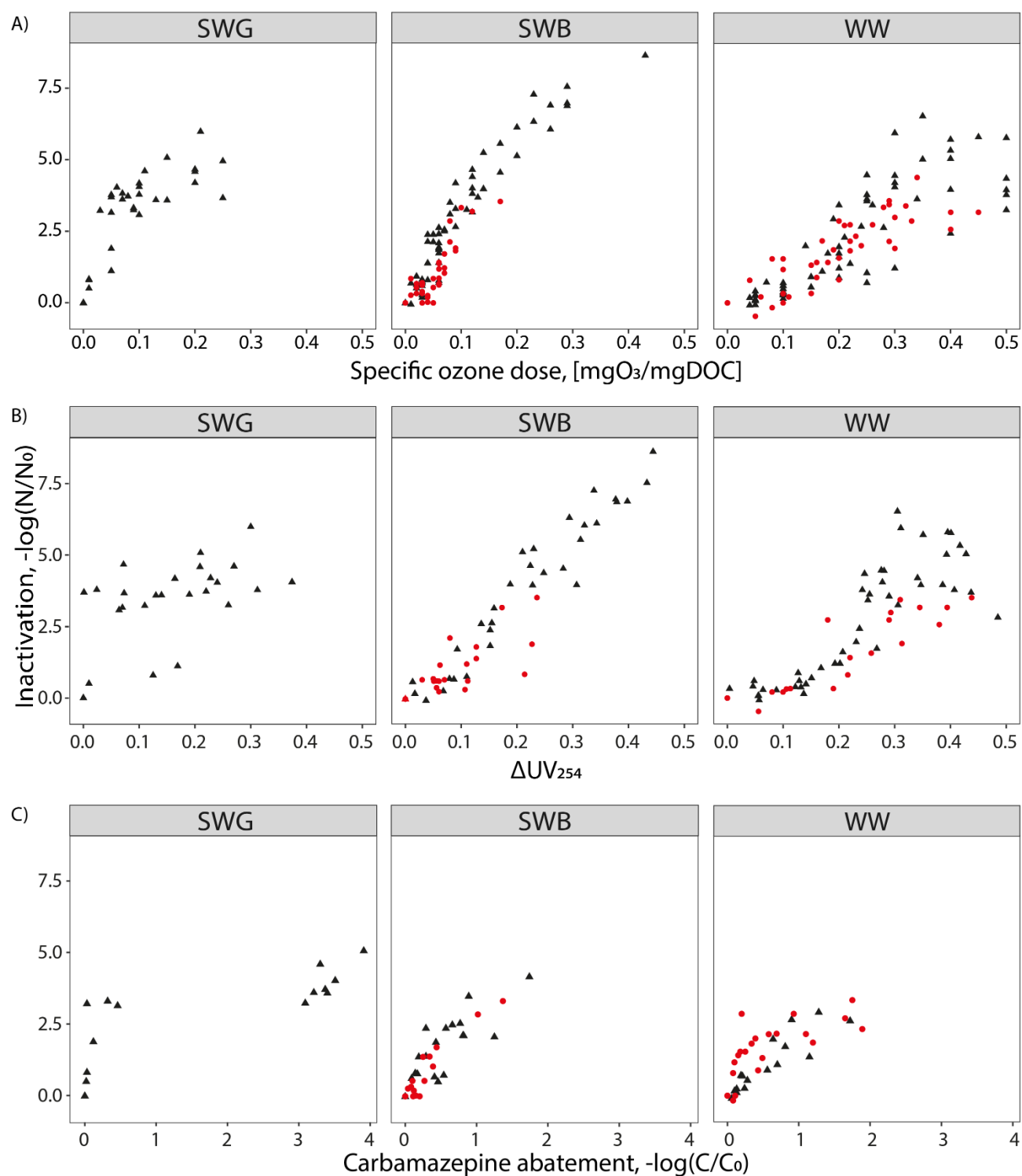


Figure 3.5 Inactivation of MS2 (black triangles) and CVB5 (red circles) in SWG, SWB and WW in function of the three proxies studied.

For  $\Delta UV_{254}$ , inactivation in SWG and SWB exhibited a roughly log-linear dependency. In WW, a lag-phase was observed up to a  $\Delta UV_{254}$  of 15%, where the inactivation stayed below 1 log<sub>10</sub>. Reaction of ozone with highly reactive moieties present in wastewater, such as phenols, which also absorb UV light,<sup>104</sup> may explain the initial reduction in UV absorbance prior to the onset of inactivation. The relationship between  $\Delta UV_{254}$  and inactivation obtained in WW corresponded well to that observed by *Gerrity et al. (2012)*.<sup>43</sup> While all of their samples exhibited reductions in  $\Delta UV_{254} < 15\%$ , the overall trend is comparable to the observations in this study (Figure 3.6). Interestingly, the data by *Gerrity et al.* includes six different wastewaters from various origins and with DOC concentrations ranging from 6.3 to 18 mg/l. Combined with the data obtained herein, this indicates that a single relationship between  $\Delta UV_{254}$  and virus inactivation applies across vastly different wastewaters.

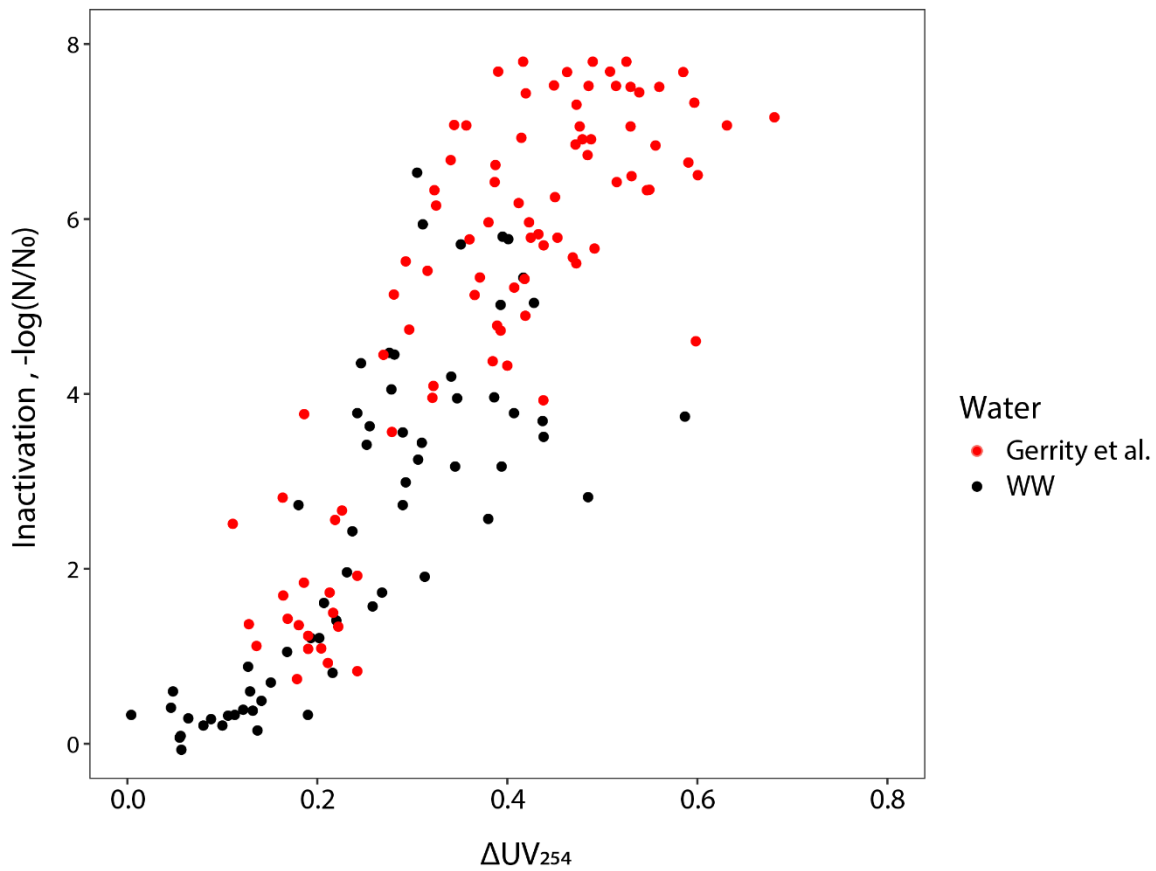


Figure 3.6 Comparison of the inactivation MS2 and CVB5 as function of the  $\Delta UV_{254}$  in WW of this study (black circles) with corresponding data for MS2 by *Gerrity et al.* (red circles). The data by *Gerrity et al.* is a compilation of five different wastewaters.

Finally, inactivation as a function of the log<sub>10</sub> CBZ abatement exhibited a maximum of ~5 log<sub>10</sub>, ~4 log<sub>10</sub> and ~3 log<sub>10</sub> in SWG, SWB and WW, respectively, before the limit of detection for CBZ abatement was reached. This relationship exhibited an initial log-linear part, followed by a plateau in all waters studied.

### Predictive relationships between proxies and virus inactivation

To establish predictive relationships between the different proxies and virus inactivation ( $\log_{10} N/N_0$ ), we first determined which system variables significantly contribute - to explaining the observed variation in inactivation. To this end, we used Bayesian model averaging (BMA)<sup>97</sup> - considering four variables: virus species, water type (i.e., surface or wastewater), DOC content, and the proxy under consideration. One result of BMA is the probability (p) that a given variable may be included in a model to explain the variation in the response variable. Secondly, it also gives an estimate of the effect size of each variable (Figure S3.6- S3.8).

BMA results for the specific  $O_3$  dose and for  $\Delta UV_{254}$  as a proxy show that, as expected, the proxy was the variable with the greatest effect (10 and 12.5 per unit of proxy for the specific  $O_3$  dose and  $\Delta UV_{254}$ , respectively). Interestingly, the water type ( $p \geq 0.98$ ) was also relevant, whereas the DOC content was not ( $p < 0.95$ ). This was expected, because the [DOC] is considered in the specific ozone dose. Therefore, the type of organic matter is decisive, and mainly its phenols content. Finally, the BMA identified the virus species as a relevant model variable ( $p \geq 0.97$ ). However, its effect is small, this may be expected given their similar inactivation rate constant and stay close to the experimental uncertainty of the infectivity assay ( $\sim 0.5 \log_{10}$ ). Moreover, it is preferable to not discriminate viral species, because the model needs to capture variabilities in their response to disinfection. Therefore, this variable will not be included in the predictive model below. For CBZ abatement as a proxy, the BMA revealed no dependence of inactivation neither on virus species, nor water type, nor DOC content. CBZ abatement is the only relevant variable needed to explain variation in inactivation. This was expected, because the extend of CBZ abatement integrates already the other factors.

To build predictive relationships between virus inactivation and proxies, we used a Bayesian model structure that considers censored inactivation data. A power function model was used to describe the relationship for each water type, to capture the observed deviations from log-linearity (Figure S3.6):

Equation 3.4 Model used to fit virus inactivation as function of the different proxies

$$\text{Log} \left( \frac{N}{N_0} \right) = \gamma_0 * \left( \text{Specific } O_3 \text{ dose OR } \log \left( \frac{CBZ}{CBZ_0} \right) \text{ OR } \Delta UV_{254} \right)^{\gamma_1}$$

Because the water type was identified by the BMA as a relevant model variable when using the specific  $O_3$  dose or  $\Delta UV_{254}$  as a proxy, separate sets of model parameters were obtained for each water type. For carbamazepine, SW and WW were fit with the same model. Model parameters for all proxies are summarized in Table 3.2.

In Figure 3.7, Bayesian power model predictions (black line), together with its 95% credible intervals (dashed lines) are shown for the two types of water and all proxies studied. For SW, the predicted inactivation for specific  $O_3$  dose of 0.4 mgO<sub>3</sub>/mgDOC, is  $9.4 \pm 1.2 \log$  (95%CI: 7 to 11.5). In WW the data is more scattered, therefore the uncertainties are relatively high. For an operational dose of 0.4 mgO<sub>3</sub>/mgDOC, the expected inactivation is  $3.8 \pm 1.3 \log_{10}$  (95%CI: 1.2 to 6.4). Thus, virus inactivation resulting from application of the operational specific ozone dose will be sufficient to inactivate virus load by at least 1.2  $\log_{10}$  and a maximum of 6.4  $\log_{10}$ , and will more likely yield around 4  $\log_{10}$ . Inactivation was also well predicted in both water types using  $\Delta UV_{254}$  as a proxy.

Importantly, both the specific ozone dose and  $\Delta UV_{254}$  could predict inactivation of up to  $\sim 8 \log_{10}$  in SW and  $\sim 5 \log_{10}$  in WW for  $\sim 50\%$  UV reduction. Furthermore, both proxies could estimate virus inactivation in both SW matrices tested (Figure S3.9 and S3.10).

Finally, CBZ abatement could predict inactivation in both SW and WW well by a single model (note that SW and WW are presented separately in Figure 3.7 for better readability only). This confirms that changes in water matrix equally impacts virus inactivation and CBZ abatement. Therefore, CBZ abatement is a good proxy for virus inactivation in all water matrices tested, independently of the type and content of the dissolved organic matter (Figure S3.11). However, CBZ is strongly abated during ozonation.<sup>42,43</sup> As such, the range over which virus inactivation may be estimated is limited by the concentration of CBZ before ozonation and its limit of quantification. In this study, inactivation could be predicted up to 4 log<sub>10</sub> with good confidence both in SW and in WW.

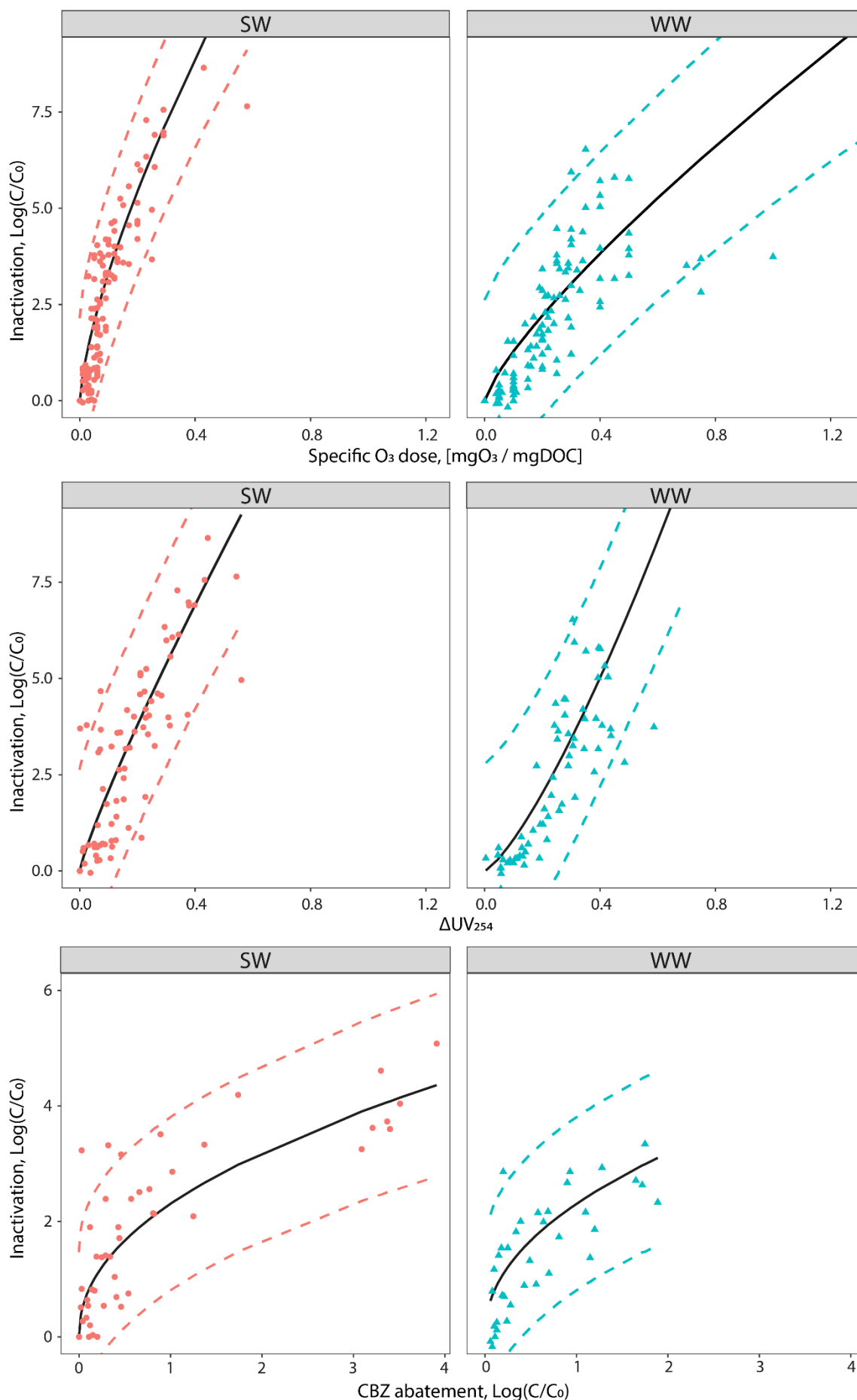


Figure 3.7 Power model (equation 5) with expected mean value (black line) and 95% credible interval (dashed lines) separate by water type (SW: circle and WW: triangle) for the three proxies studied.

Table 3.2 Summary of linear and power model parameters with the mean values, standard deviation and the 95% credible intervals in parentheses.

Specific O <sub>3</sub> dose		
Water type	$\gamma_0$	$\gamma_1$
SW	17 ± 1.116	0.7 ± 0.03
	(14.9, 19.3)	(0.64, 0.775)
WW	7.89 ± 0.52	0.79 ± 0.06
	(6.9, 9)	(0.67, 0.91)
$\Delta UV_{254}$		
Water type	$\gamma_0$	$\gamma_1$
SW	15.3 ± 1.4	0.86 ± 0.07
	(12.6, 18.2)	(0.73, 1)
WW	17 ± 2.3	1.3 ± 0.1
	(12.7, 21)	(1, 1.6)
CBZ abatement		
Water type	$\gamma_0$	$\gamma_1$
both	2.3 ± 0.1	0.46 ± 0.04
	(2.1, 2.5)	(0.38, 0.55)

As a first validation for  $\Delta UV_{254}$  as proxy, a prediction of the MS2 inactivation in WW measured by Gerrity *et al.* (2012)<sup>43</sup> was performed using their reported  $\Delta UV_{254}$  (extracted using Webplotdigitizer<sup>105</sup>, raw data is presented in Table S 3.9). Figure 3.8 A) presents the inactivation predicted by equation 3.4 (red line) together with credible intervals and the measured inactivation as a function of  $\Delta UV_{254}$  reported by Gerrity *et al.* (2012).<sup>43</sup> The measured inactivation follows our model reasonably well. Figure 3.8 B) shows a direct comparison between the calculated inactivation (eq. 5) and the measured inactivation by Gerrity *et al.* (2012).<sup>43</sup> The prediction slightly underestimates observed inactivation greater than 2 log<sub>10</sub>, though the discrepancy is minor (about 20%). Since the data of Gerrity *et al.* (2012)<sup>43</sup> comprises five different wastewaters, the good match with the model predictions established herein confirms that the inactivation -  $\Delta UV_{254}$  relationship in wastewater is independent of the concentration of DOC, and only dependent on the origin of organic matter.

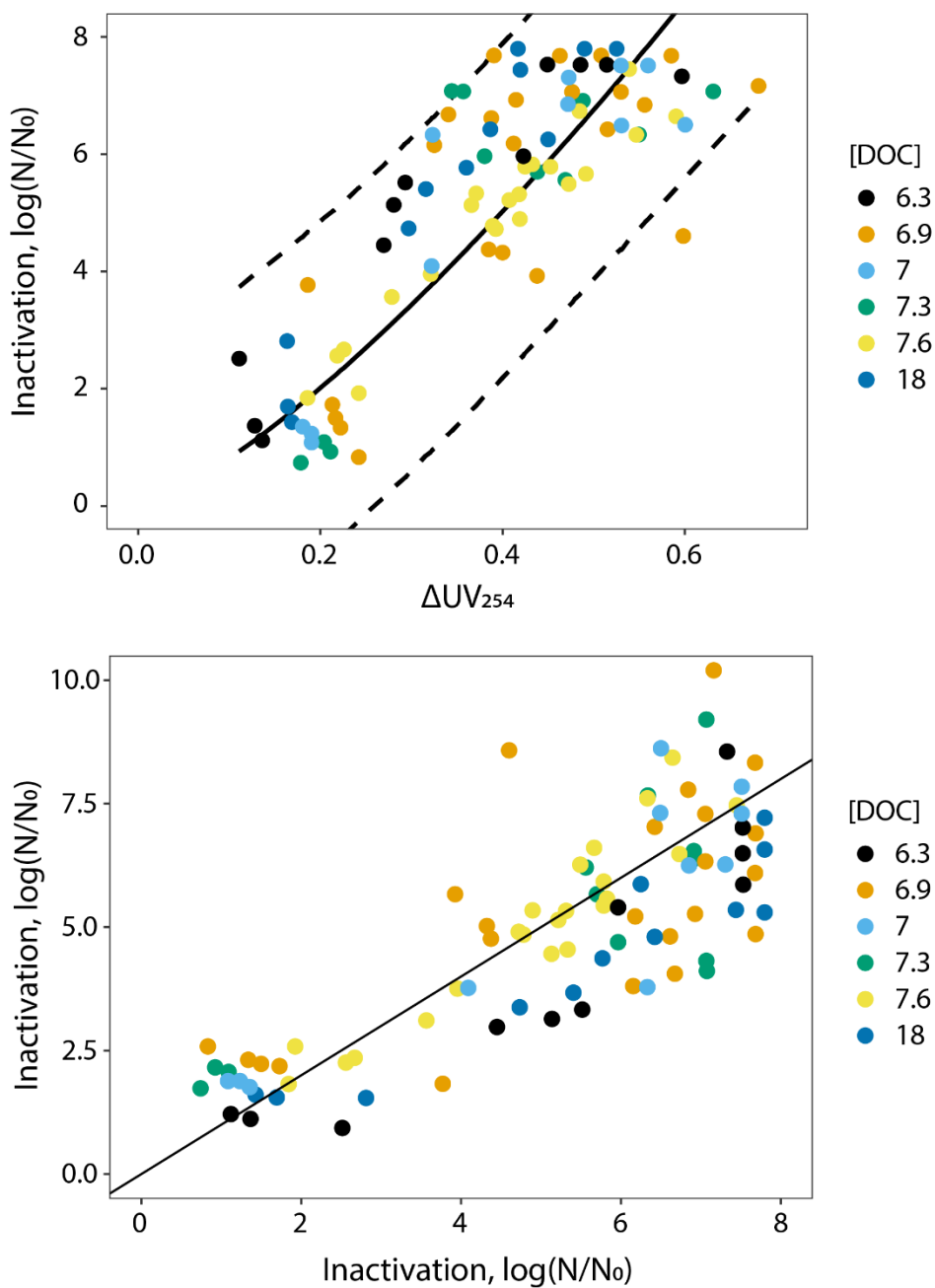


Figure 3.8 (A): Prediction of the mean MS2 inactivation (red line) and 95% CI (black dashed line) in wastewater based on equation 5, superimposed by inactivation data measured by Gerrity et al. (2012). (B): Comparison of the predicted vs measured inactivation for the data generated by Gerrity et al. (2012)<sup>40</sup> The black line indicates a 1:1 relationship.

***Proxy validation in a pilot-scale ozonation reactor***

The applicability of the developed proxy-inactivation relationships for MS2 was validated in a pilot-scale ozonation reactor described elsewhere<sup>92,93</sup>. This pilot reactor treats water from lake Zurich and was operated at two specific ozone doses (further details in Table S3.10-Table S3.11).

Figure 3.9 A) shows the MS2 inactivation throughout the ozonation reactor as a function of ozone exposure, in addition pilot data has been compared with batch experiment in SWB and WW (Figure S3.12). Residual infective MS2 concentrations could be measured throughout the reactor and in the reactor effluent for the lower specific ozone dose of 0.2 mgO<sub>3</sub>/mgDOC. In contrast, the MS2 concentration fell below the detection during the early stages of treatment for the higher specific ozone dose (0.5 mgO<sub>3</sub>/mgDOC). The inactivation data from both specific ozone doses adhered to the model described by Equation 3.4 for surface water (black line), which slightly overestimates the plateau at higher ozone exposures. As only one water matrix (SWB) was used to validate this model, further experimental data may improve the estimates. All inactivation-ozone exposure data are presented in the SI.

Figure 3.9 B)-D) show the measured inactivation of MS2, as well as the inactivation predicted by the proxy-inactivation relationships for SW developed herein. Predictions could only be experimentally validated for treatment using a specific ozone dose of 0.2 mgO<sub>3</sub>/mgDOC. For the higher specific ozone dose (0.5 mgO<sub>3</sub>/mgDOC), CBZ concentrations were below the detection limit in all treated samples, and MS2 was not detectable in the effluent sample in which  $\Delta\text{UV}_{254}$  was determined. As such, no samples were available for this specific ozone dose in which both proxy and MS2 were measurable.

As is evident from Figure 3.9, the proxies predicted the inactivation well, confirming the applicability of the proxy-inactivation relationships developed in batch systems herein for a flow-through pilot plant. For higher specific ozone doses, inactivation can be predicted based on the specific ozone dose or  $\Delta\text{UV}_{254}$ . However, because the limit of quantification (LOQ) of CBZ was exceeded, CBZ measurements can only inform on the minimal inactivation level that can be expected (red line in Figure 3.9), and this estimate will depend on the analytical methods and LOQ.



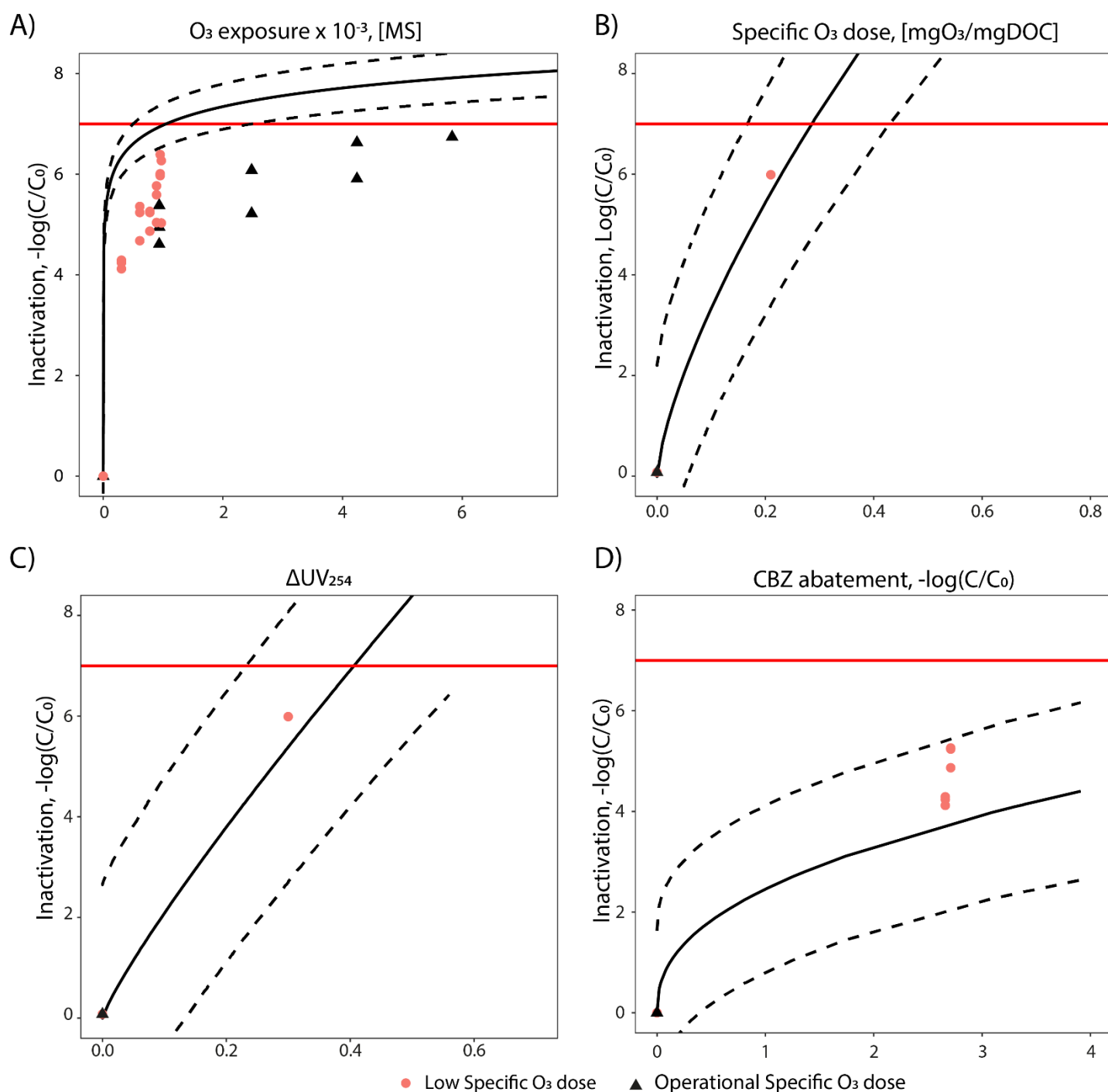


Figure 3.9 Inactivation measured in the pilot reactor as a function of ozone exposure or proxies. Red circles and black triangles represent the experimental data obtained using a specific  $O_3$  dose of 0.2 and 0.6 mg $O_3$ /mg DOC, respectively. Model predictions (expected mean: black line, 95% CI: dashed line) using the proxy-inactivation relationships developed herein are also shown. Red lines indicate the detection limit for MS2 inactivation.

To conclude, we tested the specific ozone dose and two additional proxies that allow to estimate virus inactivation over several orders of magnitude. For the specific  $O_3$  dose or  $\Delta UV_{254}$ , the proxy-inactivation relationships were influenced by the water type. Therefore, the model predictions are specific to SW or WW. In contrast, CBZ abatement and virus inactivation were affected by different water types in the same way, such that a single the proxy-inactivation relationship for CBZ abatement applied across all waters tested.

A limitation of using the specific  $O_3$  dose as a proxy is that it does not allow an online/real-time monitoring during ozonation treatment. Therefore, it cannot inform on unexpected anomalies during treatment. The main advantages of this proxy are that it does not require any specialized monitoring equipment, and is able to predict a wide range of virus inactivation. In contrast,  $\Delta UV_{254}$  is already used to monitor the efficiency in treatment plant with respect to micropollutant abatement,<sup>106</sup> and therefore its utility could easily be expanded to online/on-time monitoring of viruses. However, a limitation of  $\Delta UV_{254}$ , is that this proxy is not really suitable for low DOC waters as the absorbance is low and yields inaccurate  $\Delta UV_{254}$  measurements. Secondly, the inactivation-proxy relationship depends on water type. Finally, the use of CBZ as proxy may require specialized equipment, and its range of prediction is slightly smaller than for the other two proxies. However, it is independent of the water type and allows to monitor inactivation during the treatment.

### 3.4 ACKNOWLEDGMENTS

This study was funded by the Swiss National Science Foundation (Grant 205321\_169615). Elisabeth Salhi, Loïc Decrey and Dominique Grandjean are acknowledged for help in the laboratory.

# Chapter 4 Inactivation mechanisms

The author of this thesis, Camille Wolf, designed the experimental plan, performed the experiments, analyzed the data and wrote the chapter.

## 4.1 Introduction

A mechanistic understanding of virus inactivation is important to design effective control strategies. Consider, for example, the case of human adenovirus. This virus is resistant to monochromatic low-pressure UV irradiation,<sup>107</sup> however not to free chlorine.<sup>108</sup> Inactivation of these disinfectants is mostly attributed to genome damage, and coat protein damage, respectively.<sup>109</sup> In the first case (UV inactivation), adenovirus can still be internalized by host cells. Then, using cell's repair machinery, it can recover from genome damage and stays infectious. In the second case (free chlorine), however, the protein damage induced is irreversible, and the virus is permanently inactivated. As highlighted by this specific case, mechanistic insight into virus inactivation caused by a disinfectant to viruses is crucial to understand. This may help to design synergistic disinfection strategies that combine several disinfectants causing different types of damage. Synergies may lower risks of resistant virus escaping the treatment.

While the inactivation mechanisms of UV and free chlorine are reasonably well understood, the viral targets of ozone have not been clearly identified. Ozone may damage both the genome and viral proteins. How this damage impacts the critical steps in a virus' life cycle, however, remains unknown. Interestingly, as shown in chapter 2, the inactivation rate constants of different viruses by ozone are remarkably similar, despite the great differences in the virus' structure and composition.<sup>83</sup> This indicates that ozone may react by a mechanism that is common to all viruses studied. What this mechanism is and which steps in the viral life cycle it targets is not fully understood.

In this chapter, we investigate how ozone inactivates echovirus 11 (E11). The virus belongs to the genus *Enterovirus* of the *Picornaviridae* family. The life cycle of this virus family is complex and can be divided into different phases, all of which have to be intact for the virus to be infective.<sup>110</sup> Infection starts by binding of the virus to the cellular membrane receptor (Figure 4.1). Binding to these receptors, most of which are member of the immune-globulin-like or integrin receptor family, triggers virus entry into the host cell by endocytosis. After endocytosis, the viral particle has to uncoat to deliver its genome into the cytoplasm. Uncoating mechanisms are relatively conserved throughout the enterovirus genus. The viral capsid is gradually destabilized and this destabilization is initiated either by receptor binding, by a pH decrease, or by both. The destabilized capsid releases viral protein (VP) 4, which forms an ion-permeable channel through the plasma membrane with a size that corresponds to that of the RNA. After VP4 expulsion the remaining capsid is called A particle; its larger size allows for the release of RNA. Once in the cytosol, cellular ribosomes translate the viral genome to synthesize viral coat proteins and viral proteins involved in viral genome replication. Genome replication occurs in cytoplasmic membrane vesicles, and proceeds via the production of a double-stranded (ds) RNA intermediate. Ultimately, new progeny virus is formed and released in a stepwise process that is poorly understood.<sup>110</sup>

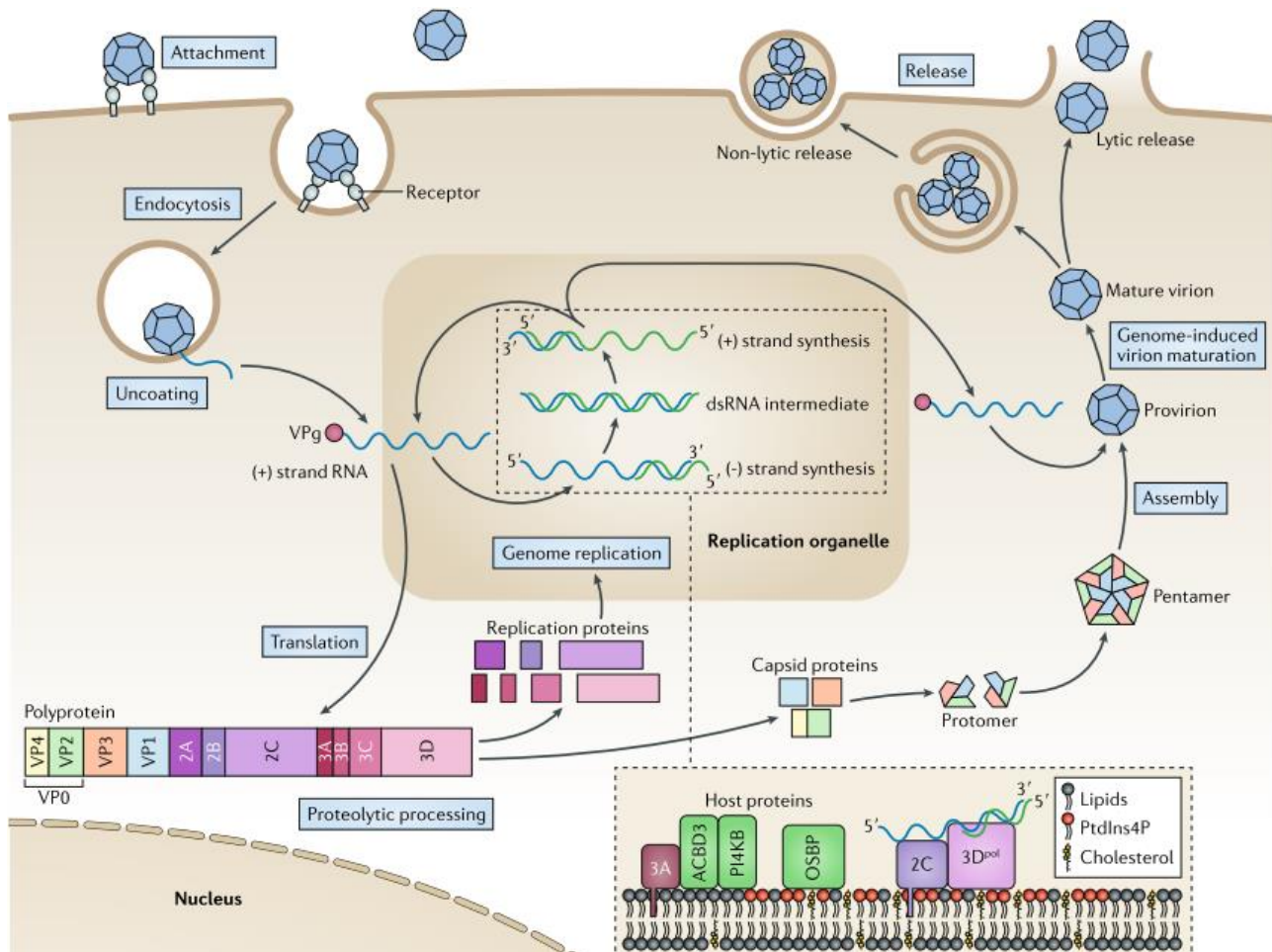


Figure 4.1 Schematic overview of the enterovirus life cycle, scheme from Baggen *et al* (2018)<sup>106</sup>

When enteroviruses are exposed to ozone, reaction with amino acids is likely to cause chemical damage and conformational changes of the viral proteins.<sup>20</sup> Among the steps in the viral life cycle described above, such changes may affect virus attachment and entry. The effect of ozone on genome replication was recently investigated by Torrey *et al.*, who quantified genome functionality using a transfection assay. Their results revealed a proportional reduction in genome functionality and infectivity after ozone treatment, indicating that ozone inhibits the virus' ability to replicate its genome.<sup>111</sup> The aim of this study was to expand on the work by Torrey *et al.* to investigate the effect of ozone not only on genome replication, but on additional steps in the viral life cycle. The main goal was to develop an experimental strategy to elucidate if ozonation impairs virus attachment and internalization, as well as replication.

To this end, we used an approach based on fluorescence confocal microscopy. Similar methodologies have previously been used to investigate steps in viral life cycles, though not in the context of disinfection. For example, using fluorescently tagged viral particles in live cells, it was determined that the internalization of a single influenza virus particle may take about ~200 seconds once the virus reaches the cell membrane.<sup>110</sup> Unfortunately, modifying virus particles with fluorescent proteins or chemical dyes may change their reactivity towards ozone, such that tagging viruses was not possible for our purposes. Instead, we use an immunostaining approach based on work by Le Cabec *et al.*<sup>112</sup> In this approach, viruses are first inactivated and exposed

to cells, and only then are the different components (e.g., viral capsid, RNA) fluorescently labelled and localized using a procedure detailed in section 4.2 below.

## 4.2 Material and Methods

### 4.2.1 Virus and cells

Echovirus type 11 Gregory strain (ATCC VR-41) was purchased from LGC Standards (Molsheim, France). E11 was propagated on buffalo green monkey kidney (BGMK) cells. BGMK cells were cultivated in minimum essential medium (MEM; Invitrogen) supplemented with penicillin (20 U mL<sup>-1</sup>; Invitrogen), streptomycin (20 µg mL<sup>-1</sup>; Invitrogen), and 2 or 10% fetal bovine serum (FBS; Invitrogen), and cells were incubated at 37°C in 5% CO<sub>2</sub> and 95% humidity.

### 4.2.2 Buffers and media

Infection media (iMEM) was 2% MEM was supplemented with 20 mM HEPES (Roth), 0.3% bovine serum albumin to minimize unspecific binding of the virus. Permeabilization buffer (PB) was composed of phosphate buffered saline (PBS; Invitrogen) supplemented with 0.1% Tween20 (AppliChem) and 1% BSA (w/v) (Sigma). PBS supplemented with Mg<sup>2+</sup> and Ca<sup>2+</sup> (Invitrogen), 0.1% BSA (w/v, Sigma) and 1% penicillin/streptomycin. Development of our staining procedure was based on protocol kindly shared by Silke Stertz (University of Zürich).

### 4.2.3 Antibodies

Primary antibodies used were monoclonal Mouse anti-echovirus (Biozol Diagnostica). As secondary antibodies, polyclonal Goat anti-mouse IGG Alexa 555 (Life technology) or Alexa 488 (Life technology) were used.

### 4.2.4 Time lapses and inactivation experiments

Two types of experiments were conducted: a time lapses experiment, where an untreated population of E11 was infected onto cells, and internalization and replication were analyzed at different points in time up to 8 hours post infection. This experiment served to identify the best time points to use in the internalization and replication assays (see below).

Inactivation experiments were conducted to measure the change in internalization and replication prior to and after ozone treatment. An ozone stock solution was prepared as described in chapter 2, and was added to E11 diluted in phosphate buffer at pH 7.5, up to a final concentration of 20 mg/l. The extent of inactivation was measured as described in chapter 2, and infective viruses were measured in most probable number (MPN) per mL.

### 4.2.5 Sample preparation and fixation

BGMK cells were seeded in a 96-well plates (6005550, Prekin Elmer) at 10'000 cells /well in 2% MEM (Invitrogen) at least twelve hours before experiments. Virus were incubated on cells for different durations ranging from 0 to 8h at 37°C or 1h at 4°C in iMEM at a MOI ~10<sup>3-4</sup>. After removing the inoculum, the cells were washed three times with 100µl of PBS to remove any unbound virus. Cells were fixed with paraformaldehyde fixative solution (ABCR) 10 min on ice. Cells were washed three times with 100 µl PBS, and 100µl of PBS was left overnight on the samples.

#### 4.2.6 Internalization assay

In order to accurately detect an object in microscopy it is recommended to have at least 5 to 10 pixels to cover the object. The smallest object that common microscopes (widefield or confocal, with an objective of 100x) can detect is ~ 250nm with a pixels size of ~50nm.<sup>113</sup> Given this limitation, and considering that a lipid bilayer is ~ 5 nm thick,<sup>114,115</sup> it is impossible to spatially resolve if labelled viruses are localized inside or outside the membrane, or if they are attached to the plasma membrane. Instead, to confirm that a virus has entered a cell, colocalization of the viruses with different labelled cell compartments has been used. For example, influenza virus migrates to the cell nucleus, and colocalization of the virus and the nucleus then indicates successful cell entry.<sup>116</sup> Similarly, the internalization process of echovirus 1 has been studied by immunostaining and colocalization with Caveolin-1, a membrane protein involved in the entry process.<sup>117</sup> However, the viruses used herein do not migrate to the nucleus, but instead replicate in the perinuclear area in a virus-induced, tubulovesicular replication organelle.<sup>110</sup> Furthermore, E11 may use caveolin-independent entry mechanisms.<sup>117</sup>

To confirm a successful virus entry into cells, we therefore used an approach inspired by Le Cabec *et al.*<sup>112</sup> These authors used a double labelling method applied prior to and after cell permeabilization, to differentiate between total and internalized bacteria in macrophages.<sup>112</sup> Here, we performed two anti-E11 labelling steps with two different secondary dyes to localize E11 inside of BGMK cells. The first dye (Alexa 555, Figure 4.2) was applied before cell permeabilization of the BGMK cells, thus labeling only external viruses. Permeabilization was done by adding 100µl of PE on cells for 1h at rt. The second dye (Alexa 488, Figure 4.3) was applied after permeabilization, such that both internalized and external viruses were labelled. Comparison of the two images then revealed the presence of internalized viruses. In addition, nucleus and cytoplasm were also labelled (as described below), to localize the cell boundaries.

Specifically, 100 µl of monoclonal Mouse anti-virus (1/500) diluted in PBS were incubated at 4°C for 1h. The cells were labelled with 100 µl Goat anti-mouse IGG Alexa 555 (1/500) diluted in PBS for 1h at room temperature. After washing, cells were permeabilized with 100 µl of PB for 1h at room temperature. Then, they were incubated with 100 µl of Mouse anti-virus (1/500) diluted in PB at 4°C for 1h, followed by incubation with a secondary antibody (Alexa 488). Finally, samples were incubated with 100 µl of HCS Cellmask (1 µg/ml, Life technology) at room temperature for 30 min, and DAPY mounting media (Vectashield, Vectorlabs) was added. Between each step, the cells were washed three times with 100 µl of PB.

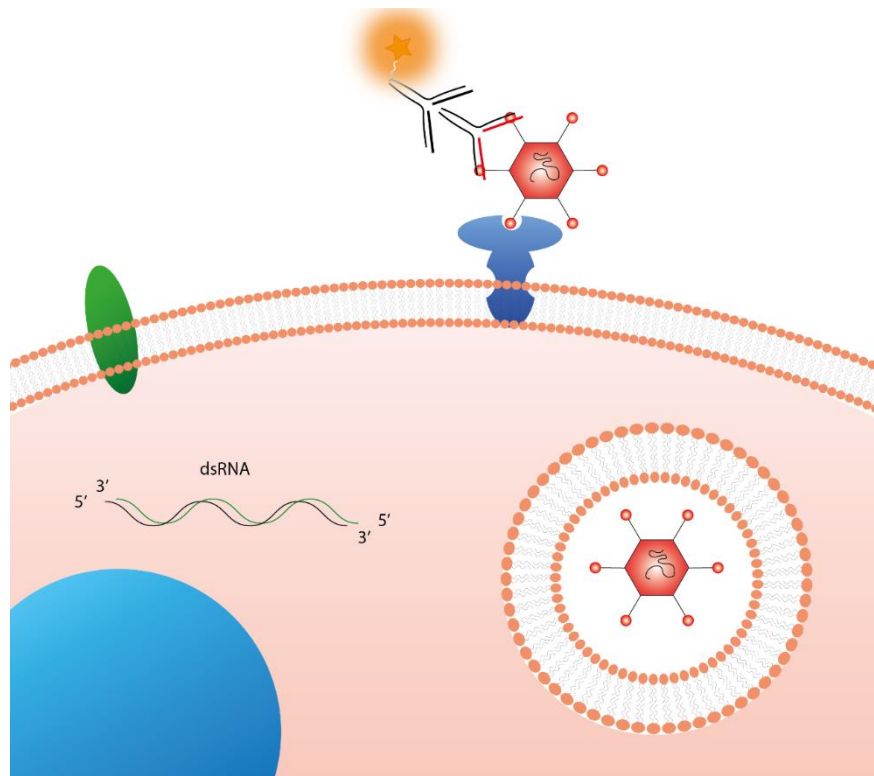


Figure 4.2 Immunostaining before permeabilization with Mouse anti-E11 (primary Ab) and Goat anti-Mouse IGG-Alexa 555 (secondary Ab). Only viruses outside of the cell are labelled.

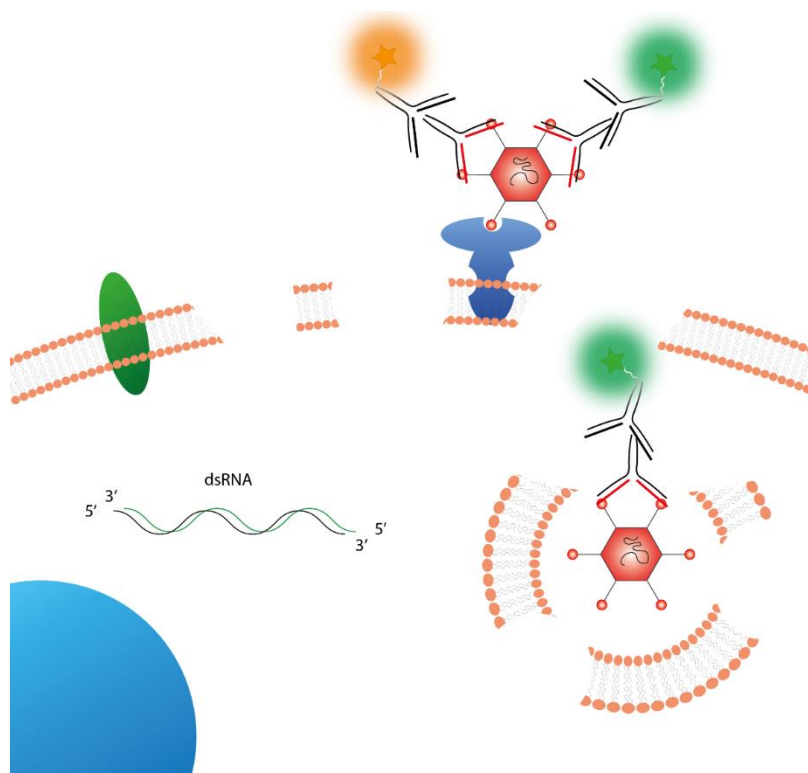


Figure 4.3 Immunostaining after permeabilization with Mouse anti-E11 (primary Ab) and Goat anti-Mouse IGG-Alexa488 (secondary Ab). Viruses outside are labelled with both Abs (Alexa 555 and Alexa 488). Viruses within the cell are labelled only with Alexa488.

#### 4.2.7 Replication assay

To detect the presence of functional genomes, Mouse J2 antibody was used to bind dsRNA, which indicates active genome replication (Alexa 488, Figure 4.4). Cells were permeabilized with 100  $\mu$ l of PB for 1h at room temperature. Then, samples were incubated with 100  $\mu$ l of J2 antibodies (1  $\mu$ g/ml, Scicons) diluted in PB at 4°C for 1h, followed by incubation with the secondary antibody (Alexa 488). Finally, samples were incubated with 100  $\mu$ l of HCS Cellmask (1  $\mu$ g/ml, Life technology) at room temperature for 30 min, and DAPY mounting media (Vectashield, Vectorlabs) was added. Between each step, the cells were washed three times with 100  $\mu$ l of PB.



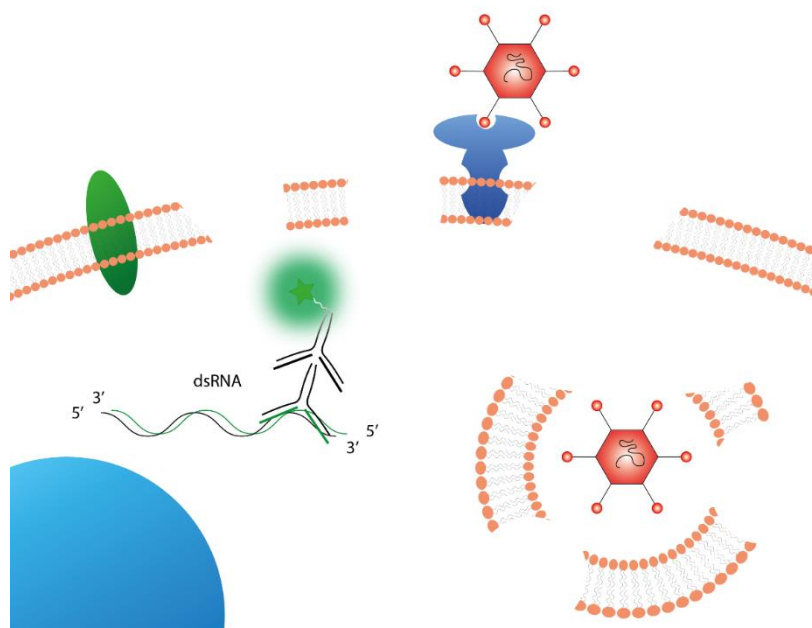


Figure 4.4 Immunostaining after permeabilization with Mouse J2 antibody (primary Ab) and Goat anti-Mouse IGG-Alexa 488 (secondary Ab). Only dsRNA is labelled.

### 4.3 Confocal microscopy

A LSM 700 inverted microscope (Carl Zeiss) was used to perform the imaging. The dilutions of secondary antibodies gave negligible background signals. Controls did not show unspecific signals between secondary antibodies. Multitracking was used for all laser lines (wavelength: 405, 488, 555, 639 nm) to avoid false colocalization.

### 4.4 Image analysis

Cell identification was performed with Cell profiler<sup>118</sup> and colocalization was performed with Fiji<sup>119</sup> based on a pipeline provided by Romain Guet from the EPFL bioimaging and optics platform. The procedure is summarized in Figure 4.5.

To detect fluorescence associated with dsRNA (replication) in time laps experiments, the nuclei were first identified and a mask was created using DAPI, expanded by 15 pixels (A.1) in order to define the perinuclear area, this area is delimited as the region of interest (ROI). Each different ROI is identified separately (A.2). Finally, the fluorescence intensity for dsRNA was measured in this defined area (A.3). For colocalization experiments, the nuclei were identified using the DAPI channel, and the cytoplasm was defined from the nucleus using the Cellmask channel (B.1). Negative control did not reveal any false positive signal from other channels. Each cell is defined separately and a mask is created. Finally, a mask was created with a gray scale identifying each cell (B.2). Then, the original images were opened in ImageJ together with the mask that

define the ROIs. The colocalization analysis was run at the cell level using JACoP plugin (B.3) applying thresholding based on negative control images and enable to colocalized pixels that were positive in before and after permeabilization channel.<sup>120</sup> Finally the colocalized area was subtracted to the area after permeabilization in order to obtain the signal area of virus inside.

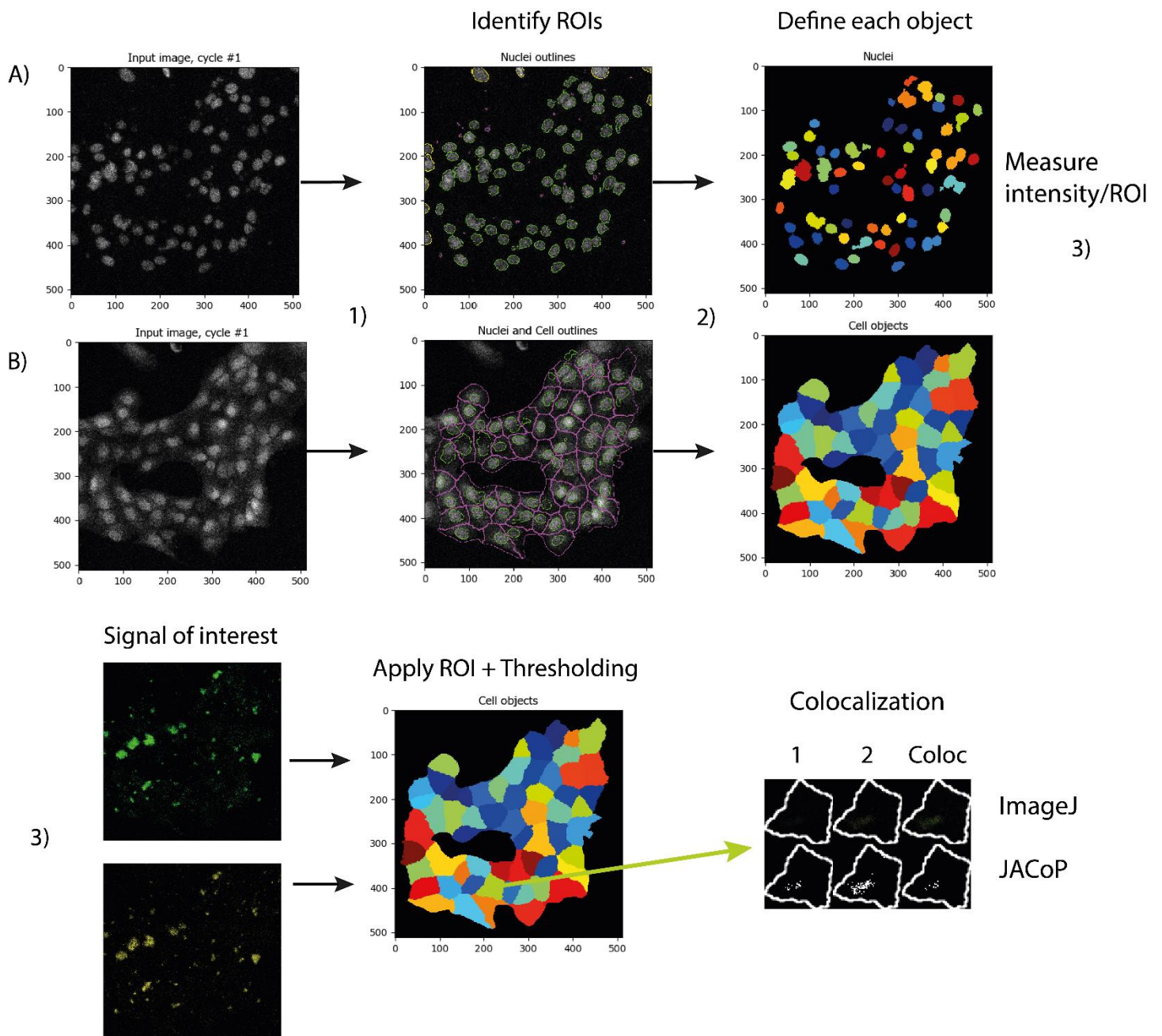


Figure 4.5 Image analysis pipelines for replication assay A) and internalization assay B).

## 4.5 Results

### 4.5.1 Time laps

To better understand the viral life cycle kinetics in BGMK cells, a time laps of infection was conducted for E11. Specifically, internalization and replication were followed over a time course of up to 8h. In Figure 4.6, images of the different channels recorded are shown for both the internalization and the replication assays at different time points up to 8 hours post-infection.

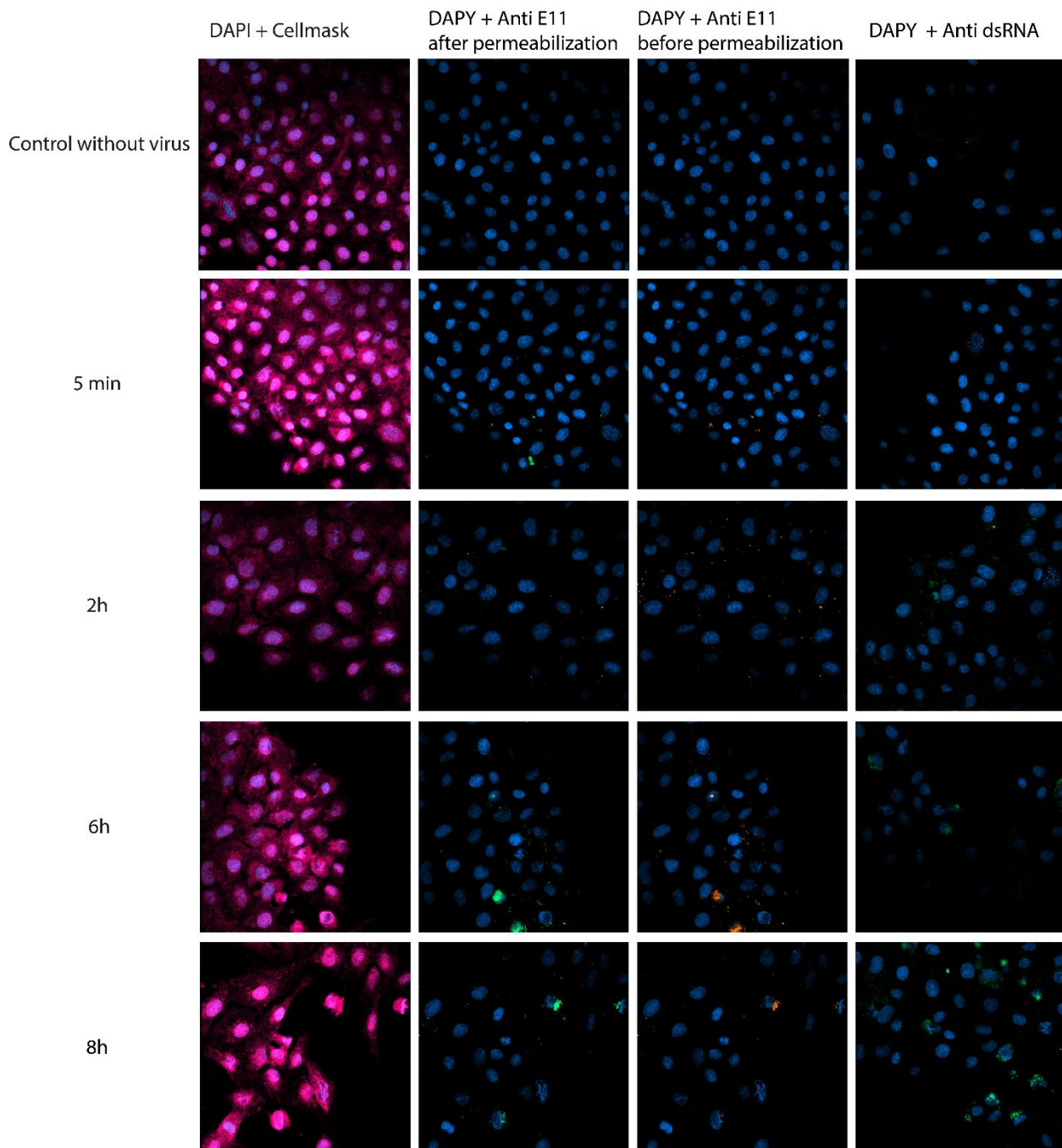


Figure 4.6 Time laps images of the cells (first column), the virus signal after cell permeabilization (2nd column), the virus signal before cell permeabilization (3rd column) and the replication signal (4th column) from 5 min up to 8h.

Recall that in the internalization assay, the orange signals stem only from viruses outside the cell (before permeabilization), whereas the green dye stained both virus inside and outside (after permeabilization). As seen in Figure 4.6, after 5 min, virus signals were already observed in both virus channels, indicating that viruses are rapidly internalized. Both signals seemed to increase over the course of 8h. The replication signal stayed relatively low up to 6 h, and then started to increase.

These visual observations are confirmed by quantification of the area of virus signal within the cell. During colocalization analysis, the area in pixels of the two signals (before ( $A_b$ ) and after permeabilization ( $A_p$ )) are recorded, together with the area where both signal colocalized ( $A_c$ ). Therefore, the area of virus signal that is only inside  $A_i$ , can be calculated by subtracting  $A_p$  to  $A_c$ . In addition, the mean fluorescence intensity of the dsRNA signal per ROI (defined previously, 1 ROI/cell). As shown in Figure 4.7, both the area of virus signal inside the cells, as well as the mean intensity of the dsRNA signal increase over time, indicating virus internalization and replication.

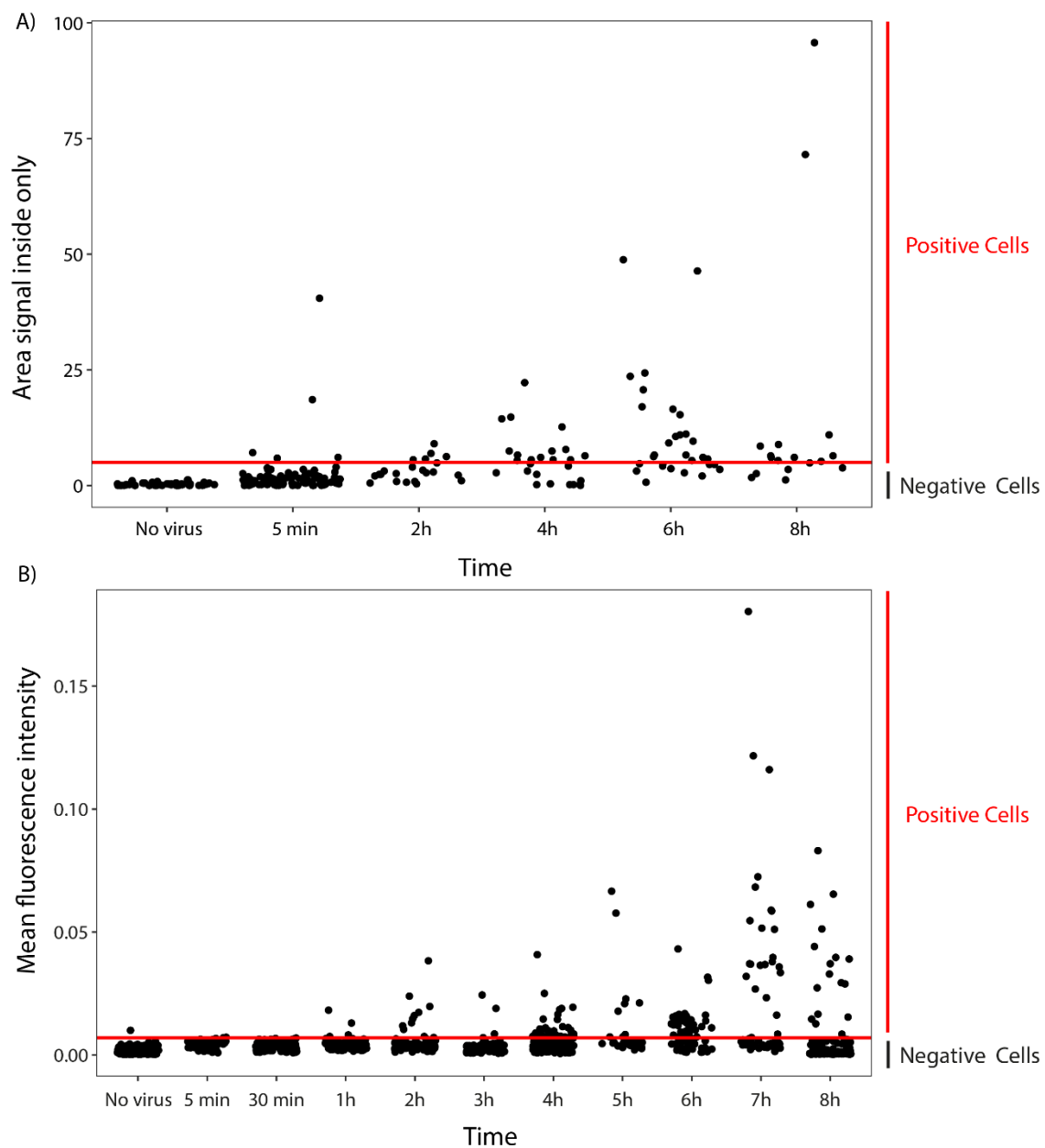


Figure 4.7 A) the area of virus signal inside the cell and B) the mean intensity of replication signal in function of the time post-infection. Each dot represents an individual cell analyzed. The estimated background signals arising from virus- or replication-negative cells are indicated with red lines.

In order to quantify the extent of virus internalization, the degree of colocalization of the two probes applied prior to and after cell permeabilization can be determined. To do so, the Mander's coefficients ( $M_i$ ) can be used which is determined by the following formula:<sup>121</sup>

$$M_1 = \frac{\sum Probe1_{coloc}}{\sum Probe1} \quad M_2 = \frac{\sum Probe2_{coloc}}{\sum Probe2}$$

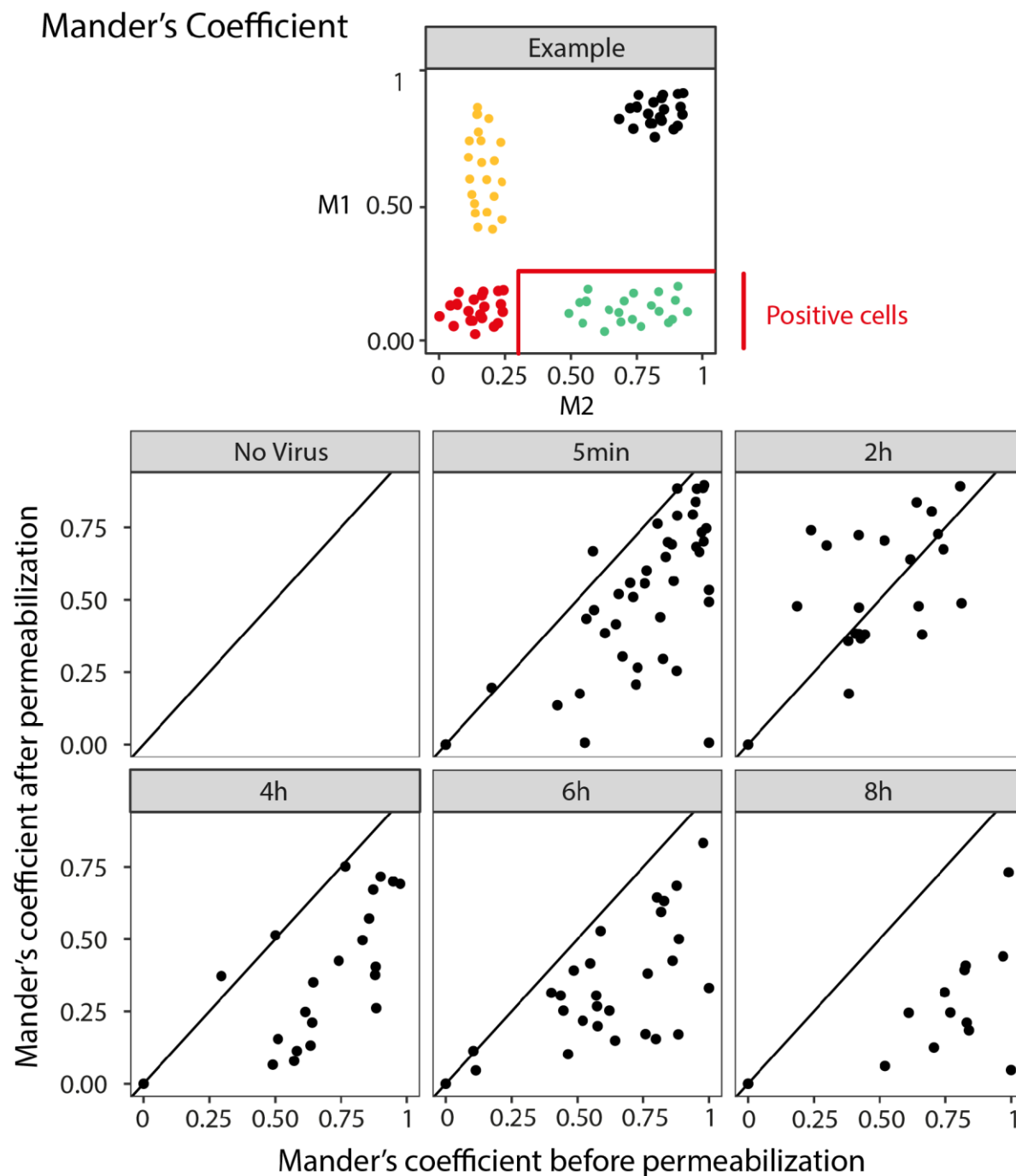


Figure 4.8 Top: example plot of  $M_1$  vs  $M_2$ . Two extreme cases are presented. The two signals colocalize well (black) or do not colocalize at all (red). The orange dots imply that most of the first signal colocalized with the second ( $M_1$  is high), but most of the second signal does not colocalize with the first; the green dots indicate the inverse case. The area where cells were considered positive to internalisation is defined by the red lines. Bottom:  $M_1$ - $M_2$  plots for the time laps experiment. The individual dots represent individual cells analyzed.

Here,  $M_1$  represents the fraction of fluorescence signal of probe 1 that colocalizes with probe 2, and inversely for  $M_2$ . If  $M_1$  is equal to zero, there is no colocalization of the two probes. If all signals of both probes colocalize, then  $M_1$  is equal to 1. In Figure 4.8, an example is given that highlights different scenarios of probe colocalization. There are two extreme cases, where the two signal colocalize well (black) or do not colocalize at all (red). The more realistic cases are indicated in orange and green. The orange dots imply that most of the first signal colocalized with the other ( $M_1$  is high), but most of the second signal does not colocalize with the first one ( $M_2$  is low). Finally, the inverse is in green.



In this study, the cells with internalized viruses will exhibit a low M1, if most of the virus signal after permeabilization stems from viruses on the inside of the cell (i.e., the green dye would not colocalize well with the orange dye, because it captures both the large, internalized fraction of the virus as well as the smaller external fraction, whereas the orange dye only captures the external fraction). The area in which the cells are considered as positive for internalized viruses are delimited by the red lines in Figure 4.8. The corresponding M1-M2 plots for the time-lapse experiment are shown in Figure 4.8 (2<sup>nd</sup> and 3<sup>rd</sup> rows). Except for 2h, several cells are present in the parts of the graphs indicating cells with internalized viruses.

Determining the area of virus signal within the cell, or the Mander's coefficient method, the number of cells with internalized viruses can be determined and their percentage with respect to the total number of cells observed are shown in Figure 4.9 below. With the Mander's coefficient methods we obtained a lower proportion of virus-positive cells. This may be explained by the a quite conservative choice of the area of positive cells. However, even though absolute percentage differ with the method, the proportion of positive cells increased with time.

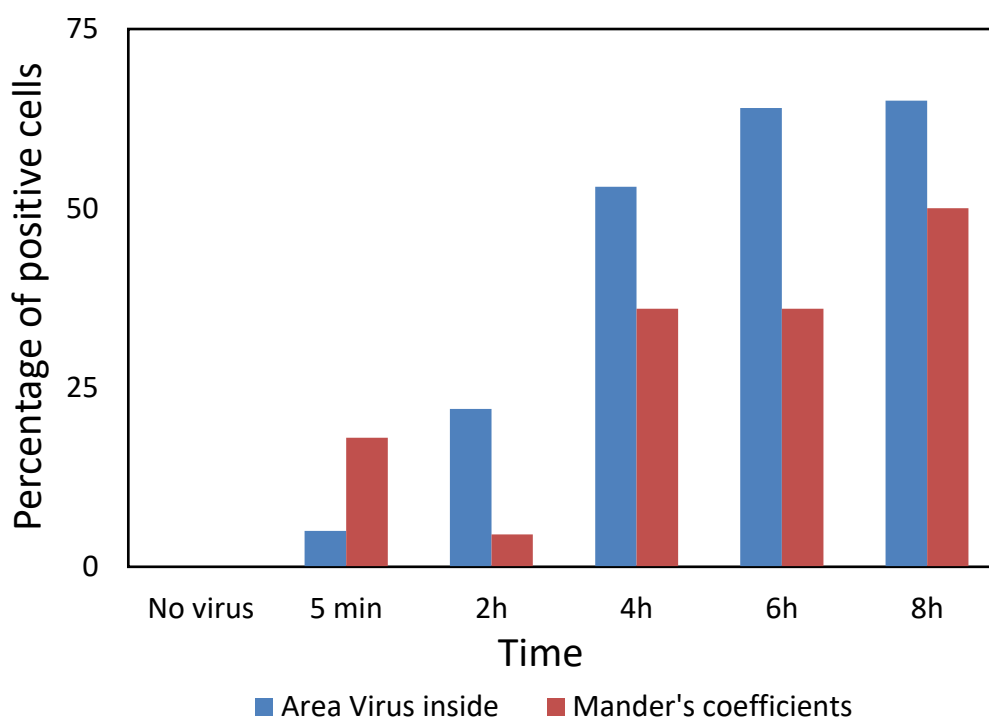


Figure 4.9 Virus-positive cells as a percentage of the total cell number, calculated using the area of virus signal inside the cells (blue) and the Mander's coefficients (orange)

#### 4.5.2 Disinfection

In order to measure the loss of virus internalization or replication after ozone treatment, we did not conduct a full time-lapse analysis, but instead analyzed two relevant time points. In order to observe internalization of treated virus, confounding effects of replication has to be avoided. In contrast, replication does have to be occurring in order to detect it. Based on our time-lapse test and on literature data<sup>117</sup>, we analyzed the extent of virus internalization at 1h post-infection, and the replication at 7h post-infection.

E11 was inactivated by ozone by 5 log<sub>10</sub> and the measured infective concentration in the treated sample was  $3.2 \times 10^3$  MPN/ml (compared to  $9.5 \times 10^8$  MPN/ml for the control). The corresponding microscopy images for the control and inactivated samples are shown in Figure 4.10. This figure shows cells with virus signals before and after cell permeabilization together with staining of dsRNA to indicate replication. After 7h, cells had a round shape and exhibited cytopathic effect (CPE). DAPI indicates nuclear fragmentation due to cell apoptosis, especially 7h post-infection, as previously described for other viruses,<sup>122</sup> unfortunately the shapes of the signal prevent the Cell Prolifer to correctly recognize the nucleus. The DAPI channel was, therefore, not used in the image analysis. Instead, only cellmask was used to define and count the number of cells.

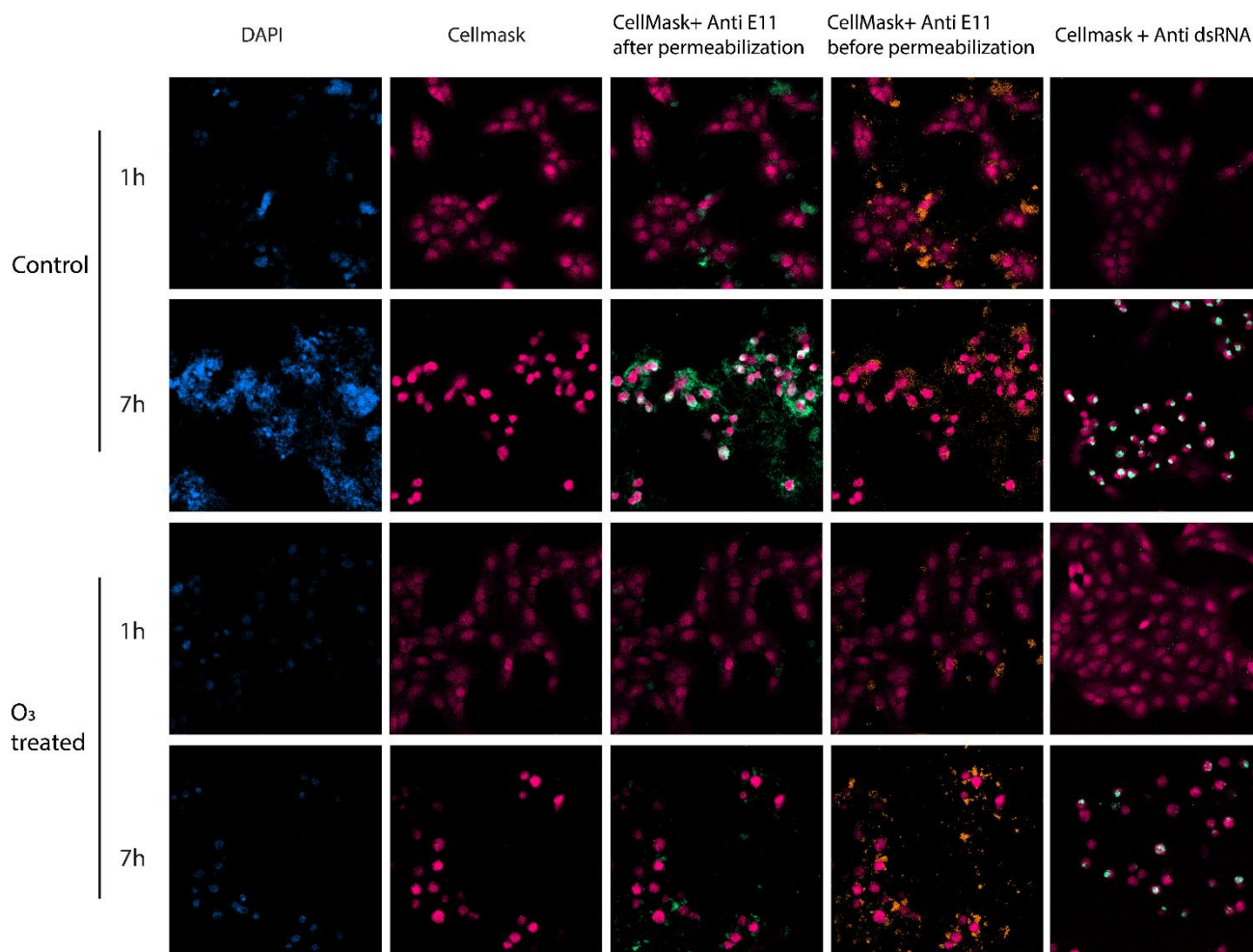


Figure 4.10 Selection of images analysed to observe loss of internalization or replication with and without ozone treatment. Nucleic acid (DAPI), cells (CellMask), the virus (before and after cell permeabilisation) and dsRNA were stained 1h or 7h post-infection.

A quantitative analysis of the effect of ozone on E11 internalization and replication are summarized in Figure 4.11. Virus internalization after ozone treatment is significantly lower than the control ( $p\text{-value} < 2 \times 10^{-12}$ ) for both 1- and 7-hours post-infection. The mean signal intensity per cell after 1h for the ozone treated sample is lower than the positive threshold, though several positives cells were observed. Whereas 70% of the cells in the untreated sample showed a virus signal intensity higher than the threshold limit, this proportion drop to 25% in the treated sample. This difference diminished at 7h post-infection, with respectively 97 and 92% of positive cells. However, this could be expected as most of the cells exhibited cytopathic effect after 7h in this experiment. The Mander's coefficient plots are presented in the Figure S4.1. Due to the relatively conservative threshold chosen previously, no cells were considered positive 1h post-infection. Nevertheless,



7h post-infection showed a clear shift with 52% of positive cells in the control sample. For the ozone treated sample, the shift is less important, with only 15% of virus-positive cells.

For virus internalization, the ozone treated sample showed significant loss of internalized virus (25% +cells) after 1h compared to the control sample (70% +cells). After 7h, the difference of internalization increased in both sample to 92% and 97% +cells. However, the mean area is significantly lower for the O<sub>3</sub> treated sample ( $p < 1e-16$ ).

For replication, the ozone treated sample exhibited a significantly lower signal intensity per cell than the control at 7h post-infection ( $p$ -value = 0.0003, respectively). In addition, at 7h post infection, 92% of the cells were replication positive in the control, whereas only 66% of the cells were positive for the ozone treated sample. In contrast, the mean signal intensity per cell measured 1h post-infection stayed below the positive thresholds for both samples.

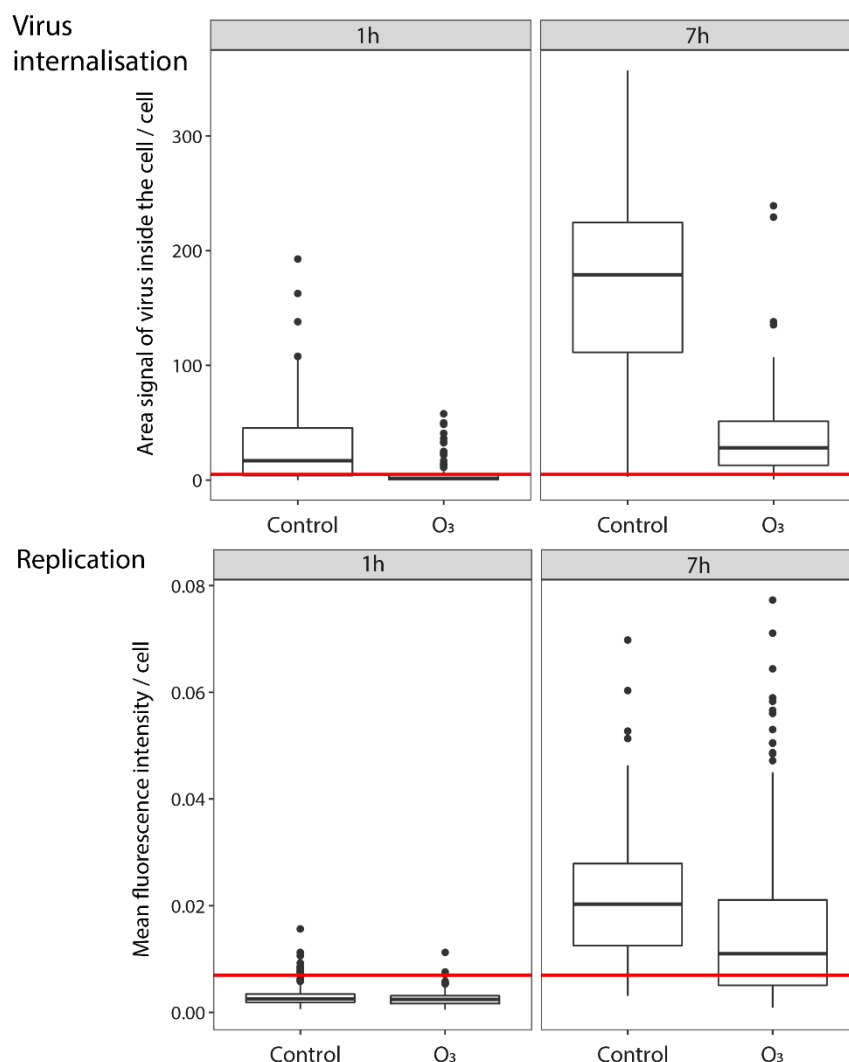


Figure 4.11 Comparison of the area of virus signal within the cells and replication signal mean intensity between control and treated sample.

In conclusion, in this chapter we demonstrate how internalization and replication evolve in time during E11 infection. Preliminary results with ozone treated samples indicate that ozone reduces internalization of the virus. In addition, a loss of replication is also observed. However, it is not known if this loss a consequence of lower internalization of treated samples compared to the control, or a consequence of genome damage induced by ozone, as suggested by Torrey *et al.*<sup>111</sup> Future work should focus on validating the experimental procedure and the image analysis process, and on including additional inactivating treatments with known mechanisms to validate the assays.

## 4.6 ACKNOWLEDGMENTS

This research was funded by the Swiss National Science Foundation (Grant 205321\_169615). Romain Guiet is acknowledged for advice in method and image analysis development and for kindly providing a code and a pipeline for the internalization assay analysis. Silke Sertz is acknowledged for kindly sharing her staining protocols.

## Chapter 5 Conclusion

Increased water demands, due to population growth and climate change, challenges safe drinking water production. This may encourage new drinking water production scheme, such as potable water reuse. As highlighted in the introduction, two main actions can be undertaken to ensure water safety. First, protect water reservoir by enhancing wastewater treatment prior to the discharge and second, add more barriers during drinking water production. Advanced oxidative treatment, such as ozonation, may be involved in either wastewater and drinking water treatment.

This thesis focused on understanding inactivation of waterborne viruses by ozone. These viruses are highly relevant because they represent a threat to human health and a barrier to safe drinking water and potable water reuse, with severe consequences, such as large viral diarrhea outbreaks, if not correctly inactivated during treatment.<sup>123</sup> Several other disinfectants have been studied, but ozone presents several advantages over others. Lower exposure is expected due to its high reactivity, and overall a better efficiency. Nevertheless, information on ozone inactivation kinetics of virus remained scarce and poorly understood.

In Chapter 2, the inactivation rate constants of 9 different viruses and bacteriophages were resolved, including two environmental strains. A simplified buffered water matrix was chosen to well characterize  $k_{O_3\text{-virus}}$  in a controlled system. Physical parameters, such as pH and temperature and their effect on  $k_{O_3\text{-virus}}$  were also investigated. These estimates provide a basis for quantitative microbial risk assessment (QMRA) of potable water reuse scheme that include ozonation. The benefits of applying ozonation may be better assessed and compared to other alternatives. In addition, the experimental method developed to quantify low ozone exposure inactivation may be applied to other pathogens.

In Chapter 3, these constants were challenged in both surface waters and wastewater secondary effluents. As expected, a deviation from simple linear model was observed due to interaction with matrix constituents. Since ozone exposure is not practical to be measured during treatment, especially for low specific ozone doses, tools were needed to measure treatment efficiency. Therefore, several proxies were tested in lab and pilot experiments for virus inactivation prediction during ozonation. These proxies may inform treatment plant operator on the expected virus inactivation during ozonation.

Additionally, an immunostaining procedure was developed to study virus internalization and replication. Preliminary results are presented in Chapter 4 and seem to indicate that ozone may induce a loss of internalization, and replication loss was also observed. However, it was not possible to differentiate the loss induced by the loss of internalization or by genome damage.

## 5.1 Main conclusion and implications

### 5.1.1 Virus inactivation in buffered system

The efficiency of ozone against viruses has been confirmed and fast inactivation kinetics were measured. Although inactivation kinetics depend on the virus species,  $k_{O_3\text{-virus}}$  was typically in the range of  $10^5\text{-}10^6\text{ M}^{-1}\text{s}^{-1}$ . Therefore, even the two genotypes of CVB5 that were the most resistant to ozone were still well inactivated. An increased temperature or pH increase  $k_{O_3\text{-virus}}$ , however, the magnitude of these effects remains relatively small. These experiments showed that inactivation has a log-linear relationship with ozone exposure.

Table 5.3 Parameters influencing  $k_{O_3\text{-virus}}$  in buffered water matrix by decreasing importance.

$O_3$ exposure	>	Viruses species	>	Temperature	>	pH
----------------	---	-----------------	---	-------------	---	----

Given the variety of virus capsid structures and genomes studied, the  $k_{O_3\text{-virus}}$  remained relatively high. Therefore, we can expect similar kinetics for other virus species. The implication of fast inactivation kinetics is that a low ozone exposure is sufficient to achieve treatment goals. As a result, the risk of disinfection byproducts (DBPs) produced during ozonation is also low. However, viruses are not the most resistant waterborne pathogens to ozone, and generally *C. parvum* oocyst is the main treatment target to determine the disinfectant exposure. In this case, DBPs formation may become a limiting factor.

Finally, knowledge of  $k_{O_3\text{-virus}}$  will benefit quantitative microbial risk assessments. Specifically, they will reduce the uncertainties with respect to the extent of inactivation achieved when evaluating risks of water matrices treated by different treatment trains.

### 5.1.2 Virus inactivation in natural matrices

Due to interaction with dissolved organic matter (DOM), inactivation curves in natural matrices deviated from the log-linear dependence on ozone exposure, and instead exhibited a strong tail. Despite these complex kinetics, this study confirmed the potential of  $\Delta UV_{254}$  and carbamazepine (CBZ) abatement as proxies for virus inactivation by ozone. The specific ozone dose also provided a good prediction of virus inactivation, even though it does not serve as a real-time monitoring tool during treatment.

The inactivation of MS2 and CVB5 were similar, despite the fact that their inactivation rate constants in homogenous buffer solutions vary by a factor ten. As such, a single proxy-inactivation relationship can be applied to several viruses. In contrast, the origin of DOM (lakewater or wastewater), influenced the proxy-inactivation relationship, though the DOM content did not. The exception is CBZ abatement, which was independent on the water type. In fact, due to their similar kinetics, both virus inactivation and CBZ abatement depend on the intrinsic ozone exposure, and these two parameters thus vary in concert, independent of the matrix. In contrast, the  $\Delta UV_{254}$  is different in SW and WW, because the UV absorbing moieties present are different.

Finally, we were able to test and validated the proxy-inactivation relationships during a pilot plan experiment in lake water. The model predictions of virus inactivation were reasonably good for all proxies investigated. The ability to predict new data confirms the potential of such relationships to estimate virus inactivation during ozonation. An overview over the benefits and limitations of the different proxies tested is given in Table 5.5.

Table 5.5 Review of proxies studied, their advantages and limitations

Proxy	Advantages	Limitations
Specific O <sub>3</sub> dose	Easy, applicable in all range of [DOC]	No online monitoring
$\Delta UV_{254}$	Already in use in TP Online monitoring	Not applicable in low [DOC]
CBZ abatement	Applicable in low and high [DOC] water	More expensive

Implications of this research in practice is a tool for treatment operators to monitor in real-time the efficiency of ozonation for inactivate viruses. In addition, proxies may be proposed as validation tools for ozone treatment, especially in the case of potable water reuse. 4 Log<sub>10</sub> removal credit are currently attributed to ozonation followed by biological filtration. However, this removal credit can increase if higher inactivation can be proven and verified. More than 7 log<sub>10</sub> inactivation were observed in wastewater during pilot testing and up to 5 log<sub>10</sub> in lab experiments for specific ozone doses typically applied for micropollutant abatement (0.5-0.6 mgO<sub>3</sub>/mgDOC). Therefore, waterborne viruses may be inactivated with relatively low specific ozone dose, and their disinfection may not induce the formation of problematic DBPs such as bromate.

Bayesian modeling is a useful tool in the context of inactivation by ozonation. Model parameter estimates in this work can be used as prior knowledge when constructing a model to predict inactivation in a specific treatment plant. These parameters can be “upgraded” with measures on-site to obtain a model that better represents the situation of a specific plant. Additionally, Bayesian models can handle censored data and construct a probability distribution of the expected inactivation. This may be more relevant in the frame of risk assesement and control of water safety.

### 5.1.3 Virus inactivation mechanism

Preliminary results shows a reduced internalization and replication after ozone disinfection. However, it is not clear yet if the decrease of replication is due to the reduction of virus internalization.

**Virus internalisation seems to be impaired by ozone treatment**

## 5.2 Limitations and further work

While virus kinetics were broadly studied in this thesis, two important viral pathogens that cause the majority of the viral gastroenteritis worldwide, rotavirus and norovirus, were not experimentally investigated. Given the high reactivity of ozone, we expect these viruses to present similar inactivation kinetics as the rest of virus species studied. However, experimental validation may be important to confirm their susceptibility to ozone.

In order to apply proxies as predictive tools in water treatment, further testing may help to validate the current model and to account for variability among matrices. In addition, model validation in a wastewater pilot plant will be valuable in order to confirm that high inactivation can be achieved. More variability may be expected in wastewater matrices compared to surface water. In the case of potable water reuse, we may expect that the wastewater model for the specific ozone dose and the UV absorbance reduction may correspond better than the surface water model. However, this will depend where ozonation is applied in the treatment train and the different treatments applied upstream.

Experiments presented in Chapter 4 need further replication in order to support the preliminary findings. In addition, exchanging the dye used for the internalization assay is necessary to verify that similar results are obtained. The experimental procedure for coxsackievirus B5 should be optimized and the results post-disinfection should be compared to echovirus 11 to determine if there is a difference in internalization ability. Internalization of viruses treated with other disinfectants could also be studied. Finally, fluorescence flow cytometry can be used to study the host binding.

In conclusion, this thesis provides new information on the efficacy of ozone disinfection of waterborne viruses with implications in research and for water treatment. Furthermore, as practical outcomes, it delivers tools to monitor virus inactivation during water and wastewater treatment in real-time.

## Supporting information for Chapter 2

### Chemicals and solutions

Sodium chloride (NaCl), sodium monophosphate ( $\text{NaH}_2\text{PO}_4$ ) and sodium di-phosphate ( $\text{Na}_2\text{HPO}_4$ ) were purchased from Acros. EDTA ( $\text{C}_{10}\text{H}_{12}\text{O}_8\text{CaN}_2\text{Na}_2 \cdot 2\text{H}_2\text{O}$ ) was purchased from Carl Roth GmbH. Trans-cinnamic acid ( $\text{C}_6\text{H}_5\text{CHCHCOOH}$ ; recrystallized for quenched-flow experiments), tert-butanol (2-methyl-2-propanol), carbamazepine ( $\text{C}_{15}\text{H}_{12}\text{N}_2\text{O}$ ), benzaldehyde ( $\text{C}_7\text{H}_6\text{O}$ ) and 1 M HCl were purchased from Sigma-Aldrich. HPLC grade solvents were purchased from Biosolve chimie SARL.

### Phages and bacteria

Coliphages MS2 (DSMZ 13767),  $\Phi$ X174 (DSMZ 4497) and their host *Escherichia coli* (DSMZ 5695 and DSMZ 13127) were purchased from the German Collection of Microorganisms and Cell Cultures (DSMZ, Braunschweig, Germany). Coliphage Q $\beta$  was provided by Joan Jofre (University of Barcelona), and coliphage T4 and its *E. coli* B1 host were supplied by Petr Leiman (École Polytechnique Fédérale de Lausanne, Switzerland). All phages were propagated and enumerated as described previously,<sup>55</sup> except that *E. coli* B1 was grown in the absence of antibiotics.

### Viruses and cells

Human adenovirus (HAdV) type 2 was kindly provided by Rosina Gironès (University of Barcelona). Echovirus (EV) type 11 Gregory strain (ATCC VR-41) and coxsackievirus (CVF) B5 Faulkner strain (ATCC VR-185), were purchased from LGC Standards (Molsheim, France). Two environmental strains of coxsackievirus B5 (CVLEnv1 and CVLEnv2) were isolated from the Vidy wastewater treatment plant (Lausanne, Switzerland) on 03/03/2015 and 06/08/2015, respectively, as described elsewhere.<sup>124</sup> HAdV was propagated on A549 human lung carcinoma epithelial cells and EV, CVF, CVLEnv1 and CVLEnv2 on buffalo green monkey kidney (BGMK) cells. Viruses were propagated and purified using the PEG- chloroform procedure as reported previously.<sup>55</sup> A549 cells were kindly provided by the Lausanne University Hospital (Switzerland) and BGMK cells by the Spiez Laboratory (Switzerland). A549 cells were cultivated in high-glucose pyruvate Dulbecco's modified Eagle's medium (DMEM; Invitrogen), and BGMK cells were cultivated in minimum essential medium (MEM; Invitrogen). Both media were supplemented with penicillin ( $20 \text{ U mL}^{-1}$ ; Invitrogen), streptomycin ( $20 \mu\text{g mL}^{-1}$ ; Invitrogen), and 2 or 10% fetal bovine serum (FBS; Invitrogen), and cells were incubated at  $37^\circ\text{C}$  in 5%  $\text{CO}_2$  and 95% humidity.

## Procedure for the purification of MS2 by QA monolith liquid chromatography

A MS2 culture in broth was supplemented with 5 mL of chloroform and stored overnight, then centrifuged and filtered through a 0.45 µm membrane (Millipore). Samples were then purified with a CIM monolith column (QA 1 mL, BIA Separation) mounted onto an ÄKTA pure 150 LC system (GE healthcare). The column was equilibrated according to manufacturer instructions. A 5 mL/min flow rate was used to load the MS2 broth in VDB pH 7.5 (1:1) onto the column. MS2 was eluted by a step-gradient using milliQ water and 2M NaCl as detailed in Table S2.1. The MS2 peak was identified by UV absorbance at 280 nm and by testing for the presence of infective virus by a plaque assay, and the corresponding fraction was collected and concentrated using a 100K Amicon ultrafiltration column (Millipore).

Table S2.1 : Step-gradient sequence applied for MS2 purification by monolith QA.

Column volumes	% NaCl eluent
5	2.5-6
12	6
5	6-16
12	16
5	16-33
10	33
5	33-100
5	100



## Activation energy for the reaction of trans-cinnamic acid with ozone

O<sub>3</sub> was reacted with an excess of CA (1:10 molar ratio) at various temperatures (5 to 35°C). The absorbance at 266 nm was recorded after a dead time of 1.5 ms to follow the decrease of CA concentration over time. Hereby the degradation of CA was maximally 10 %, such that pseudo-first-order conditions were maintained. The software Kinetic Studio<sup>125</sup> was used to fit the apparent pseudo first-order rate constant ( $k_{obs}$ ; Equation S2.1).

Equation S2.1 Pseudo first-order rate CA reaction with ozone

$$\frac{d[CA]}{dt} = k_{obs}[O_3]$$

where  $k_{obs} = k_{O_3-CA}[CA]$

To obtain the second-order rate constant ( $k_{O_3-CA}$ ) at a given temperature,  $k_{obs}$  was divided by the CA concentration. Finally, the activation energy  $E_a$  was obtained using the Arrhenius equation as shown in Figure S2.1

Equation S2.2 Arrhenius equation

$$\ln(k) = \frac{-E_a}{RT} + \ln(A)$$

Table S2.2 presents the pseudo first-order reaction rate constants ( $k_{obs}$ ) and related second order reaction rate constants ( $k_{O_3-CA}$ ) for the reaction of  $O_3$  with CA and the temperature at which they were measured. The values of  $k_{O_3-CA}$  are used in the Arrhenius plot (Figure S2.1) to determine the activation energy of the reaction. Values of  $k_{O_3-CA}$  calculated based on the Arrhenius equation for the three temperatures investigated in this work are shown in Table S2.3.

Table S2.2 Reaction rate constants at different temperatures, measured by stopped-flow for the reaction of trans-cinnamic acid and ozone.  $k_{obs}$  is the pseudo first-order rate constant of  $O_3$  consumption in excess of CA, and  $k_{O_3-CA}$  is the second-order rate constant of the reaction of  $O_3$  with CA.

Temp (°C)	1/T (K <sup>-1</sup> ) x10 <sup>3</sup>	$k_{obs}$ (s <sup>-1</sup> )	$k_{O_3-CA}$ (M <sup>-1</sup> s <sup>-1</sup> )	ln( $k_{O_3-CA}$ )
10.5	3.525	33.00	5.34 x 10 <sup>5</sup>	13.189
9	3.544	30.67	4.97 x 10 <sup>5</sup>	13.116
10.3	3.528	30.73	4.98 x 10 <sup>5</sup>	13.117
10	3.532	29.85	4.83 x 10 <sup>5</sup>	13.088
9.7	3.535	31.11	5.04 x 10 <sup>5</sup>	13.130
15.9	3.460	38.00	6.15 x 10 <sup>5</sup>	13.330
16.1	3.457	36.90	5.97 x 10 <sup>5</sup>	13.301
16.2	3.456	35.70	5.78 x 10 <sup>5</sup>	13.267
16.1	3.457	37.26	6.03 x 10 <sup>5</sup>	13.310
16.1	3.457	35.97	5.82 x 10 <sup>5</sup>	13.275
21.1	3.398	48.46	7.85 x 10 <sup>5</sup>	13.573
20.9	3.401	45.50	7.37 x 10 <sup>5</sup>	13.510
20.9	3.401	43.60	7.06 x 10 <sup>5</sup>	13.467
21	3.400	43.13	6.98 x 10 <sup>5</sup>	13.456
21.1	3.398	43.12	6.98 x 10 <sup>5</sup>	13.456
29.5	3.304	58.23	9.43 x 10 <sup>5</sup>	13.757
29.5	3.304	57.03	9.23 x 10 <sup>5</sup>	13.736
29.6	3.303	57.15	9.25 x 10 <sup>5</sup>	13.738
29.5	3.304	57.99	9.39 x 10 <sup>5</sup>	13.752
29.5	3.304	52.11	8.44 x 10 <sup>5</sup>	13.646
34.9	3.246	66.63	1.08 x 10 <sup>6</sup>	13.891
34.9	3.246	62.46	1.01 x 10 <sup>6</sup>	13.827
34.9	3.246	61.16	9.90 x 10 <sup>5</sup>	13.806
34.9	3.246	61.58	9.97 x 10 <sup>5</sup>	13.813
34.9	3.246	62.84	1.02 x 10 <sup>6</sup>	13.833

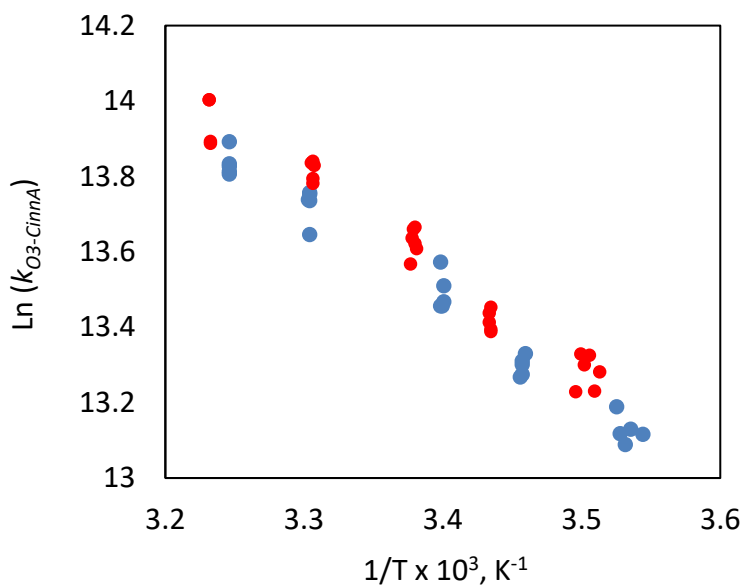


Figure S2.1 Arrhenius plot of  $k_{O3-CA}$  versus temperature, where the slope corresponds to  $E_a/R$ . Two replicate experiments are highlighted in blue and red.

Table S2.3 : Second order rate constants  $k_{O3-CA}$  for the reactions of CA with ozone at 2, 12 and 22°C, calculated using the Arrhenius equation and an activation energy of 21.2 kJ mol<sup>-1</sup>.

Activation Energy, [kJ mol <sup>-1</sup> ]	21.2 ± 0.72
$k_{O3-CA}$ at 2°C, [M <sup>-1</sup> s <sup>-1</sup> ]	4.0 x 10 <sup>5</sup>
$k_{O3-CA}$ at 12°C, [M <sup>-1</sup> s <sup>-1</sup> ]	5.6 x 10 <sup>5</sup>
$k_{O3-CA}$ at 22°C, [M <sup>-1</sup> s <sup>-1</sup> ]	7.6 x 10 <sup>5</sup>

## HPLC analyses

In virus ozonation experiments, benzaldehyde was quantified using an EC 125/3 Nucleosil 100-5-C18 column (Marcherey-Nagel) on an Agilent Infinity II 1260 (Agilent Technologies) HPLC with a multiple wavelength diode array detector recording the absorbance at 254 nm. 20  $\mu$ L of the sample were injected and an isocratic flow (85% milliQ water/ 15% Acetonitrile) with a flow rate of 1 mL/min. The benzaldehyde retention time was 6 min, the limit of detection (LOD) was 0.17  $\mu$ M and the limit of quantification (LOQ) was 0.6  $\mu$ M. The measured benzaldehyde concentrations ranged from 10-175  $\mu$ M. Alternatively, after quench-flow experiments, benzaldehyde was quantified using an Ultimate 3000 HPLC system (ThermoScientific, Sunnyvale, CA, USA) with a multiple wavelength diode array detector (250 nm). The injection volume was 50  $\mu$ L, and an isocratic flow (60% 10mM H<sub>3</sub>PO<sub>4</sub>/40% MeOH) was used on a Cosmosil-C18-MS-II column (100 mmx 3.0mm ID, 5 $\mu$ m; Nacalai Tesque Inc., Kyoto, Japan) with a flow rate of 1 mL/min. The retention time was 7.8 min, the LOD was 0.04  $\mu$ M and the LOQ was 0.13  $\mu$ M. Benzaldehyde concentrations were measured over the range of 4-6  $\mu$ M.

In carbamazepine (CBZ) ozonation experiments, benzaldehyde and CBZ were quantified simultaneously using the Ultimate 3000 HPLC system described above. A gradient methods (details in Table S2.6) was used on a Cosmosil-C18-MS-II column (100 mmx 3.0mm ID, 5 $\mu$ m; Nacalai Tesque Inc., Kyoto, Japan) with a flow rate of 1 mL/min. UV absorbances at 250nm (benzaldehyde) and 285nm (CBZ) were recorded. 50  $\mu$ L of the sample were injected, and the retention times were 7.8 min and 9.5 min for benzaldehyde and CBZ, respectively. CBZ had an LOD of 0.003  $\mu$ M and an LOQ of 0.009  $\mu$ M. The CBZ concentration range measured was 0.7-2  $\mu$ M, and the benzaldehyde concentration range was 25-35  $\mu$ M.

## Experimental details for quench-flow experiments to measure the kinetics of MS2 inactivation

Table S2.4 : Ozone concentration [O<sub>3</sub>], flow rate, aging time, ozone exposure and corresponding MS2 inactivation (ln(N/N<sub>0</sub>)) for quench-flow experiments using a 500 µL loop. Asterisks (\*) indicate blank samples used to determine the initial O<sub>3</sub> concentration. In the blank samples, the ozone exposure was not determine (ND).

[O <sub>3</sub> ], [µM]	Flow rate, [µL/ms]	Aging time, [ms]	Ozone exposure, [M s]	ln(N/N <sub>0</sub> )
6.66	2.50	53	ND	*
6.02	2.50	53	3.32E-07	-5.26
5.98	1.67	79	4.96E-07	-5.50
6.02	1.25	105	6.58E-07	-9.65
5.97	0.83	158	9.77E-07	-12.63
5.82	0.63	211	1.29E-06	-13.76
5.75	0.56	237	1.44E-06	-13.50
5.70	0.42	316	1.90E-06	-14.05
5.70	0.36	369	2.19E-06	-14.46
5.28	0.31	422	2.48E-06	-14.28
6.37	2.50	53	3.32E-07	-5.84
5.44	2.50	53	ND	*
5.57	2.50	53	ND	*
4.92	2.50	53	3.33E-07	-5.02
4.77	1.67	79	4.98E-07	-6.26
4.90	1.11	118	7.43E-07	-6.97
4.86	1.00	132	8.24E-07	-8.41
4.81	0.83	158	9.86E-07	-10.43
4.80	0.71	184	1.15E-06	-11.11
4.80	0.63	211	1.31E-06	-9.65
4.68	0.42	316	1.93E-06	-13.16
4.53	0.28	475	2.84E-06	-13.48
4.40	0.25	528	3.13E-06	-14.27
5.10	2.50	53	3.33E-07	-4.68
5.40	2.50	53	ND	*
5.32	2.50	53	3.32E-07	-3.87
5.31	1.67	79	4.95E-07	-5.92
5.26	1.11	118	7.37E-07	-7.41
5.13	1.00	132	8.17E-07	-8.32
5.19	0.83	158	9.76E-07	-9.93
5.02	0.71	184	1.13E-06	-11.43
4.91	0.63	211	1.29E-06	-11.64
4.73	0.42	316	1.89E-06	-10.87
4.30	0.28	475	2.75E-06	-13.09
4.10	0.25	528	3.02E-06	-13.03

## Experimental details for quench-flow experiments to measure the kinetics of carbamazepine (CBZ) abatement

Table S2.5: Loop volume, ozone concentration [O<sub>3</sub>], aging time, flow rate, ozone exposures and corresponding CBZ abatement (ln (CBZ/CBZ<sub>0</sub>)) for quench-flow experiments. Asterisks (\*) indicate blank sample used to the initial O<sub>3</sub> concentration. In the blank samples, the ozone exposure was not determine (ND).

Loop volume, [μL]	[O <sub>3</sub> ], [M]	Flow rate, [μL/ms]	Aging time, [ms]	Ozone exposure, [M s]	Ln (CBZ/CBZ <sub>0</sub> )
40	3.46E-05	0.20	6	ND	*
	3.46E-05	0.20	6	2.08E-07	-0.15
	3.36E-05	0.09	14	4.50E-07	-0.27
	3.25E-05	0.05	24	7.87E-07	-0.43
	3.11E-05	0.04	30	9.40E-07	-0.50
	3.17E-05	0.029	42	1.34E-06	-0.70
	3.12E-05	0.025	48	1.51E-06	-0.77
	3.14E-05	0.02	60	1.90E-06	-0.96
500	3.06E-05	2.5	53	ND	*
	3.01E-05	2.5	53	1.59E-06	-1.14
	2.93E-05	1.1	118	3.48E-06	-2.15
	2.98E-05	0.83	158	4.72E-06	-2.84
	2.85E-05	0.62	211	6.02E-06	-3.70
	2.87E-05	0.55	238	6.82E-06	-4.15
	2.91E-05	2.5	53	1.54E-06	-0.97

## HPLC method to measure benzaldehyde and carbamazepine (CBZ)

Table S2.6 : Eluent gradient to analyze benzaldehyde and CBZ by HPLC

Time, [min]	Flowrate, [mL/min]	Acetonitrile, %	10mM H <sub>3</sub> PO <sub>4</sub> (pH=6.5), %
0	1	10	90
4	1	10	90
10	1	50	50
12	1	50	50
14	1	10	90
19	1	10	90

Comparison of MS2 inactivation measured in batch experiments and by quench-flow.

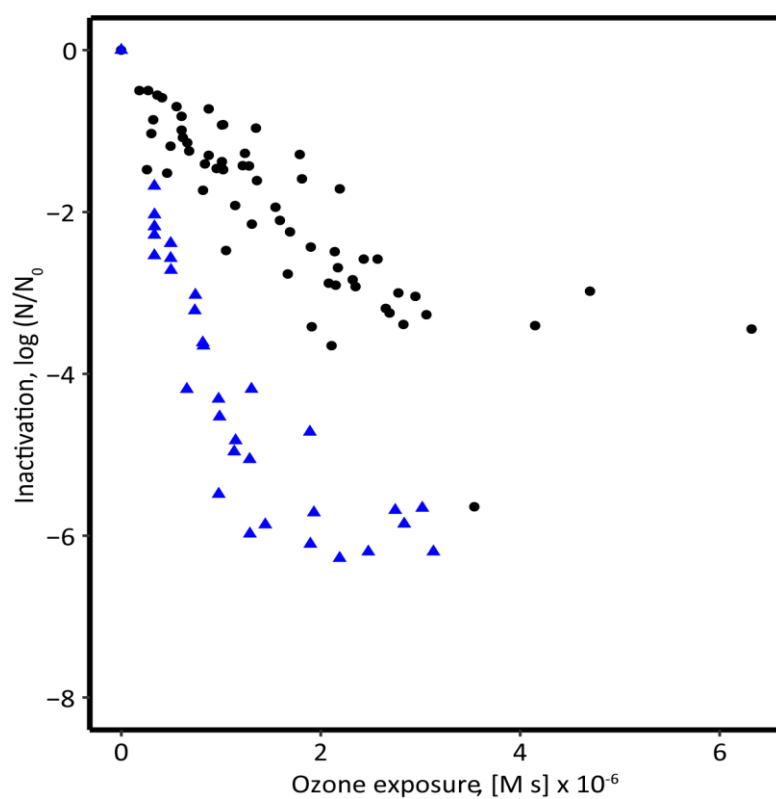


Figure S2.2 MS2 inactivation measured in batch (black dots; 13 replicate experiments) and by quench-flow (blue triangles; three replicate experiments)



## Effect of the purification method on $k_{03-MS2}$

The effect of virus purification on  $k_{03-MS2}$  was assessed by a multiple linear regression model for MS2 inactivation, which includes a “Purification” categorical variable (factor):

Equation S2.3 Statistical model to test for purification effect

$$\ln \left( \frac{N}{N_0} \right) = \beta_0 + \beta_1 * \text{Ozone exposure} + \beta_2 * \text{Purification}$$

Hereby  $\beta_1$  corresponds to the second-order inactivation rate constant determined as a function of the ozone exposure ( $k_{03-MS2}$ ), and  $\beta_2$  is the corresponding coefficient associated with different purification procedures. As shown Table S2.7, PEG-chloroform and liquid chromatography purification yield to equivalent inactivation (p-value > 0.05), while simply filtering the virus-containing broth significantly changed the inactivation kinetics measured.

Table S2.7 MS2 inactivation rate constants and effect of purification procedures, and corresponding F-statistics. A p-value > 0.05 indicates that a sample is statistically equivalent to a representative reference experiment (\*) obtained under “standard conditions”

Purification	$\beta_1$	$\beta_2$	<i>p-value for <math>\beta_2</math></i>
PEG		-	*
CIM/LC	$-2.1 \pm 0.1 \times 10^6$	$0.9 \pm 0.6$	0.14
Filtered broth		$1.93 \pm 0.5$	$5.3 \times 10^{-4}$

## Reproducibility of batch approach and effect of initial virus concentration

For the analysis of reproducibility and replicate variability, thirteen replicate experiments of MS2 inactivation by ozone were performed and the following model was formulated:

Equation S2.4 Statistical model to test the different replicate

$$\ln \left( \frac{N}{N_0} \right) = \beta_0 + \beta_1 * \text{Ozone exposure} + \beta_2 * \text{Replicate}$$

Hereby, “Replicate” was included as categorical variable (factor) to evaluate if different replicates yield different inactivation rate constants. The MS2 inactivation rate constant as a function of ozone exposure ( $k_{\text{O}_3\text{-MS}_2}$ ) corresponds to  $\beta_1$ , and the corresponding coefficient for different replicates is  $\beta_2$ . In Table S2.8, a selection of four replicates is presented. Despite their different MS2 starting concentrations, the observed inactivation is statistically equivalent. This indicates that  $k_{\text{O}_3\text{-MS}_2}$  is independent of the initial MS2 concentration.

Table S2.8 Second-order MS2 inactivation rate constants for experiments conducted at different MS2 starting concentrations, and corresponding F-statistics. A p-value > 0.05 indicates that a sample is equivalent to a representative reference experiment (\*) obtained

MS2, [PFU/mL]	Purification	$\beta_1$	$\beta_2$	p-value
$4 \times 10^8$	PEG	$-2.1 \pm 0.1 \times 10^6$	$0.0 \pm 0.9$	0.98
$2 \times 10^8$	PEG		-	*
$9 \times 10^6$	PEG		$0.4 \pm 0.7$	0.61
$8 \times 10^6$	LC		$-0.8 \pm 0.6$	0.14

Overall, two replicates out of 13 were found to be different from the others (p-values = 0.0001 and 0.0002). However, as shown in Figure S2.3,  $k_{\text{O}_3\text{-MS}_2}$  changed by only about 4 % if this replicate effect was considered, indicating that the influence of replicates, while statistically significant, was biologically negligible.

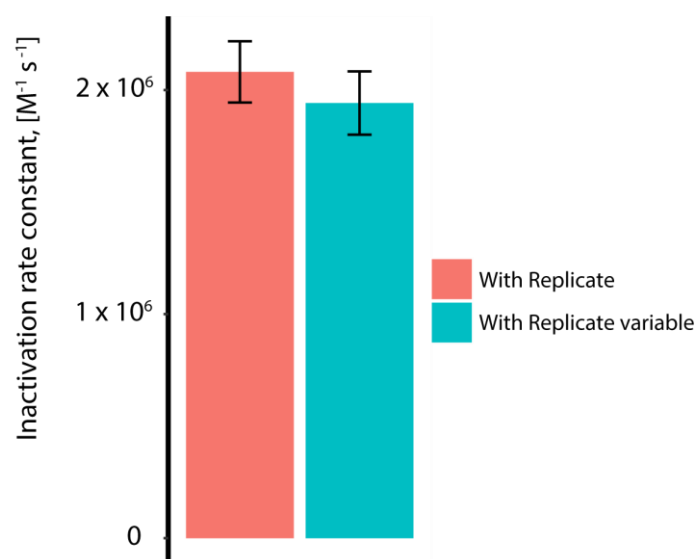


Figure S2.3 Second order MS2 inactivation rate constants for the reaction with ozone obtained by including or excluding the “replicate” variable in the linear model.

## Effect of temperature and pH

The effect of ozone exposure, temperature and pH on  $k_{O3-MS2}$  were assessed using the following multiple linear regression model:

Equation S2.5 Statistical model to infer pH and Temperature effect on inactivation

$$\ln\left(\frac{N}{N_0}\right) = \beta_0 + \beta_1 * \text{Ozone exposure} + \beta_2 * \text{Temp} + \beta_3 * \text{pH}$$

Where the parameters  $\beta_n$  represent the contribution per unit of each variable to the overall inactivation.  $\beta_n$ , standard errors, p-value and adjusted  $R^2$  are presented in Table S2.9. The parameters  $\beta$  associated with all three variables were significantly different from zero, indicating that pH, temperature and ozone exposure all influence virus inactivation by ozone.

Table S2.9 Contributions of the variables ozone exposure, temperature and pH to inactivation, with corresponding F-test statistics.

	$\beta$	p-value	Adjusted $R^2$
Intercept	$5.6 \pm 1.1$	$3.4 \times 10^{-7}$	
Ozone exposure, [M s]	$-2.1 \pm 0.1 \times 10^6$	$<2 \times 10^{-16}$	
Temp, [°C]	$-1.2 \pm 0.1 \times 10^{-1}$	$1.7 \times 10^{-15}$	
pH	$-6.5 \pm 1.3 \times 10^{-1}$	$1.9 \times 10^{-6}$	
Overall model	-	-	0.68

## Activation energy of MS2 inactivation by ozone

The activation energy ( $E_a$ ) of MS2 inactivation by ozone was estimated based on experiments conducted at different temperatures and analyzed by the Arrhenius equation Equation S2.2. Experiments were conducted at two different pH levels. The data are presented in Table S2.10 and Figure S2.4.

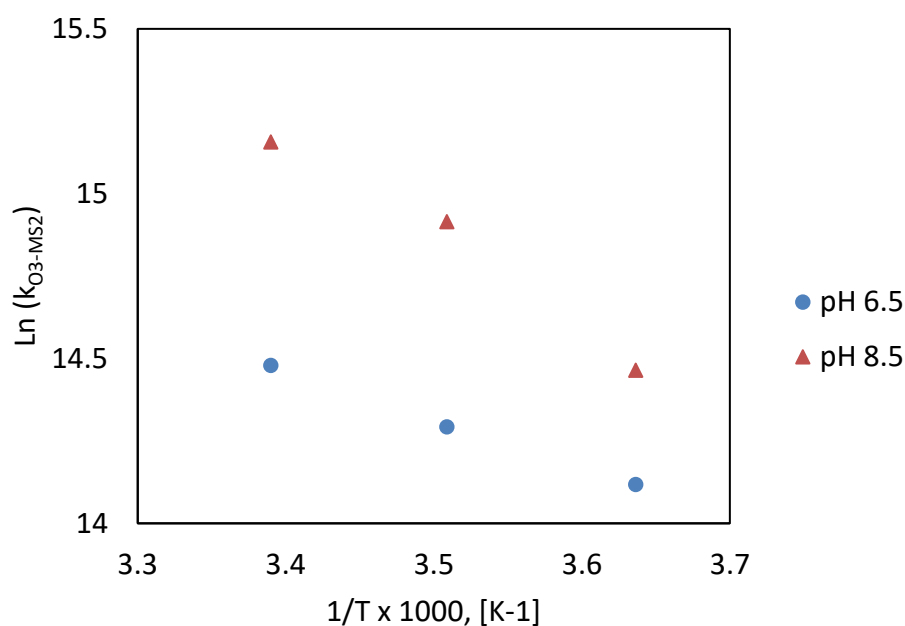


Figure S2.4 pH-dependence of Arrhenius plot for  $k_{O_3-MS2}$  for 2, 12 and 22 °C.

Table S2.10 Data used to estimate activation energy of MS2 inactivation by ozone ( $T= 2, 12, 22^\circ\text{C}$ )

pH	$\ln(k_{O_3-MS2})$	$1/T \times 1000, [K^{-1}]$	Slope	Calculated $E_a$ , [kJ mol <sup>-1</sup> ] from Figure S4
6.5	14.118	3.636	-1.46	~12.2
	14.292	3.509		
	14.479	3.381		
8.5	14.465	3.636	-2.81	~23.4
	14.915	3.509		
	15.157	3.389		

## Supportive information for Chapter 3

### S3.1 O<sub>3</sub> depletion profiles in natural matrices

The following figures show the depletion of the ozone concentration over time for the different specific ozone doses (grey title) in SWB and WW. The decay was measured repeatedly several weeks apart and showed good reproducibility (data not shown).

#### *R script of calc\_ct function*

```
calc_ct<- function(x) {
  #Load the needed library
  library(flux)
  library(caTools)

  #Here data is the ensemble of the data point for ozone decay of the different Ozone dose for 1 specific water
  # Split the data frame into a list according to different doses
  x <- split.data.frame(x, x[, "Dose"])

  CT<- NULL
  d<- NULL
  date<- NULL
  selected_data<- NULL

  #Check if there is duplicate of time points
  for (i in 1:length(x)) {
    #          Select the data corresponding to one dose and order it by Time
    selected_data <- x[[i]]
    selected_data<- selected_data[order(selected_data$Time),]

    #          Calculation of CT & Plot the decay curve
    CT[i]<- auc(selected_data$Time, selected_data$ConcO3)          #Store CT value
    d[i]<- selected_data[1,"Dose"]                                #Store Dose value
    date[i]<- selected_data[1,"Date"]

  }
```

```
# Store data in a new dataframe
exposure <- data.frame(cbind(d,CT, date),stringsAsFactors = FALSE)    #Add CT and dose value, return table
colnames(exposure) <- c("Dose", "Exposure", "Date")
exposure[, "Dose"] <- as.numeric(exposure[, "Dose"])
exposure[, "Exposure"] <- as.numeric(exposure[, "Exposure"])
return (exposure)
}
```

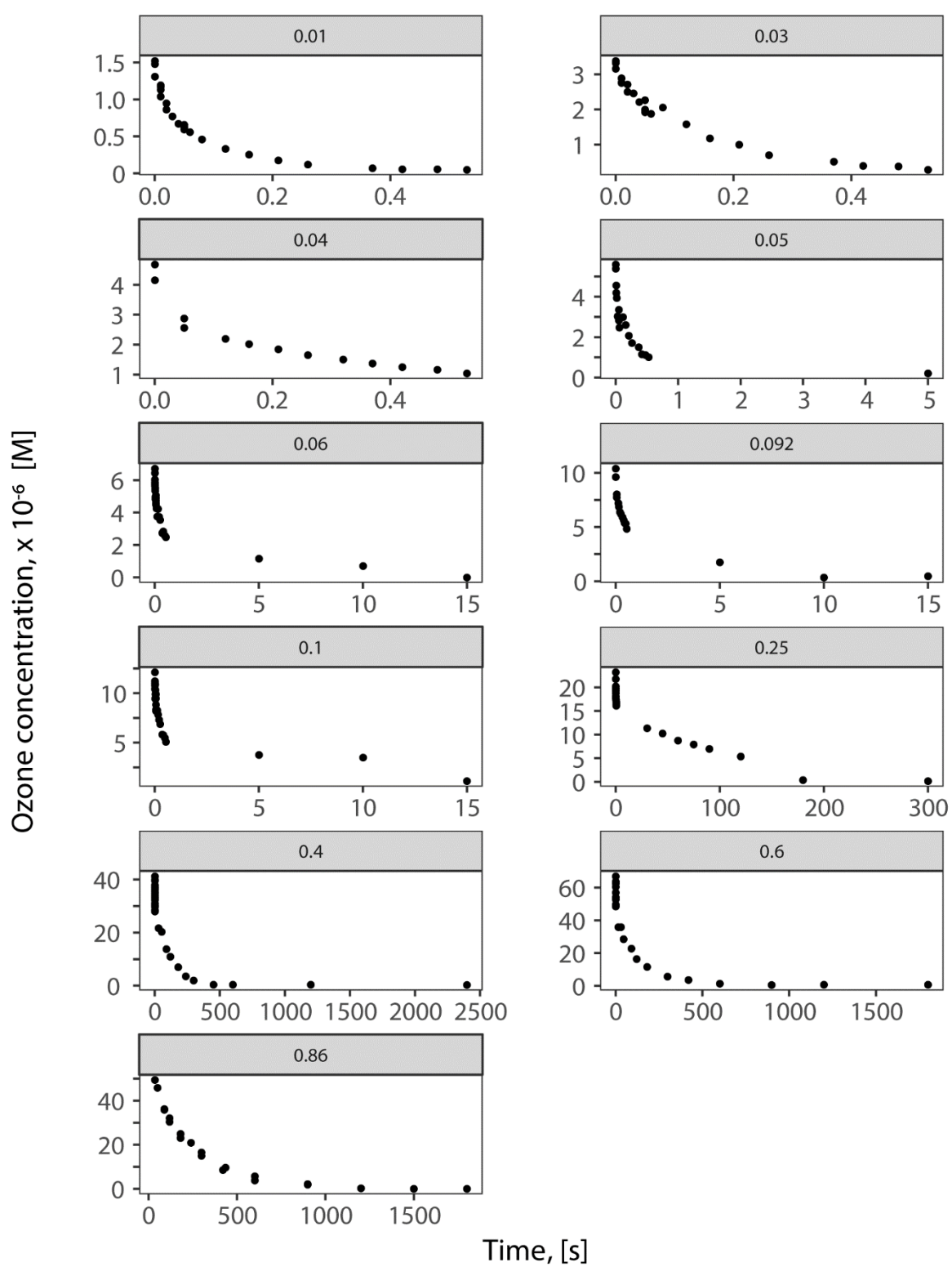


Figure S3.1 Depletion of the ozone concentration over time for the different specific ozone doses (grey title) in SWB.



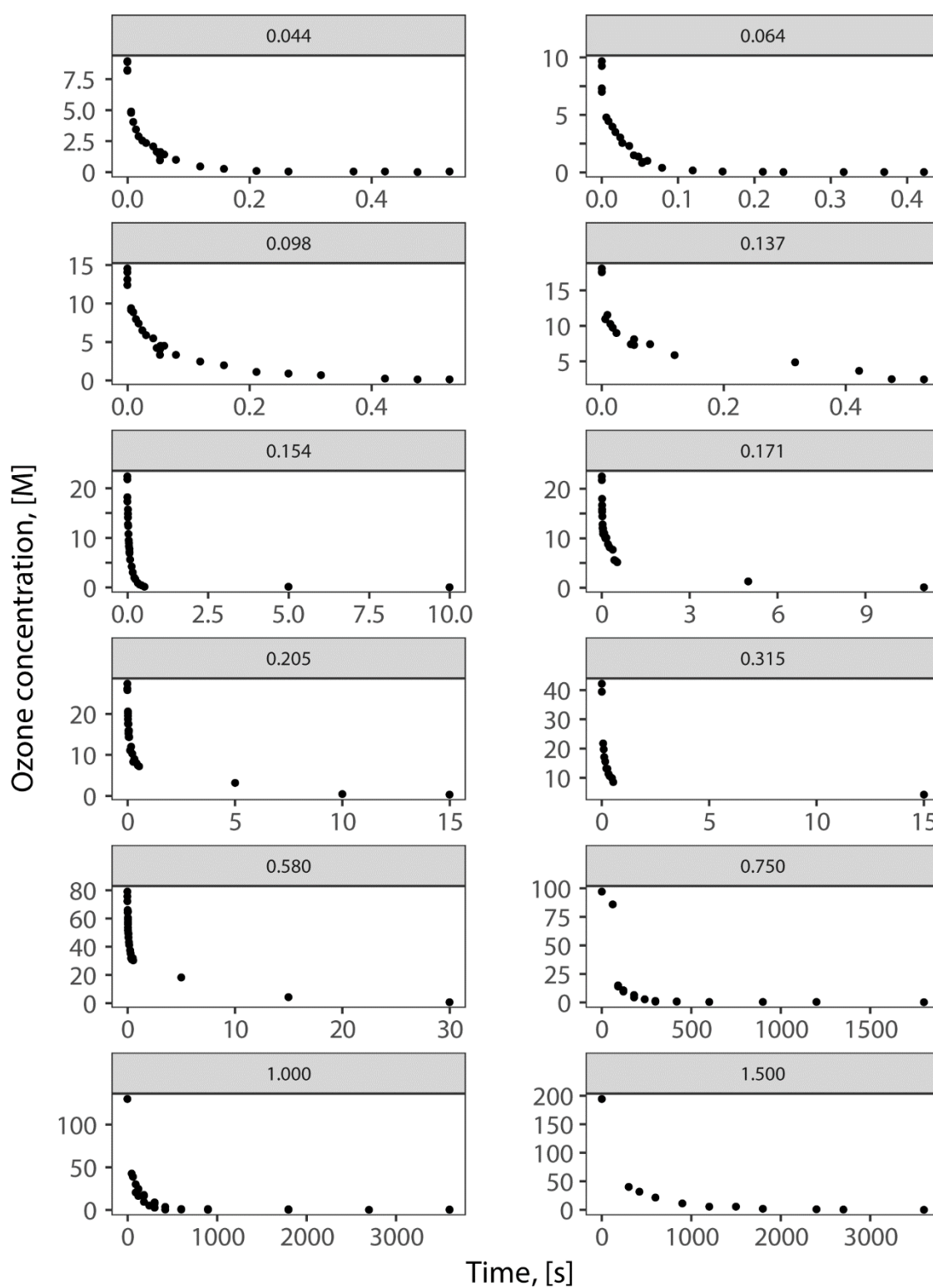


Figure S3.2 Depletion of the ozone concentration over time for the different specific ozone doses (number in grey title, in  $\text{mgO}_3/\text{mgDOC}$ ) in WW.

## S3.2 HPLC analyses

In quench-flow experiments, benzaldehyde was quantified using an Ultimate 3000 HPLC system (ThermoScientific, Sunnyvale, CA, USA) with a multiple wavelength diode array detector (250 nm). The injection volume was 100  $\mu$ L, and an isocratic flow (60% 10mM  $\text{H}_3\text{PO}_4$ /40% MeOH) was used on a Cosmosil-C18-MS-II column (100 mm x 3.0mm ID, 5 $\mu$ m; Nacalai Tesque Inc., Kyoto, Japan) with a flow rate of 1 mL/min. The retention time was 7.8 min, the LOD was 0.002  $\mu$ M and the LOQ was 0.008  $\mu$ M. Benzaldehyde concentrations were measured over the range of 0.15-70  $\mu$ M.

Carbamazepine (CBZ) was analyzed using an Ultimate 3000 HPLC system (ThermoScientific, Sunnyvale, CA, USA) with a multiple wavelength diode array detector (250 nm). CBZ was quantified by a gradient methods,<sup>83</sup> on an EC 125/3 Nucleosil 100-5-C18 column (Marcherey-Nagel). 100  $\mu$ L of the sample were injected, a flowrate of 1mL/min was applied and the retention times were 10.3 min CBZ, respectively. CBZ had an LOD of 0.003  $\mu$ M and an LOQ of 0.009  $\mu$ M. The CBZ concentration was measured in the range 0.01-1  $\mu$ M.

### S3.3 Conditions for the SPE online and UPLC MS/MS analysis (adapted from <sup>91</sup>)

Five ml of sample were loaded via a 5 ml loop at a flow rate of 2 ml min<sup>-1</sup> into the SPE cartridge (2.1 × 20 mm, with Oasis HLB 25 µm phase, Waters), which was previously conditioned around 20 min. at 1 ml min<sup>-1</sup> with H<sub>2</sub>O with 1% (v/v) formic acid. The cartridge was then progressively eluted in back-flush mode with the gradient of solvents used for the UPLC at 0.4 ml min<sup>-1</sup> during 11 min. The SPE effluent was directly injected into the UPLC column and served as UPLC mobile phase. Compounds were separated on the UPLC column (Acquity UPLC system, with HSS T3, 2.1 x 100 mm, 1.8 µm, Waters) at 30°C, eluted with an aqueous-organic mobile phase (SPE effluent) composed of (v/v) 94.9% H<sub>2</sub>O, 5% acetonitrile and 0.1% formic acid (solvent A2) and 5% H<sub>2</sub>O, 94.9% acetonitrile and 0.1% formic acid (solvent B2) in gradient mode, from 5 to 95% solvent B2 (v/v) in 11 min at 0.4 ml min<sup>-1</sup>. The column was previously equilibrated during 4.5 min at 0.4 ml min<sup>-1</sup> with 95% solvent A2 and 5% solvent B2. More details of the loading and elution phase are given in Figure S3.3.

Steps		Pump Loading				SPE		Pump Elution				MS
		min	ml min <sup>-1</sup>	A1	B1			min	ml min <sup>-1</sup>	A2	B2	
1	Load sample in loop (2 min)			100	0				0.4	95	5	
2	Load sample on SPE (2.5 min)											
	Load sample on SPE (2 min)	initial	2	100	0			initial	0.4	95	5	Run MS (15 min)
3	Analysis (~10 min) & syringe washing	2.00	2	95	5							
		2.80	0.1	50	50			2.50	0.4	95	5	
								10.00	0.4	5	95	
		11.00	0.1	50	50							
								11.00	0.4	5	95	
		12.00	2	0	100			12.00	0.4	95	5	
		13.00	2	0	100							
		13.50	2	100	0							
		15.00	2	100	0			15.00	0.4	95	5	

Eluent:

Pump Loading

A199% H2O, 1% AF

B1100% MeOH

Pump Elution

A295% H2O, 5% ACN, 0.1% AF

B295% ACN, 5% H2O, 0.1% AF

Figure S3.3 Details loading and elution phase of the SPE online procedure.

CBZ was identified and quantified using tandem mass spectrometry (MS/MS) (Xevo TQ MS, Waters) as described here:

Table S3.1 Detailed ions used for CBZ quantification

Compound	Deuterated compound	Parents ion [m/z]	Daughter ion used for quantification [m/z]
Carbamazepine	Carbamazepin-d10	237.3	165.15

### S3.4 Experimental plan

Table S3.2 summarizes the different types of experiments that were performed for each water and each proxy.

Table S3.2 Summary of the experiments that conducted for each water.

<b>Water</b>	<b>Surface water</b>	<b>Surface water</b>	<b>Secondary effluent wastewater</b>
Water matrix	SWG	SWB	WW
[DOC], [mg/l]	1.2	5.3	6.3
Virus	MS2	MS2 + CVB5	MS2 + CVB5
$K_{O3-virus}$	-	X	X
Specific O <sub>3</sub> dose	X	X	X
$\Delta UV_{254}$	X	X	X
Carbamazepine	X	X	X

### S3.5 R Script of the power model

This model structure has been used for

# Model formulation:

```
Model_string <- "
```

```
model {
```

```
# Likelihood
```

```
for ( i in 1:N) {
```

```
    isCensored[i] ~ dinterval(y[i], censorlimitVec[i])
```

```
    y[i] ~ dnorm(mu[i], tau)
```

```
    mu[i] <- alpha * xun[i]^beta
```

```
}
```

```
# Priors
```

```
    alpha ~ dnorm (0, 0.001)
```

```
    beta ~ dnorm (mu.b1, tau.b1) T(0,)
```

```
    tau ~ dgamma (0.001, 0.001)
```

```
    mu.b1 ~ dnorm( 0, 0.001)
```

```
    tau.b1 ~ dgamma(0.001, 0.001)
```

```
}
```

```
"
```

### S3.6 Ozone exposure model : Model parameters and details

Model parameters for equation 2 are shown in Table S3.3. Model fits are presented (red and blue lines); gray line represents 95% confidence interval of prediction, and black dashed line 95% intervals of the confidence.<sup>42</sup>

Table S3.3 Model parameters and relevant statistics for O<sub>3</sub> exposure model in function of specific O<sub>3</sub> dose [mgO<sub>3</sub>/mgDOC] for the two waters studied.

Water	Model parameter	Estimate	p value	adjusted R <sup>2</sup>
SWB	a	2.9 ± 0.16	2.34E-05	0.969
	b	-3.4 ± 0.16	2.66E-08	
	model		2.65E-08	
WW	a	3.74 ± 0.23	4.64E-07	0.9586
	b	- 4.73 ± 0.41	1.90E-08	
	model		1.90E-08	

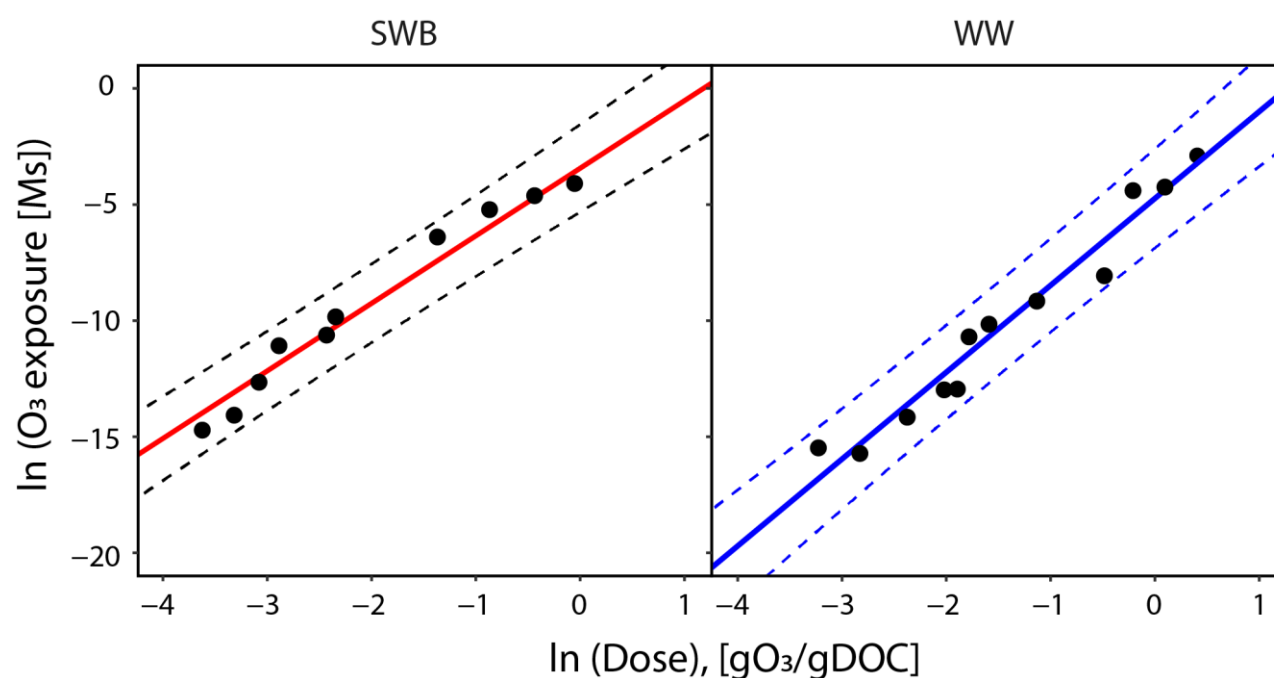


Figure S3.4 Model with expected mean (red and blue for SW and WW, respectively), 95% confidence interval (dashed line) and data of ln(O<sub>3</sub> exposure) in function of the specific O<sub>3</sub> dose applied for the SWB and WW.

### S3.7 Inactivation as a function of the ozone exposure

Table S3.4 presents a summary of the statistical model (equation 3.3).

Table S3.4 Summary of the O<sub>3</sub> exposure model statistics (estimate, standard deviation, p-value and adjusted R<sup>2</sup>)

Water	Model parameter	Estimate	Credible interval
SWB	$\alpha_0$	$15.7 \pm 1.1$	(13.52, 17.9)
	$\alpha_1$	$0.12 \pm 0.01$	(0.11, 0.13)
WWD	$\alpha_0$	$21.6 \pm 2.86$	(16.2, 27.3)
	$\alpha_1$	$0.21 \pm 0.02$	(0.18, 0.24)

### S3.8 Proxies as a function of the specific ozone dose: comparison with published data

Proxies are shown as a function of the specific ozone dose in the main text (Figure S3.3). The model parameters obtained from the power regression (Equation S3.1) are compared with published data.<sup>43,84</sup>

Equation S3.1 Model for Uv in function of the specific ozone dose

$$\Delta UV_{254} = c * Dose^d \quad (S3.2)$$

Table S3.5 summarizes the estimates of model coefficients. For UV, estimates obtained are close to previously published data.

Table S3.5 Power function and quadratic function parameters (slope, standard deviation, 95% credible intervals) for the three studied waters and comparison with previously published data.

$\Delta UV_{254}$		This study			from Gamage et al. (2013)	from Carjaval et. al (2017)
Water	SWG	SWB	WW	WW	WW	
<i>c</i>						
Credible interval (95%)	0.74 ± 0.14 (0.48, 1.0)	0.94 ± 0.07 (0.8, 1.08)	0.54 ± 0.02 (0.51, 0.57)	0.48 (0.46, 0.51)	0.71 (0.63, 0.8)	
<i>d</i>						
Credible interval (95%)	0.67 ± 0.05 (0.39, 0.96)	0.69 ± 0.05 (0.6, 0.78)	0.55 ± 0.03 (0.49, 0.61)	0.53 (0.44, 0.63)	0.75 (0.63, 0.88)	



CBZ abatement as a function of the specific ozone dose was compared to data published by Lester *et al.* (2013)<sup>103</sup> (data extracted using WebPlotdigitiliser<sup>105</sup>). WW data obtained herein is similar to the observations by Lester *et al.* (2013)<sup>103</sup> when looking at all datasets (Figure S3.5). The WW datasets presents several replicated experiments. For the literature data it has been extracted from a plot presenting a single replicate. That may explain the variability in our datasets. Our two SW data sets seem closer together than to WW one.

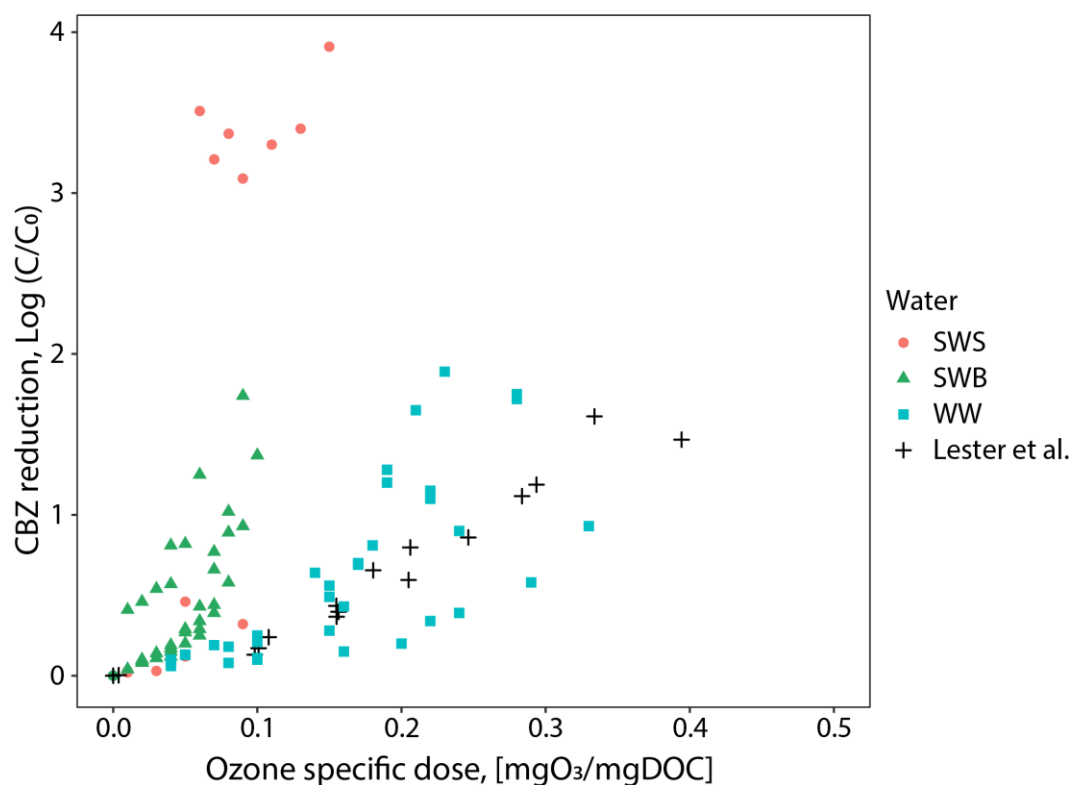


Figure S3.5 CBZ abatement as a function of the specific ozone dose for the three selected waters and data extracted from Lester *et al.* (2012)

### S3.9 Bayesian model averaging (BMA)

The “BAS” package provides functions to perform Bayesian model averaging in linear and generalized linear models. In this study the model used is presented in equation S4. Prior distributions of coefficients were based on the Jeffreys-Zellner-Siow Cauchy prior,<sup>126</sup> and an adaptive algorithm to sample without replacement from Markov chain Monte Carlo (MCMC) sampling was used. The variables with high inclusion probabilities (the probability that a variable has a coefficient ( $\beta_i$ ) different from zero) are likely to be important to explain predictions or data. The Highest Probability Model (HPM) was used to construct a posterior probability distribution of variable estimates (Figure S3.6 to S3.7). This analysis was performed with batch experiment datasets of the three water matrices, without censored data as “BAS” package does not treat censored data.

$$\text{Log} \left( \frac{N}{N_0} \right) = \beta_0 + \beta_1 * \text{Water type} + \beta_2 * \text{Virus species} + \beta_3 * [\text{DOC}] + \beta_4 \\ * \text{Specific O}_3 \text{ dose OR } \log \left( \frac{\text{CBZ}}{\text{CBZ}_0} \right) \text{ OR } \Delta UV_{254} \text{ (S4)}$$

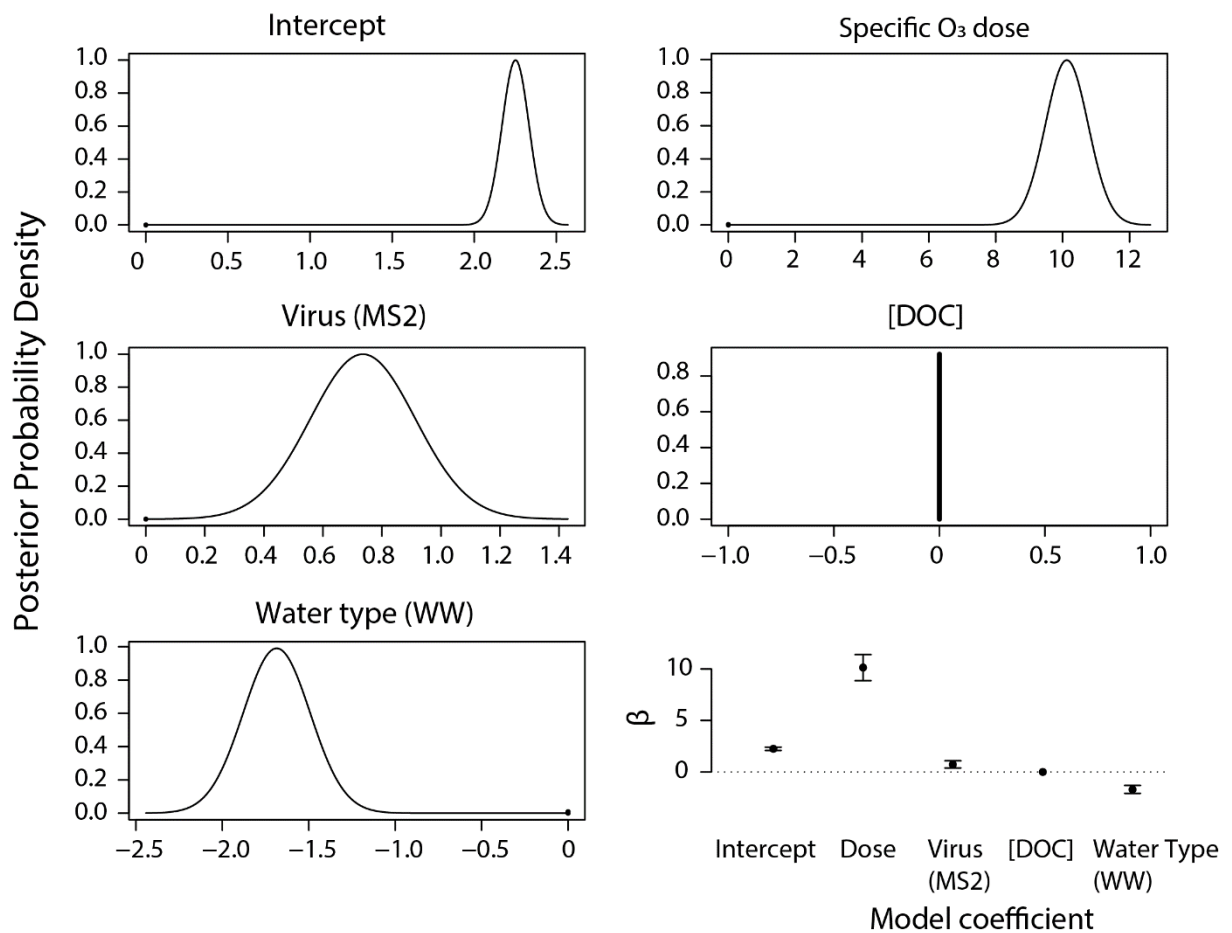
The goal was to determine the probability of the coefficients  $\beta_i$  in equation S4 to be different from 0, using inclusion probabilities. If this later was > 95%, the variable was considered unimportant in explaining variation in inactivation. Finally, a most probable model (model1) was used to compute parameter posterior distributions.

BMA summary tables below (Table S3.6 to Table S3.8) group the five models with the highest posterior probabilities. In addition, the inclusion probabilities (1<sup>st</sup> column) are also computed. Bayes factors of each model to the highest probability model are also presented. Here, a value < 1 indicated evidence in favor of model1. Posterior probabilities (Poast probability) for each model are also computed, the higher the probability the more likely the model is. Logmarg indicates the log marginal likelihood of the model compared to a base model with intercept only.

In Figure S3.6 to S3.8, the posterior probability distributions obtained from BMA using the highest probability model (model1 in Table S3.6 to Table S3.8) are shown, without prior knowledge or censored data incorporation.

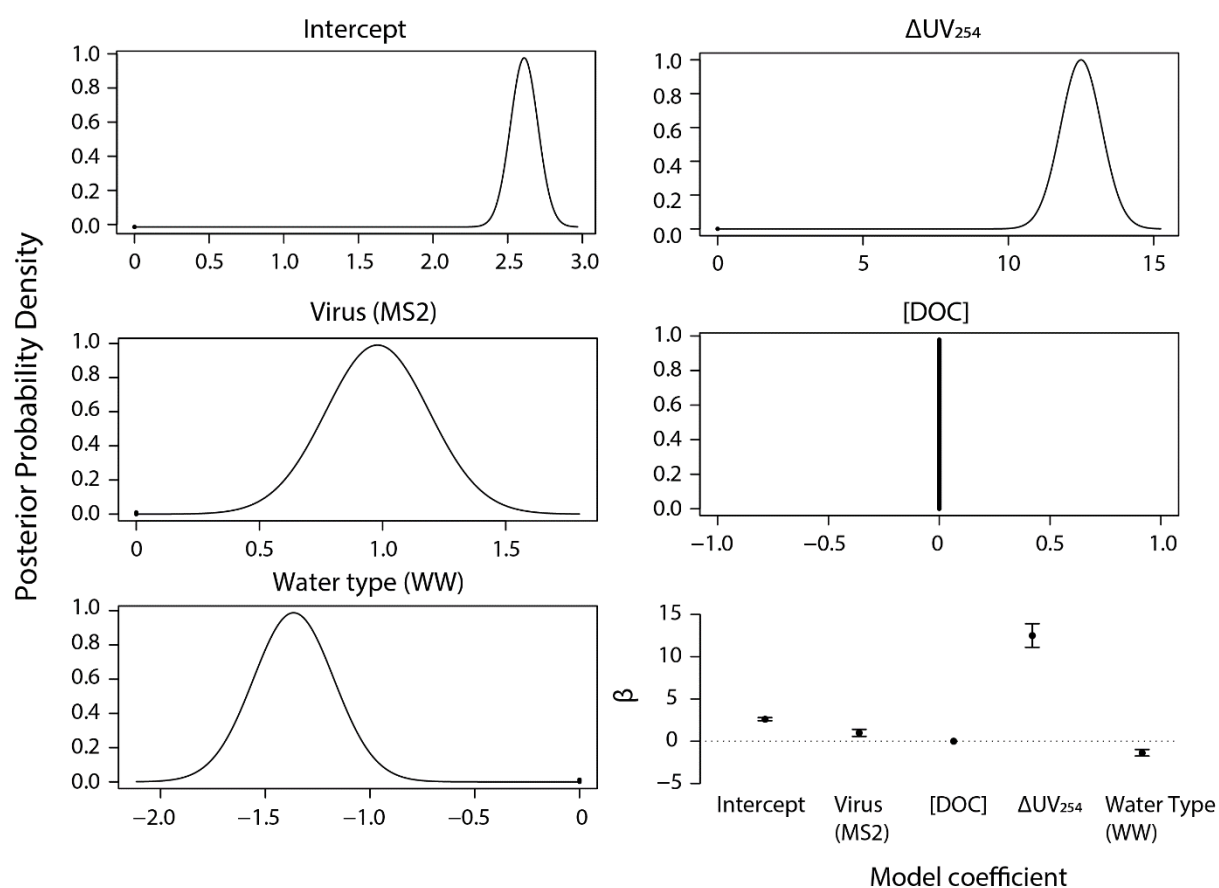
**Specific O<sub>3</sub> Dose**Table S3.6 Summary statistics of Bayesian model averaging for variable selection for the specific O<sub>3</sub> dose as a proxy. Five probable models are presented with their statistics.

Specific O <sub>3</sub> Dose	P(B != 0   Y)	model 1	model 2	model 3	model 4	model 5
<b>Intercept</b>	1	1	1	1	1	1
<b>Dose</b>	0.996	1	1	0	1	1
<b>Virus (MS2)</b>	0.97	1	1	0	0	0
<b>[DOC]</b>	0.13	0	1	0	0	1
<b>Water type (WW)</b>	0.99	1	1	1	0	1
<b>Bayes Factor</b>	NA	1.00	0.11	3E-39	3E-18	1.5E-03
<b>Post Probability</b>	NA	0.84	0.12	6.2E-03	6.2E-03	6.2E-03
<b>R<sup>2</sup></b>	NA	0.55	0.55	0.52	0.00	0.54
<b>Model dimension</b>	NA	4	5	3	1	4
<b>logmarg</b>	NA	88.65	86.48	0	48	82.19

Figure S3.6 Posterior probability distribution for the  $\beta_i$  coefficients of each variable (five first graphs) and summary of beta value and 95% credible intervals (third row on the right) for the model using  $\Delta UV_{254}$  as a proxy. I don't understand: I was under the impression that we are discussing the specific ozone dose here

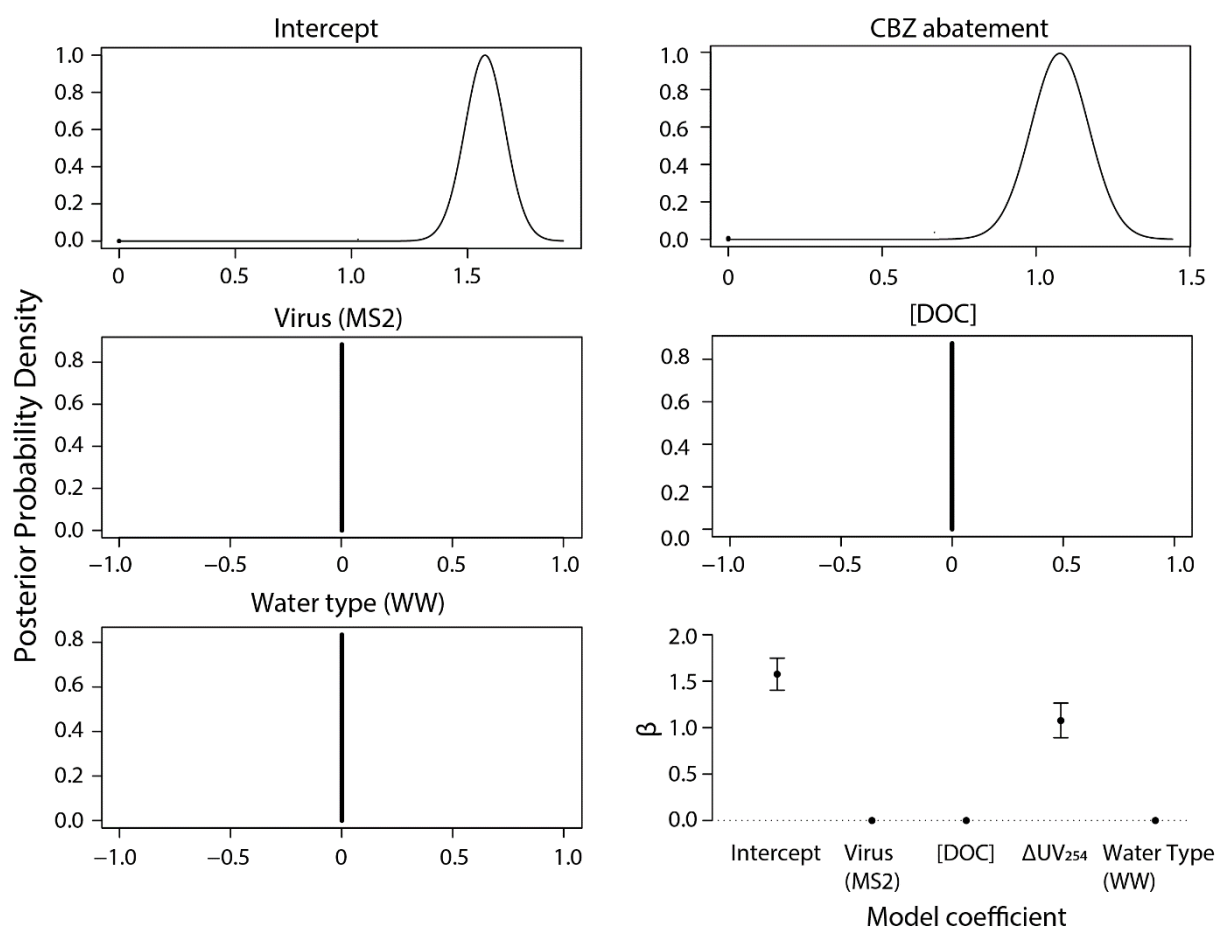
$\Delta UV_{254}$ Table S3.7 Summary statistics of Bayesian model averaging for variable selection for  $\Delta UV_{254}$  as a proxy. Five probable models are presented with their statistics.

$\Delta UV_{254}$	$P(B \neq 0 \mid Y)$	model 1	model 2	model 3	model 4	model 5
<b>Intercept</b>	1	1	1	1	1	1
<b>Virus (MS2)</b>	0.98	1	1	0	0	0
<b>[DOC]</b>	0.05	0	1	1	0	0
<b><math>\Delta UV_{254}</math></b>	0.99	1	1	1	0	1
<b>Water type (WW)</b>	0.98	1	1	0	0	0
<b>Bayes Factor</b>	NA	1	0.09	1.4E-07	5.74E-39	2.5E-12
<b>Post Probability</b>	NA	0.92	0.05	9.3E-03	6.2E-03	6.2E-03
<b><math>R^2</math></b>	NA	0.73	0.73	0.65	0.00	0.58
<b>dim</b>	NA	4	5	3	1	2
<b>logmarg</b>	NA	88.05	85.61	72	0.00	61.3

Figure S3.7 Posterior probability distribution for  $\beta_i$  coefficient of each variable (five first graphs) and summary of beta values and 95% credible intervals (third row on the right) for the model using  $\Delta UV_{254}$  as a proxy.

**CBZ abatement**Table S3.8 Summary statistics of Bayesian model averaging for variable selection for  $\Delta UV_{254}$  as a proxy. Five probable models are presented with their statistics.

	$P(B \neq 0   Y)$	model 1	model 2	model 3	model 4	model 5
<b>Intercept</b>	1	1	1	1	1	1
<b>Virus (MS2)</b>	0.09	0	0	0	1	0
<b>[DOC]</b>	0.09	0	1	0	0	0
<b>CBZ abatement</b>	0.99	1	1	1	1	0
<b>Water type (WW)</b>	0.03	0	0	1	0	0
<b>Bayes Factor</b>	NA	1.00	0.11	0.09	0.09	6E-17
<b>Post Probability</b>	NA	0.72	0.07	0.07	0.03	9.3E-03
<b><math>R^2</math></b>	NA	0.60	0.61	0.6	0.6	0
<b>dim</b>	NA	2	3	3	3	1
<b>logmarg</b>	NA	37.29	35.06	34.93	34.94	0

Figure S3.8 Posterior probability distribution for  $\beta_i$  coefficients of each variables (five first graphs) and summary of beta values and 95% credible intervals (third row on the right) for the model using CBZ abatement as a proxy.

### Specific $O_3$ dose

No cluster of points is observed neither for the water type nor for the virus species. The repartitioning seems also closer to the 1:1 slope, which indicated a better predictability.

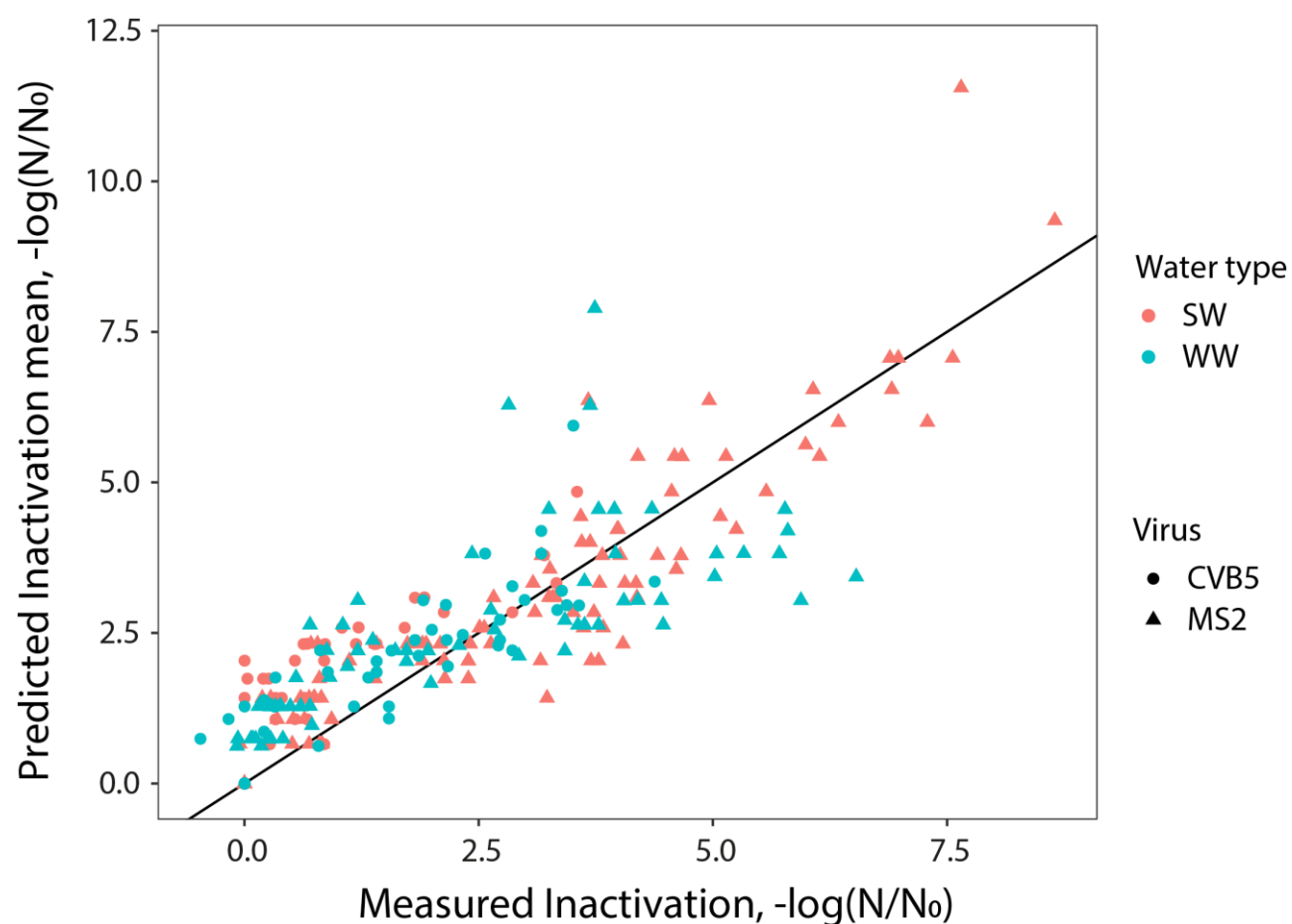


Figure S3.9 Power model: Predicted vs measured inactivation using specific  $O_3$  dose as proxy; virus species, water types and the 1:1 slope (black line) are highlighted.

$\Delta UV_{254}$ 

Figure S3.10 shows the predicted mean using  $\Delta UV_{254}$  as proxy in function of the measured inactivation. The inactivation is slightly overestimated for lower inactivation value (up to 2.5), however, for higher inactivation predicted value are closer to the measured one. No clear cluster is observed.

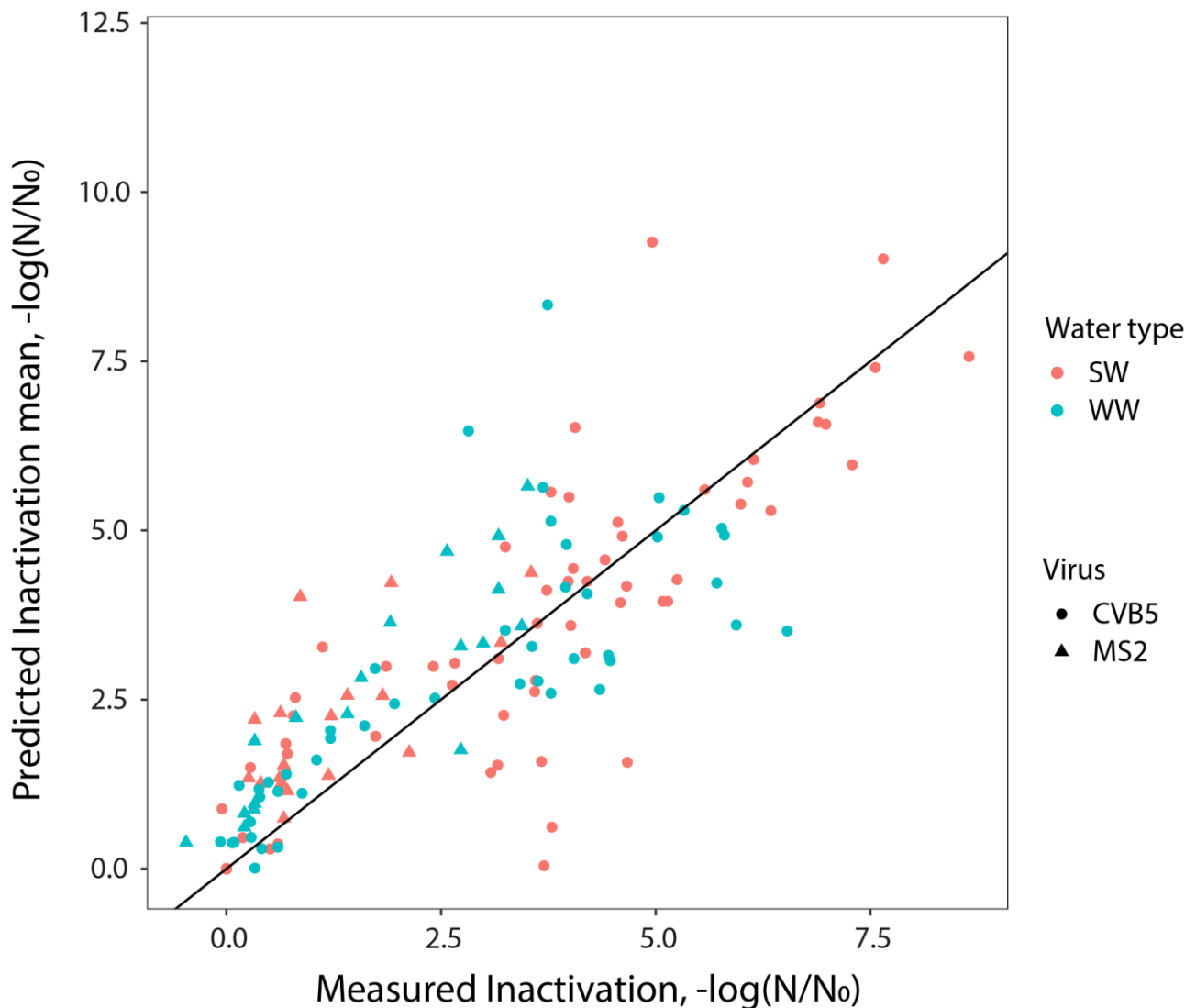


Figure S3.10 Power model: predicted vs measured inactivation using UV reduction as proxy, virus species, water types and the 1:1 slope (black line) are highlighted.

### Carbamazepine abatement

Compared to linear model, the power model is much more convincing. Except for a few outliers, the point lies along the 1:1 line and no clear cluster is observed.

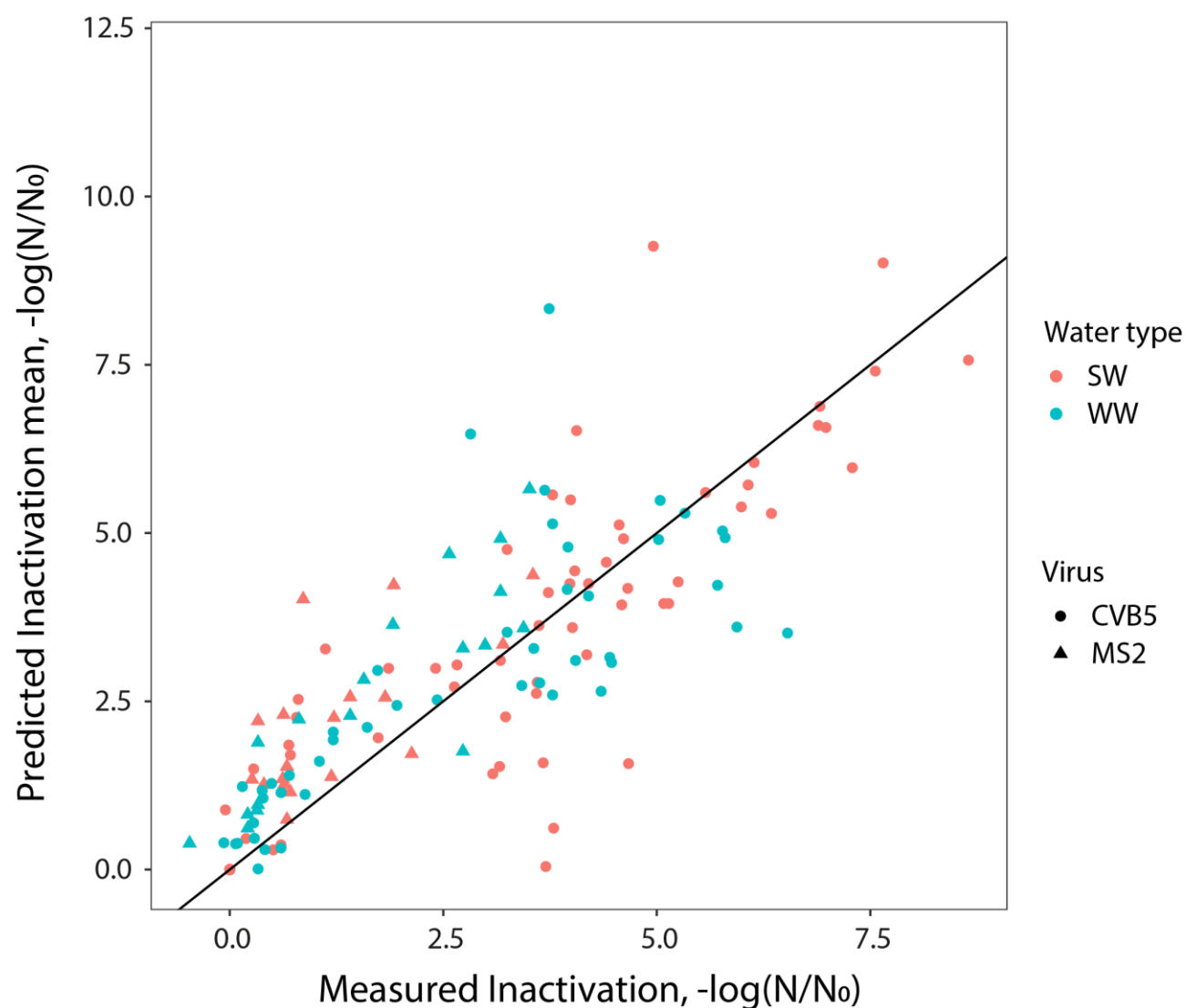


Figure S3.11 Power function model predicted vs measured inactivation using CBZ as a proxy, virus species, water types and the 1:1 slope (black line) are highlighted.



## S3.11 Gerrity et al. extracted data

Table S 3.9 Extracted data from Gerrity et al. (2012)

UV reduction	Log	Water.type	DOC
0.18	0.74	WW	7.3
0.21	0.92	WW	7.3
0.20	1.09	WW	7.3
0.47	5.56	WW	7.3
0.44	5.70	WW	7.3
0.38	5.96	WW	7.3
0.55	6.34	WW	7.3
0.63	7.07	WW	7.3
0.36	7.07	WW	7.3
0.34	7.08	WW	7.3
0.48	6.91	WW	7.3
0.49	6.91	WW	7.3
0.19	1.84	WW	7.6
0.24	1.92	WW	7.6
0.22	2.56	WW	7.6
0.23	2.67	WW	7.6
0.28	3.56	WW	7.6
0.32	3.95	WW	7.6
0.39	4.72	WW	7.6
0.39	4.78	WW	7.6
0.42	4.90	WW	7.6
0.37	5.13	WW	7.6
0.37	5.33	WW	7.6
0.41	5.22	WW	7.6
0.42	5.31	WW	7.6
0.47	5.49	WW	7.6
0.49	5.66	WW	7.6
0.45	5.78	WW	7.6
0.42	5.78	WW	7.6
0.43	5.82	WW	7.6
0.59	6.65	WW	7.6
0.48	6.73	WW	7.6
0.54	7.45	WW	7.6
0.55	6.33	WW	7.6
0.24	0.83	WW	6.9
0.22	1.34	WW	6.9
0.22	1.50	WW	6.9
0.21	1.73	WW	6.9
0.19	3.77	WW	6.9

0.44	3.93	WW	6.9
0.40	4.32	WW	6.9
0.38	4.37	WW	6.9
0.60	4.60	WW	6.9
0.41	6.18	WW	6.9
0.32	6.15	WW	6.9
0.34	6.67	WW	6.9
0.39	6.62	WW	6.9
0.41	6.93	WW	6.9
0.48	7.06	WW	6.9
0.53	7.06	WW	6.9
0.56	6.84	WW	6.9
0.52	6.42	WW	6.9
0.68	7.16	WW	6.9
0.59	7.68	WW	6.9
0.46	7.68	WW	6.9
0.51	7.68	WW	6.9
0.39	7.68	WW	6.9
0.17	1.43	WW	18
0.16	1.69	WW	18
0.16	2.81	WW	18
0.30	4.73	WW	18
0.32	5.41	WW	18
0.36	5.77	WW	18
0.45	6.25	WW	18
0.39	6.42	WW	18
0.42	7.44	WW	18
0.42	7.80	WW	18
0.49	7.80	WW	18
0.53	7.80	WW	18
0.14	1.12	WW	6.3
0.13	1.37	WW	6.3
0.11	2.51	WW	6.3
0.27	4.45	WW	6.3
0.28	5.14	WW	6.3
0.29	5.52	WW	6.3
0.42	5.96	WW	6.3
0.60	7.33	WW	6.3
0.51	7.52	WW	6.3
0.49	7.52	WW	6.3
0.45	7.53	WW	6.3
0.19	1.08	WW	7
0.19	1.23	WW	7
0.18	1.35	WW	7

0.32	4.09	WW	7
0.53	6.49	WW	7
0.60	6.50	WW	7
0.47	6.85	WW	7
0.32	6.33	WW	7
0.47	7.31	WW	7
0.53	7.51	WW	7
0.56	7.51	WW	7

### S3.12 Pilot experiment

Table S3.10 Water parameters of the pilot experiments during the two runs performed

Water parameter	Specific O <sub>3</sub> dose: 0.2 mgO <sub>3</sub> /mgDOC	Specific O <sub>3</sub> dose: 0.5 mgO <sub>3</sub> /mgDOC
Temperature, [°C]	8.6	8.5
Conductivity, [μS/cm] at 20°C	274	274
pH	7.98	8.02
Alkalinity, [mmol/L]	2.69	2.69
Hardness, [mmol/L]	1.48	1.49
Dissolved organic carbon (DOC), [mg/L]	1.4	1.6

Table S3.11 Summary of the different sampling points in the pilot reactor together with which proxy measurement locations.

Sampling points	Proxy			
	O3 exposure	UV <sub>254</sub>	Dose	CBZ abatement
Inlet (E1) before O <sub>3</sub>	x	x		x
Inlet (after O <sub>3</sub> )	x			x
P1	x			x
P2	x			x
P3	x			x
P4	x			x
Outlet (M263)	x			x
Outlet without quenching		x	x	x

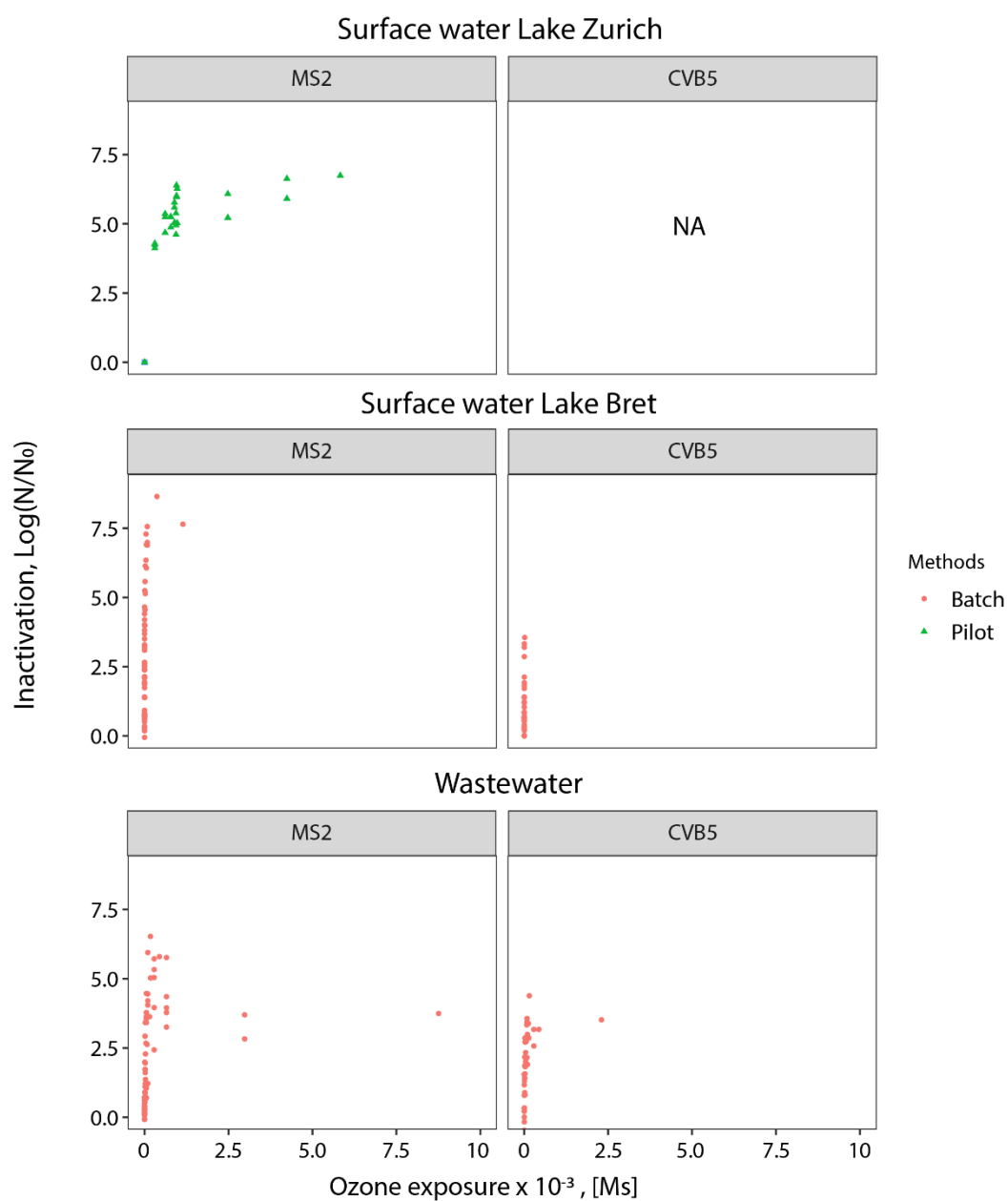


Figure S3.12 Complete inactivation profile of MS2 & CVB5 in function the computed ozone exposure in SW Lake Bret and WW. In addition, MS2 inactivation profile for Pilot experiments with surface water Lake Zurich is presented for comparison.

## Supportive information for Chapter 4

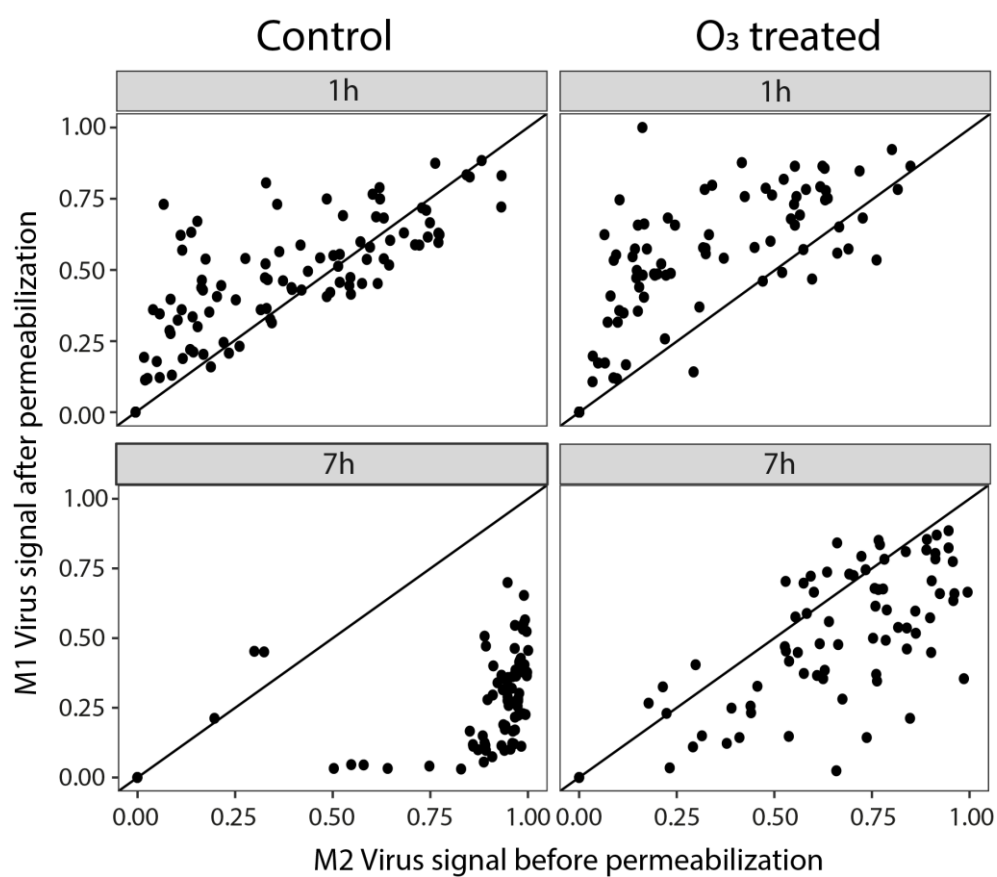


Figure S4.1 Mander's coefficients after and before permeabilization for 1h and 7h for the sample with an without ozone treatment.



## References

- (1) WWAP. *Water in a changing world: the United Nations world water development report 3*; 2009.
- (2) Bhagowati, B.; Ahamad, K. U. A Review on Lake Eutrophication Dynamics and Recent Developments in Lake Modeling. *Ecohydrol. Hydrobiol.* **2018**. <https://doi.org/10.1016/j.ecohyd.2018.03.002>.
- (3) Verlicchi, P.; Al Aukidy, M.; Zambello, E. Occurrence of Pharmaceutical Compounds in Urban Wastewater: Removal, Mass Load and Environmental Risk after a Secondary Treatment—A Review. *Sci. Total Environ.* **2012**, *429*, 123–155. <https://doi.org/10.1016/j.scitotenv.2012.04.028>.
- (4) Luo, Y.; Guo, W.; Ngo, H. H.; Nghiem, L. D.; Hai, F. I.; Zhang, J.; Liang, S.; Wang, X. C. A Review on the Occurrence of Micropollutants in the Aquatic Environment and Their Fate and Removal during Wastewater Treatment. *Sci. Total Environ.* **2014**, *473–474*, 619–641. <https://doi.org/10.1016/j.scitotenv.2013.12.065>.
- (5) Naidoo, S.; Olaniran, A. O. Treated Wastewater Effluent as a Source of Microbial Pollution of Surface Water Resources. *Int. J. Environ. Res. Public Health* **2014**, *11* (1), 249–270. <https://doi.org/10.3390/ijerph110100249>.
- (6) Vörösmarty, C. J.; McIntyre, P. B.; Gessner, M. O.; Dudgeon, D.; Prusevich, A.; Green, P.; Glidden, S.; Bunn, S. E.; Sullivan, C. A.; Liermann, C. R.; et al. Global Threats to Human Water Security and River Biodiversity. *Nature* **2010**, *467* (7315), 555–561. <https://doi.org/10.1038/nature09440>.
- (7) WHO | Guidelines for drinking-water quality, fourth edition [http://www.who.int/water\\_sanitation\\_health/publications/dwq-guidelines-4/en/](http://www.who.int/water_sanitation_health/publications/dwq-guidelines-4/en/) (accessed Jul 26, 2017).
- (8) World Health Organization. Potable Reuse Guidance for producing safe drinking-water [http://www.who.int/water\\_sanitation\\_health/publications/potable-reuse-guidelines/en/](http://www.who.int/water_sanitation_health/publications/potable-reuse-guidelines/en/) (accessed May 8, 2018).
- (9) Koeman, J. H.; Brauw, M. C. T. N. D.; Vos, R. H. D. Chlorinated Biphenyls in Fish, Mussels and Birds from the River Rhine and the Netherlands Coastal Area. *Nature* **1969**, *221* (5186), 1126. <https://doi.org/10.1038/2211126a0>.
- (10) Edder, P.; Ortelli, D.; Klein, A.; Ramseier, S. *METALS AND ORGANIC MICROPOLLUTANTS IN RIVERS AND GENEVA LAKE WATERS*; Comm. int. prot. eaux Léman contre pollut., 2007.
- (11) Qualité de l'eau : révision de l'ordonnance sur la protection des eaux <https://www.bafu.admin.ch/bafu/fr/home/themes/formation/communiqués.msg-id-59323.html> (accessed Jan 28, 2019).
- (12) Locas, A.; Martinez, V.; Payment, P. Removal of Human Enteric Viruses and Indicator Microorganisms from Domestic Wastewater by Aerated Lagoons. *Can. J. Microbiol.* **2010**, *56* (2), 188–194. <https://doi.org/10.1139/W09-124>.
- (13) Doultree, J. C.; Druce, J. D.; Birch, C. J.; Bowden, D. S.; Marshall, J. A. Inactivation of Feline Calicivirus, a Norwalk Virus Surrogate. *J. Hosp. Infect.* **1999**, *41* (1), 51–57. [https://doi.org/10.1016/S0195-6701\(99\)90037-3](https://doi.org/10.1016/S0195-6701(99)90037-3).
- (14) Sigmon, C.; Shin, G.-A.; Mieog, J.; Linden, K. G. Establishing Surrogate–Virus Relationships for Ozone Disinfection of Wastewater. *Environ. Eng. Sci.* **2015**, *32* (6), 451–460. <https://doi.org/10.1089/ees.2014.0496>.
- (15) WHO | Guidelines for drinking-water quality - Volume 1: Recommendations [http://www.who.int/water\\_sanitation\\_health/dwq/gdwq3rev/en/](http://www.who.int/water_sanitation_health/dwq/gdwq3rev/en/) (accessed Oct 19, 2015).
- (16) Gerrity, D.; Pecson, B. M.; Trussell, R. S.; Trussell, R. R. Potable Reuse Treatment Trains throughout the World. *AQUA* **2013**, *62* (6), 321–338. <https://doi.org/DOI: 10.2166/aqua.2013.041>.
- (17) von Gunten, U.; von Sonntag, C. *Chemistry of Ozone in Water and Wastewater Treatment, from Basic Principles to Applications*; IWA publishing: London, UK, 2012.

- (18) Buffle, M.-O.; Schumacher, J.; Salhi, E.; Jekel, M.; von Gunten, U. Measurement of the Initial Phase of Ozone Decomposition in Water and Wastewater by Means of a Continuous Quench-Flow System: Application to Disinfection and Pharmaceutical Oxidation. *Water Res.* **2006**, *40* (9), 1884–1894. <https://doi.org/10.1016/j.watres.2006.02.026>.
- (19) Buffle, M.-O.; Schumacher, J.; Meylan, S.; Jekel, M.; Gunten, U. von. Ozonation and Advanced Oxidation of Wastewater: Effect of O<sub>3</sub> Dose, PH, DOM and HO•-Scavengers on Ozone Decomposition and HO• Generation. *Ozone Sci. Eng.* **2006**, *28* (4), 247–259. <https://doi.org/10.1080/01919510600718825>.
- (20) Wigginton, K. R.; Kohn, T. Virus Disinfection Mechanisms: The Role of Virus Composition, Structure, and Function. *Curr. Opin. Virol.* **2012**, *2* (1), 84–89. <https://doi.org/10.1016/j.coviro.2011.11.003>.
- (21) NAJM, I. An Alternative Interpretation of Disinfection Kinetics. *J. Am. Water Works Assoc.* **2006**, *98* (10), 93–101.
- (22) Elovitz, M. S.; Gunten, U. von. Hydroxyl Radical/Ozone Ratios During Ozonation Processes. I. The Rct Concept. *Ozone Sci. Eng.* **1999**, *21* (3), 239–260. <https://doi.org/10.1080/01919519908547239>.
- (23) von Gunten, U. Ozonation of Drinking Water: Part II. Disinfection and by-Product Formation in Presence of Bromide, Iodide or Chlorine. *Water Res.* **2003**, *37* (7), 1469–1487. [https://doi.org/10.1016/S0043-1354\(02\)00458-X](https://doi.org/10.1016/S0043-1354(02)00458-X).
- (24) Rennecker, J. L.; Mariñas, B. J.; Owens, J. H.; Rice, E. W. Inactivation of Cryptosporidium Parvum Oocysts with Ozone. *Water Res.* **1999**, *33* (11), 2481–2488. [https://doi.org/10.1016/S0043-1354\(99\)00116-5](https://doi.org/10.1016/S0043-1354(99)00116-5).
- (25) Wickramanayake, G. B.; Rubin, A. J.; Sproul, O. J. Inactivation of Giardia Lamblia Cysts with Ozone. *Appl. Environ. Microbiol.* **1984**, *48* (3), 671–672.
- (26) Betancourt, W. Q.; Rose, J. B. Drinking Water Treatment Processes for Removal of Cryptosporidium and Giardia. *Vet. Parasitol.* **2004**, *126* (1), 219–234. <https://doi.org/10.1016/j.vetpar.2004.09.002>.
- (27) Passos, T. M.; Silva, L. H. M. da; Moreira, L. M.; Zângaro, R. A.; Santos, R. da S.; Fernandes, F. B.; Lima, C. J. de; Fernandes, A. B. Comparative Analysis of Ozone and Ultrasound Effect on the Elimination of Giardia Spp. Cysts from Wastewater. *Ozone Sci. Eng.* **2014**, *36* (2), 138–143. <https://doi.org/10.1080/01919512.2013.864227>.
- (28) Li, J.; Li, K.; Zhou, Y.; Li, X.; Tao, T. Kinetic Analysis of Legionella Inactivation Using Ozone in Wastewater. *Chemosphere* **2017**, *168*, 630–637. <https://doi.org/10.1016/j.chemosphere.2016.11.014>.
- (29) Kuchta, J. M.; States, S. J.; McNamara, A. M.; Wadowsky, R. M.; Yee, R. B. Susceptibility of Legionella Pneumophila to Chlorine in Tap Water. *Appl. Environ. Microbiol.* **1983**, *46* (5), 1134–1139.
- (30) Guillot, E.; Loret, J. *Waterborne Pathogens: Review for the Drinking Water Industry*; iwa publishing: London, UK, 2010.
- (31) WHO | Metrics: Disability-Adjusted Life Year (DALY) [https://www.who.int/healthinfo/global\\_burden\\_disease/metrics\\_daly/en/](https://www.who.int/healthinfo/global_burden_disease/metrics_daly/en/) (accessed Feb 13, 2019).
- (32) Havelaar A H; De Hollander A E; Teunis P F; Evers E G; Van Kranen H J; Versteegh J F; Van Koten J E; Slob W. Balancing the Risks and Benefits of Drinking Water Disinfection: Disability Adjusted Life-Years on the Scale. *Environ. Health Perspect.* **2000**, *108* (4), 315–321. <https://doi.org/10.1289/ehp.00108315>.
- (33) Outbreak of E. coli Infections Linked to Romaine Lettuce | E. coli Infections Linked to Romaine Lettuce | November 2018 | E. coli | CDC <https://www.cdc.gov/ecoli/2018/o157h7-11-18/index.html> (accessed Jan 25, 2019).
- (34) de Graaf, M.; Beck, R.; Caccio, S. M.; Duim, B.; Fraaij, P. L.; Le Guyader, F. S.; Lecuit, M.; Le Pendu, J.; de Wit, E.; Schultsz, C. Sustained Fecal-Oral Human-to-Human Transmission Following a Zoonotic Event. *Curr. Opin. Virol.* **2017**, *22*, 1–6. <https://doi.org/10.1016/j.coviro.2016.11.001>.
- (35) American Academy of Pediatrics. *Red Book : 2012 Report of the Committee on Infectious Diseases*; 2012.
- (36) Gall, A. M.; Mariñas, B. J.; Lu, Y.; Shisler, J. L. Waterborne Viruses: A Barrier to Safe Drinking Water. *PLoS Pathog.* **2015**, *11* (6). <https://doi.org/10.1371/journal.ppat.1004867>.



- (37) Vaughn, J. M.; Chen, Y. S.; Thomas, M. Z. Inactivation of Human and Simian Rotaviruses by Chlorine. *ResearchGate* **1986**, 51 (2), 391–394.
- (38) Roy, D.; Wong, P. K.; Engelbrecht, R. S.; Chian, E. S. Mechanism of Enteroviral Inactivation by Ozone. *Appl. Environ. Microbiol.* **1981**, 41 (3), 718–723.
- (39) Kim, C. K.; Gentile, D. M.; Sproul, O. J. Mechanism of Ozone Inactivation of Bacteriophage F2. *Appl. Environ. Microbiol.* **1980**, 39 (1), 210–218.
- (40) Shinriki, N.; Ishizaki, K.; Yoshizaki, T.; Miura, K.; Ueda, T. Mechanism of Inactivation of Tobacco Mosaic Virus with Ozone. *Water Res.* **1988**, 22 (7), 933–938. [https://doi.org/10.1016/0043-1354\(88\)90031-0](https://doi.org/10.1016/0043-1354(88)90031-0).
- (41) Lee, Y.; Gerrity, D.; Lee, M.; Bogeat, A. E.; Salhi, E.; Gamage, S.; Trenholm, R. A.; Wert, E. C.; Snyder, S. A.; von Gunten, U. Prediction of Micropollutant Elimination during Ozonation of Municipal Wastewater Effluents: Use of Kinetic and Water Specific Information. *Environ. Sci. Technol.* **2013**, 47 (11), 5872–5881. <https://doi.org/10.1021/es400781r>.
- (42) Lee, Y.; Kovalova, L.; McArdell, C. S.; von Gunten, U. Prediction of Micropollutant Elimination during Ozonation of a Hospital Wastewater Effluent. *Water Res.* **2014**, 64, 134–148. <https://doi.org/10.1016/j.watres.2014.06.027>.
- (43) Gerrity, D.; Gamage, S.; Jones, D.; Korshin, G. V.; Lee, Y.; Pisarenko, A.; Trenholm, R. A.; von Gunten, U.; Wert, E. C.; Snyder, S. A. Development of Surrogate Correlation Models to Predict Trace Organic Contaminant Oxidation and Microbial Inactivation during Ozonation. *Water Res.* **2012**, 46 (19), 6257–6272. <https://doi.org/10.1016/j.watres.2012.08.037>.
- (44) Gamage, S.; Gerrity, D.; Pisarenko, A. N.; Wert, E. C.; Snyder, S. A. Evaluation of Process Control Alternatives for the Inactivation of Escherichia Coli, MS2 Bacteriophage, and Bacillus Subtilis Spores during Wastewater Ozonation. *Ozone Sci. Eng.* **2013**, 35 (6), 501–513. <https://doi.org/10.1080/01919512.2013.833852>.
- (45) von Gunten, U. Ozonation of Drinking Water: Part I. Oxidation Kinetics and Product Formation. *Water Res.* **2003**, 37 (7), 1443–1467. [https://doi.org/10.1016/S0043-1354\(02\)00457-8](https://doi.org/10.1016/S0043-1354(02)00457-8).
- (46) Ternes, T. A.; Stüber, J.; Herrmann, N.; McDowell, D.; Ried, A.; Kampmann, M.; Teiser, B. Ozonation: A Tool for Removal of Pharmaceuticals, Contrast Media and Musk Fragrances from Wastewater? *Water Res.* **2003**, 37 (8), 1976–1982. [https://doi.org/10.1016/S0043-1354\(02\)00570-5](https://doi.org/10.1016/S0043-1354(02)00570-5).
- (47) Eggen, R. I. L.; Hollender, J.; Joss, A.; Schäfer, M.; Stamm, C. Reducing the Discharge of Micropollutants in the Aquatic Environment: The Benefits of Upgrading Wastewater Treatment Plants. *Environ. Sci. Technol.* **2014**, 48 (14), 7683–7689. <https://doi.org/10.1021/es500907n>.
- (48) Joss, A.; Siegrist, H.; Ternes, T. A. Are We about to Upgrade Wastewater Treatment for Removing Organic Micropollutants? *Water Sci. Technol.* **2008**, 57 (2), 251–255. <https://doi.org/10.2166/wst.2008.825>.
- (49) Lee, Y.; Gunten, U. von. Advances in Predicting Organic Contaminant Abatement during Ozonation of Municipal Wastewater Effluent: Reaction Kinetics, Transformation Products, and Changes of Biological Effects. *Environ. Sci. Water Res. Technol.* **2016**, 2 (3), 421–442. <https://doi.org/10.1039/C6EW00025H>.
- (50) Tchobanoglous, G.; Cotruvo, J.; Crook, J.; McDonald, J.; Olivieri, A.; Salveson, A.; Trussell, R. S. *Framework for Direct Potable Reuse*; Water Reuse, American Water Works Association, Water environment Federation, National Water Research Institute, 2015.
- (51) Finch, G. R.; Fairbairn, N. Comparative Inactivation of Poliovirus Type 3 and MS2 Coliphage in Demand-Free Phosphate Buffer by Using Ozone. *Appl. Environ. Microbiol.* **1991**, 57 (11), 3121–3126.
- (52) Thurston-Enriquez, J. A.; Haas, C. N.; Jacangelo, J.; Gerba, C. P. Inactivation of Enteric Adenovirus and Feline Calicivirus by Ozone. *Water Res.* **2005**, 39 (15), 3650–3656. <https://doi.org/10.1016/j.watres.2005.06.006>.
- (53) Roy, D.; Englebrecht, R. S.; Chian, E. S. K. Comparative Inactivation of Six Enteroviruses by Ozone. *J. Am. Water Works Assoc.* **1982**, 74 (12), 660–664.
- (54) Beltrán, F. J. *Ozone Reaction Kinetics for Water and Wastewater Systems*; Lewis Publishers: Boca Raton, Fla., 2004.

- (55) Pecson, B. M.; Martin, L. V.; Kohn, T. Quantitative PCR for Determining the Infectivity of Bacteriophage MS2 upon Inactivation by Heat, UV-B Radiation, and Singlet Oxygen: Advantages and Limitations of an Enzymatic Treatment to Reduce False-Positive Results. *Appl. Environ. Microbiol.* **2009**, *75* (17), 5544–5554. <https://doi.org/10.1128/AEM.00425-09>.
- (56) Oksanen, H. M.; Domanska, A.; Bamford, D. H. Monolithic Ion Exchange Chromatographic Methods for Virus Purification. *Virology* **2012**, *434* (2), 271–277. <https://doi.org/10.1016/j.virol.2012.09.019>.
- (57) Carratalà, A.; Calado, A. D.; Mattle, M. J.; Meierhofer, R.; Luzi, S.; Kohn, T. Solar Disinfection of Viruses in Polyethylene Terephthalate Bottles. *Appl. Environ. Microbiol.* **2016**, *82* (1), 279–288. <https://doi.org/10.1128/AEM.02897-15>.
- (58) Bader, H.; Hoigne, J. Determination of Ozone in Water by the Indigo Method. *Water Res.* **1981**, *15* (4), 449–456. [https://doi.org/10.1016/0043-1354\(81\)90054-3](https://doi.org/10.1016/0043-1354(81)90054-3).
- (59) Jans, U. Radikalbildung aus ozon in atmosphärischen wassern - einfluss von licht, gelösten stoffen und russpartikeln. Doctoral Thesis, ETH Zurich, 1996. <https://doi.org/10.3929/ethz-a-001705058>.
- (60) Leitzke, A.; Reisz, E.; Flyunt, R.; Sonntag, C. von. The Reactions of Ozone with Cinnamic Acids: Formation and Decay of 2-Hydroperoxy-2-Hydroxyacetic Acid. *J. Chem. Soc. Perkin Trans. 2* **2001**, No. 5, 793–797. <https://doi.org/10.1039/B009327K>.
- (61) von Gunten, Urs.; Hoigne, Juerg. Bromate Formation during Ozonization of Bromide-Containing Waters: Interaction of Ozone and Hydroxyl Radical Reactions. *Environ. Sci. Technol.* **1994**, *28* (7), 1234–1242. <https://doi.org/10.1021/es00056a009>.
- (62) Heeb, M. B.; Kristiana, I.; Trogolo, D.; Arey, J. S.; von Gunten, U. Formation and Reactivity of Inorganic and Organic Chloramines and Bromamines during Oxidative Water Treatment. *Water Res.* **2017**, *110*, 91–101. <https://doi.org/10.1016/j.watres.2016.11.065>.
- (63) Nieto-Juarez, J. I.; Pierzchła, K.; Sienkiewicz, A.; Kohn, T. Inactivation of MS2 Coliphage in Fenton and Fenton-like Systems: Role of Transition Metals, Hydrogen Peroxide and Sunlight. *Environ. Sci. Technol.* **2010**, *44* (9), 3351–3356. <https://doi.org/10.1021/es903739f>.
- (64) Czekalski, N.; Imminger, S.; Salhi, E.; Veljkovic, M.; Kleffel, K.; Drissner, D.; Hammes, F.; Bürgmann, H.; von Gunten, U. Inactivation of Antibiotic Resistant Bacteria and Resistance Genes by Ozone: From Laboratory Experiments to Full-Scale Wastewater Treatment. *Environ. Sci. Technol.* **2016**, *50* (21), 11862–11871. <https://doi.org/10.1021/acs.est.6b02640>.
- (65) R Core Team (2016). *R: A Language and Environment for Statistical Computing.*; Foundation for Statistical Computing, Vienna, Austria, 2016.
- (66) Tuszynski, J. *CaTools: Tools: Moving Window Statistics, GIF, Base64, ROC AUC, Etc.* *R Package Version 1.17.1*; 2014.
- (67) Jurasinski, G.; Koebsch, F.; Guenther, A.; Beetz, S. *Flux Rate Calculation from Dynamic Closed Chamber Measurements.* *R Package Version 0.3-0*; 2014.
- (68) Soetaert, K.; Petzoldt, T. Solving Differential Equations in R: Package DeSolve. *Journal of Statistical Software* **2010**, *33* (9), 1–25. <https://doi.org/10.18637/jss.v033.i09>.
- (69) Wickham, H. *Ggplot2: Elegant Graphics for Data Analysis*; New York, 2009.
- (70) Hothorn, T.; Bretz, F.; Westfall, P. Simultaneous Inference in General Parametric Models. *Biometrical Journal* **2008**, *50* (3), 346–363.
- (71) Huber, M. M.; Canonica, S.; Park, G.-Y.; von Gunten, U. Oxidation of Pharmaceuticals during Ozonation and Advanced Oxidation Processes. *Environ. Sci. Technol.* **2003**, *37* (5), 1016–1024. <https://doi.org/10.1021/es025896h>.
- (72) Roy, D.; Chian, E.; Engelbrecht, R. Kinetics of Enteroviral Inactivation by Ozone. *J. Environ. Eng. Div.-Asce* **1981**, *107* (5), 887–901.
- (73) Li Hanbin; Gyürék Lyndon L.; Finch Gordon R.; Smith Daniel W.; Belosevic Miodrag. Effect of Temperature on Ozone Inactivation of Cryptosporidium Parvum in Oxidant Demand-Free Phosphate Buffer. *J. Environ. Eng.* **2001**, *127* (5), 456–467. [https://doi.org/10.1061/\(ASCE\)0733-9372\(2001\)127:5\(456\)](https://doi.org/10.1061/(ASCE)0733-9372(2001)127:5(456)).
- (74) Cromeans, T. L.; Kahler, A. M.; Hill, V. R. Inactivation of Adenoviruses, Enteroviruses, and Murine Norovirus in Water by Free Chlorine and Monochloramine. *Appl. Environ. Microbiol.* **2010**, *76* (4), 1028–1033. <https://doi.org/10.1128/AEM.01342-09>.

- (75) Mattle, M. J.; Vione, D.; Kohn, T. Conceptual Model and Experimental Framework to Determine the Contributions of Direct and Indirect Photoreactions to the Solar Disinfection of MS2, PhiX174, and Adenovirus. *Environ. Sci. Technol.* **2015**, *49* (1), 334–342. <https://doi.org/10.1021/es504764u>.
- (76) Soltermann, F.; Abegglen, C.; Tschui, M.; Stahel, S.; von Gunten, U. Options and Limitations for Bromate Control during Ozonation of Wastewater. *Water Res.* **2017**, *116* (Supplement C), 76–85. <https://doi.org/10.1016/j.watres.2017.02.026>.
- (77) Bourgin, M.; Beck, B.; Boehler, M.; Borowska, E.; Fleiner, J.; Salhi, E.; Teichler, R.; von Gunten, U.; Siegrist, H.; McArdell, C. S. Evaluation of a Full-Scale Wastewater Treatment Plant Upgraded with Ozonation and Biological Post-Treatments: Abatement of Micropollutants, Formation of Transformation Products and Oxidation by-Products. *Water Res.* **2018**, *129* (Supplement C), 486–498. <https://doi.org/10.1016/j.watres.2017.10.036>.
- (78) Harakeh, M.; Butler, M. Factors Influencing the Ozone Inactivation of Enteric Viruses in Effluent. *Ozone-Sci. Eng.* **1984**, *6* (4), 235–243. <https://doi.org/10.1080/01919518408551029>.
- (79) Kuo, D. H.-W.; Simmons, F. J.; Blair, S.; Hart, E.; Rose, J. B.; Xagorarakis, I. Assessment of Human Adenovirus Removal in a Full-Scale Membrane Bioreactor Treating Municipal Wastewater. *Water Res.* **2010**, *44* (5), 1520–1530. <https://doi.org/10.1016/j.watres.2009.10.039>.
- (80) World Health Organization. *Potable Reuse: Guidance for Producing Safe Drinking-Water*; 2017.
- (81) Bicknell, D. L.; Jain, R. K. Ozone Disinfection of Drinking Water — Technology Transfer and Policy Issues. *Environ. Eng. Policy* **2001**, *3* (1), 55–66. <https://doi.org/10.1007/s100220100043>.
- (82) Rice, R. G.; Evison, L. M.; Robson, C. M. Ozone Disinfection of Municipal Wastewater – Current State-of-the-Art. *Ozone Sci. Eng.* **1981**, *3* (4), 239–272. <https://doi.org/10.1080/01919518108550929>.
- (83) Wolf, C.; von Gunten, U.; Kohn, T. Kinetics of Inactivation of Waterborne Enteric Viruses by Ozone. *Environ. Sci. Technol.* **2018**, *52* (4), 2170–2177. <https://doi.org/10.1021/acs.est.7b05111>.
- (84) Carvajal, G.; Branch, A.; Michel, P.; Sisson, S. A.; Roser, D. J.; Drewes, J. E.; Khan, S. J. Robust Evaluation of Performance Monitoring Options for Ozone Disinfection in Water Recycling Using Bayesian Analysis. *Water Res.* **2017**, *124*, 605–617. <https://doi.org/10.1016/j.watres.2017.07.079>.
- (85) Meister, S.; Verbyla, M. E.; Klinger, M.; Kohn, T. Variability in Disinfection Resistance between Currently Circulating Enterovirus B Serotypes and Strains. *Environ. Sci. Technol.* **2018**, *52* (6), 3696–3705. <https://doi.org/10.1021/acs.est.8b00851>.
- (86) Carratala Ripolles, A.; Dionisio Calado, A.; Mattle, M. J.; Meierhofer, R.; Luzi, S.; Kohn, T. Solar Disinfection (SODIS) of Viruses in PET Bottles. *Appl. Environ. Microbiol.* **2015**.
- (87) Road, N. L. 1-6 F.; Totnes; Devon; Sle, T. Chemistry of Ozone in Water and Wastewater Treatment: From Basic Principles to Applications <http://www.nhbs.com/title/192404/chemistry-of-ozone-in-water-and-wastewater-treatment> (accessed Jun 22, 2017).
- (88) Hoigné, J.; Bader, H. Characterization Of Water Quality Criteria for Ozonation Processes. Part II: Lifetime of Added Ozone. *Ozone Sci. Eng.* **1994**, *16* (2), 121–134. <https://doi.org/10.1080/01919519408552417>.
- (89) Morasch, B.; Bonvin, F.; Reiser, H.; Grandjean, D.; De Alencastro, L. F.; Perazzolo, C.; Chèvre, N.; Kohn, T. Occurrence and Fate of Micropollutants in the Vidy Bay of Lake Geneva, Switzerland. Part II: Micropollutant Removal between Wastewater and Raw Drinking Water. *Environ. Toxicol. Chem.* **2010**. <https://doi.org/10.1002/etc.222>.
- (90) Bonvin, F. Spatio-Temporal Presence of Micropollutants and Their Metabolites in Lake Geneva and Susceptibility to Direct and Indirect Photodegradation Processes. *Thesis N°5677* **2013**, EPFL.
- (91) Margot, J. Micropollutant Removal from Municipal Wastewater - From Conventional Treatments to Advanced Biological Processes. *Thesis N° 6505* **2015**, EPFL.
- (92) Bourgin, M.; Borowska, E.; Helbing, J.; Hollender, J.; Kaiser, H.-P.; Kienle, C.; McArdell, C. S.; Simon, E.; von Gunten, U. Effect of Operational and Water Quality Parameters on Conventional Ozonation and the Advanced Oxidation Process O<sub>3</sub>/H<sub>2</sub>O<sub>2</sub>: Kinetics of Micropollutant Abatement, Transformation Product and Bromate Formation in a Surface Water. *Water Res.* **2017**, *122*, 234–245. <https://doi.org/10.1016/j.watres.2017.05.018>.

- (93) Kaiser, H.-P.; Köster, O.; Gresch, M.; Périsset, P. M. J.; Jäggi, P.; Salhi, E.; Gunten, U. von. Process Control For Ozonation Systems: A Novel Real-Time Approach. *Ozone Sci. Eng.* **2013**, *35* (3), 168–185. <https://doi.org/10.1080/01919512.2013.772007>.
- (94) Morasch, B.; Bonvin, F.; Reiser, H.; Grandjean, D.; Alencastro, L. F. de; Perazzolo, C.; Chèvre, N.; Kohn, T. Occurrence and Fate of Micropollutants in the Vidy Bay of Lake Geneva, Switzerland. Part II: Micropollutant Removal between Wastewater and Raw Drinking Water. *Environ. Toxicol. Chem.* **2010**, *29* (8), 1658–1668. <https://doi.org/10.1002/etc.222>.
- (95) Fernández i Marín, X. Ggmcmc : Analysis of MCMC Samples and Bayesian Inference. **2016**, *70* (9), 1–20. <https://doi.org/10.18637/jss.v070.i09>.
- (96) Clyde, M. A.; Ghosh, J.; Littman, M. L. Bayesian Adaptive Sampling for Variable Selection and Model Averaging. *J. Comput. Graph. Stat.* **2011**, *20* (1), 80–101.
- (97) Clyde, M. *BAS: Bayesian Variable Selection and Model Averaging Using Bayesian Adaptive Sampling*; 2018.
- (98) Derwood, M. J. Runjags: An R Package Providing Interface Utilities, Model Templates, Parallel Computing Methods and Additional Distributions for MCMC Models in JAGS. *Journal of Statistical Software* **2016**, *71* (9), 1–25. <https://doi.org/doi:10.18637/jss.v071.i09>.
- (99) Plummer, M. *JAGS : Just Another Gibbs Sampler*; 2017.
- (100) Kruschke, J. K. *Doing Bayesian Data Analysis: A Tutorial with R and BUGS*, 1st ed.; Academic Press, Inc.: Orlando, FL, USA, 2010.
- (101) Plummer, M.; Best, N.; Cowles, K.; Vines, K. CODA: Convergence Diagnosis and Output Analysis for MCMC. *R News* *6* (1), 7–11.
- (102) Peleg, M.; Cole, M. B. Reinterpretation of Microbial Survival Curves. *Crit. Rev. Food Sci. Nutr.* **1998**, *38* (5), 353–380. <https://doi.org/10.1080/10408699891274246>.
- (103) Lester, Y.; Mamane, H.; Zucker, I.; Avisar, D. Treating Wastewater from a Pharmaceutical Formulation Facility by Biological Process and Ozone. *Water Res.* **2013**, *47* (13), 4349–4356. <https://doi.org/10.1016/j.watres.2013.04.059>.
- (104) Chon, K.; Salhi, E.; von Gunten, U. Combination of UV Absorbance and Electron Donating Capacity to Assess Degradation of Micropollutants and Formation of Bromate during Ozonation of Wastewater Effluents. *Water Res.* **2015**, *81*, 388–397. <https://doi.org/10.1016/j.watres.2015.05.039>.
- (105) Ankit Rohatgi. *WebPlotDigitizer*; 2018.
- (106) Wittmer, A.; Heisele, A.; McArdell, C. S.; Böhler, M.; Longree, P.; Siegrist, H. Decreased UV Absorbance as an Indicator of Micropollutant Removal Efficiency in Wastewater Treated with Ozone. *Water Sci. Technol.* **2015**, *71* (7), 980–985. <https://doi.org/10.2166/wst.2015.053>.
- (107) Eischeid, A. C.; Meyer, J. N.; Linden, K. G. UV Disinfection of Adenoviruses: Molecular Indications of DNA Damage Efficiency. *Appl. Environ. Microbiol.* **2009**, *75* (1), 23–28. <https://doi.org/10.1128/AEM.02199-08>.
- (108) Thurston-Enriquez, J. A.; Haas, C. N.; Jacangelo, J.; Gerba, C. P. Chlorine Inactivation of Adenovirus Type 40 and Feline Calicivirus. *Appl. Environ. Microbiol.* **2003**, *69* (7), 3979–3985. <https://doi.org/10.1128/AEM.69.7.3979-3985.2003>.
- (109) Zhong, Q.; Carratalà, A.; Ossola, R.; Bachmann, V.; Kohn, T. Cross-Resistance of UV- or Chlorine Dioxide-Resistant Echovirus 11 to Other Disinfectants. *Front. Microbiol.* **2017**, *8*. <https://doi.org/10.3389/fmicb.2017.01928>.
- (110) Baggen, J.; Thibaut, H. J.; Strating, J. R. P. M.; Kuppeveld, F. J. M. van. The Life Cycle of Non-Polio Enteroviruses and How to Target It. *Nat. Rev. Microbiol.* **2018**, *16* (6), 368. <https://doi.org/10.1038/s41579-018-0005-4>.
- (111) Torrey, J.; von Gunten, U.; Kohn, T. Differences in Viral Disinfection Mechanisms as Revealed by Quantitative Transfection of Viral Genomes. *Submitted to Applied and Environmental Microbiology*.
- (112) Cabec, V. L.; Cols, C.; Maridonneau-Parini, I. Nonopsonic Phagocytosis of *Zymosan* and *Mycobacterium Kansasii* by CR3 (CD11b/CD18) Involves Distinct Molecular Determinants and Is or Is Not Coupled with NADPH Oxidase Activation. *Infect. Immun.* **2000**, *68* (8), 4736–4745. <https://doi.org/10.1128/IAI.68.8.4736-4745.2000>.

- (113) The Diffraction Barrier in Optical Microscopy <https://www.microscopyu.com/techniques/super-resolution/the-diffraction-barrier-in-optical-microscopy> (accessed Feb 17, 2019).
- (114) Rule of thumb for width of biological hydroph - Generic - BNID 107247 <https://bionumbers.hms.harvard.edu/bionumber.aspx?&id=107247> (accessed Feb 12, 2019).
- (115) van Meer, G.; Voelker, D. R.; Feigenson, G. W. Membrane Lipids: Where They Are and How They Behave. *Nat. Rev. Mol. Cell Biol.* **2008**, *9* (2), 112–124. <https://doi.org/10.1038/nrm2330>.
- (116) Pohl, M. O.; Stertz, S. Measuring Attachment and Internalization of Influenza A Virus in A549 Cells by Flow Cytometry. *J. Vis. Exp. JoVE* **2015**, No. 105. <https://doi.org/10.3791/53372>.
- (117) Marjomäki, V.; Pietiäinen, V.; Matilainen, H.; Upla, P.; Ivaska, J.; Nissinen, L.; Reunanen, H.; Huttunen, P.; Hyypiä, T.; Heino, J. Internalization of Echovirus 1 in Caveolae. *J. Virol.* **2002**, *76* (4), 1856–1865. <https://doi.org/10.1128/JVI.76.4.1856-1865.2002>.
- (118) Carpenter, A. E.; Jones, T. R.; Lamprecht, M. R.; Clarke, C.; Kang, I. H.; Friman, O.; Guertin, D. A.; Chang, J. H.; Lindquist, R. A.; Moffat, J.; et al. CellProfiler: Image Analysis Software for Identifying and Quantifying Cell Phenotypes. *Genome Biol.* **2006**, *7* (10), R100. <https://doi.org/10.1186/gb-2006-7-10-r100>.
- (119) Schindelin, J.; Arganda-Carreras, I.; Frise, E.; Kaynig, V.; Longair, M.; Pietzsch, T.; Preibisch, S.; Rueden, C.; Saalfeld, S.; Schmid, B.; et al. Fiji: An Open-Source Platform for Biological-Image Analysis. *Nat. Methods* **2012**, *9* (7), 676–682. <https://doi.org/10.1038/nmeth.2019>.
- (120) Bolte, S.; Cordelières, F. P. A Guided Tour into Subcellular Colocalization Analysis in Light Microscopy. *J. Microsc.* **2006**, *224* (Pt 3), 213–232. <https://doi.org/10.1111/j.1365-2818.2006.01706.x>.
- (121) Dunn, K. W.; Kamocka, M. M.; McDonald, J. H. A Practical Guide to Evaluating Colocalization in Biological Microscopy. *Am. J. Physiol. - Cell Physiol.* **2011**, *300* (4), C723–C742. <https://doi.org/10.1152/ajpcell.00462.2010>.
- (122) Son, K.-N.; Liang, Z.; Lipton, H. L. Double-Stranded RNA Is Detected by Immunofluorescence Analysis in RNA and DNA Virus Infections, Including Those by Negative-Stranded RNA Viruses. *J. Virol.* **2015**, *89* (18), 9383–9392. <https://doi.org/10.1128/JVI.01299-15>.
- (123) Kukkula, M.; Maunula, L.; Silvennoinen, E.; von Bonsdorff, C.-H. Outbreak of Viral Gastroenteritis Due to Drinking Water Contaminated by Norwalk-like Viruses. *J. Infect. Dis.* **1999**, *180* (6), 1771–1776. <https://doi.org/10.1086/315145>.
- (124) Klinger, M. Disinfection of Environment Isolates of Coxsackieviruses. Master thesis, EPFL: Lausanne, Switzerland, 2016.
- (125) Ianni, J. C. A Comparison of the Bader-Deuflhard and the Cash-Karp Runge-Kutta Integrators for the GRI-MECH 3.0 Model Based on the Chemical Kinetics Code Kintecus. *Computational Fluid and Solid Mechanics* **2003**, 1368–1372.
- (126) Liang, F.; Paulo, R.; Molina, G.; Clyde, M. A.; Berger, J. O. Mixtures of g Priors for Bayesian Variable Selection. *J. Am. Stat. Assoc.* **2008**, *103* (481), 410–423. <https://doi.org/10.1198/016214507000001337>.

# Curriculum Vitae

## CONTACT INFORMATION

### CAMILLE WOLF

Plans-Praz 1, 1337 Vallorbe, 079 338 32 28  
camille.wolf@epfl.ch

## PERSONAL INFORMATION

## EDUCATION

**PhD es Science in environmental engineering** 2019

ECOLE POLYTECHNIQUE FEDERALE DE LAUSANNE (EPFL)

PhD realized in the environmental chemistry laboratory under supervision of Prof. Tamar Kohn.

**Master in Molecular and Biological Chemistry** 2014

ECOLE POLYTECHNIQUE FEDERALE DE LAUSANNE (EPFL)

- Master thesis: *“Isolation and characterization of breast cancers Extracellular vesicles (EVs)”*, 5 months project in Prof. Vogel’s laboratory (LCCPM).
  - Acquired competencies: Isolation (by ultracentrifugation) and purification with a size exclusion chromatography (AKTA purifier) of breast cancer cell EVs. Analysis of these latter by confocal microscopy, fluorescence correlation spectroscopy (FCS), Surface plasmon resonance (SPR). Results published in Analytical chemistry July 7, 2014.
- Semester project : *“Functional study of mouse KH domain of Bicaudal C protein, 8 weeks in Prof. Constam’s Laboratory at EPFL*
  - Acquired competencies : Production and purification of recombinant proteins in *E.coli*, GST-pull down, *in vitro* transcription and purification of RNAs, Luciferase assays, Electrophoretic Mobility Shift Assays

**Bachelor in chemistry at EPFL, Lausanne /VD** 2008-2012

- Erasmus at Strathclyde University, Glasgow/ UK 2011-2012  
Internship in Precy’s laboratory
  - Synthesis and characterization by NMR ( $^1\text{H}$ ,  $^{13}\text{C}$ ,  $^{19}\text{F}$ , COSY, HSQC, HMBC) and mass spectrometry of sylilenoether compound
- 5 week Internship in Prof. Heinis’ laboratory at EPFL. summer 2011  
DNA purification and peptide purification with HPLC

## CONFERENCES

Oral presentation at « *Ma Thèse en 180s* » Finale EPFL 2019  
 Oral presentation at the *Food and environmental virology conference* in Arizona, 7th-10th October 2018, Tempe Arizona  
 Oral presentation at the *Ozone and advanced oxidation solutions for emerging pollutants of concern to the water and the environment*, Lausanne, 7th-8th September 2018  
 Poster presentation at *International symposium on Health-Related Water Microbiology and IWA symposium*, Chapel hill, North Carolina, 15th-19th May 2017  
 Honorable mention for poster presentation at Gordon conference: *Environmental Sciences : Water*, New Hampshire, 25th June to 1<sup>st</sup> July 2016

## WORKSHOPS

Workshop Innoseed « *Design Thinking* », 1-day hand-on crash course, 2018  
 Several courses at the Swiss Bioinformatics institute (SIB), « *Introduction to R* », « *Intermediate R* », « *Advanced R* », « *R packaging* », « *Introduction to statistics* », « *Advanced statistical modelling* », « *Mass Spectrometry-based Proteomics* », UNIL, de 2015 à 2018  
 Cuso course « *Basics in Academic Writing « Rhetorical and Language Features in the Parts of a Scientific Article: Academic Writing 1»*, Uni Neuchatel, 2016  
 Workshop Cuso « *MALDI-TOF Mass-spectrometry in medical and environmental microbiology* », Bellinzona, 2015  
 Summer school « *Bayesian statistics for environmental research* » EAWAG, Dübendorf, 2015  
 Workshop Cuso « *Dual use of highly pathogenic microbes*», Spiez labor, 2014  
 Workshop Cuso « *Innate defense against microbes*», CHUV Lausanne, 2014

## PROFESSIONAL QUALIFICATIONS

- Laboratory work: BSL1, BSL2
- Office software: Word, Excel, PowerPoint
- Scientific software: R Statistics software (e.g. ggplot2 graphics, frequentist and Bayesian statistics)  
 Chromeleon Chromatography data system  
 Zen lite (Microscopy)  
 Cellprofiler and Image J (Image analysis)
- Illustration: Adobe Illustrator

## PUBLICATIONS

WYSS, R.; GRASSO, L.; WOLF, C.; GROSSE, W.; DEMURTAS, D.; VOGEL H. MOLECULAR AND DIMENSIONAL PROFILING OF HIGHLY PURIFIED EXTRACELLULAR VESICLES BY FLUORESCENCE FLUCTUATION SPECTROSCOPY, *ANAL. CHEM.*, 2014, 86 (15), 7229-7233, [HTTPS://DOI.ORG/10.1021/AC501801M](https://doi.org/10.1021/ac501801m)

WOLF, C.; VON GUNTEN, U.; KOHN, T. KINETICS OF INACTIVATION OF WATERBORNE ENTERIC VIRUSES BY OZONE. *ENVIRON. SCI. TECHNOL.* 2018, 52 (4), 2170–2177. [HTTPS://DOI.ORG/10.1021/ACS.EST.7B05111](https://doi.org/10.1021/ACS.EST.7B05111).

**INTERESTS**

- Ice Hockey      Player in HC féminin Lausanne in National League B; Committee Member, I am responsible for the organization of sports events and leisure for the team (for example: training camp)  
In addition, I organized and budgeted the founding dinner to raise money to pay part of team seasons
- Beer brewing  
and tasting      Like to apply some of my knowledge to different environment
- Sports          Boxing, running, biking, swimming, hiking





